Behavior and Strength of Steel Fiber Reinforced Concrete Columns Using Recycled Aggregate

A Dissertation Submitted to the Council of the Erbil Technical Engineering Collage at Erbil Polytechnic University in Partial Fulfillment of the Requirements for the Degree of PhD in Structural Engineering

By

Bakhtyar Nassih Najar

BSc. Civil Engineering – Salahaddin University-Erbil-1993

MSCE Structural Engineering – Portland State University-2008

Supervised By

Prof. Dr. Mereen Hassan Fahmi Rasheed

Asst. Prof. Dr. Bahman Omar Taha

Erbil- Kurdistan

June 2024

بِسْمِ اللَّهِ الرَّحْمَنِ الرَّحِيمِ

اقْرَأْ بِاسْمِ رَبِّكَ الَّذِي خَلَقَ ﴿١﴾ خَلَقَ الْإِنْسَانَ مِنْ عَلَقٍ ﴿٢﴾ اقْرَأْ وَرَبُّكَ الْأَكْرَمُ ﴿٣﴾ الَّذِي عَلَّمَ بِالْقَلَمِ ﴿٤﴾ عَلَّمَ الْإِنْسَانَ مَا لَمْ يَعْلَمْ ﴿٥﴾

سورة العلق

DECLARATION

I declare that the PhD dissertation entitled: **Behavior and Strength of Steel Fiber Reinforced Concrete Columns Using Recycled Aggregate** is my own original work, and hereby I certify that unless stated, all work contained within this dissertation is my own independent research and has not been submitted for the award of any other degree at any institution, except where due acknowledgment is made in the text.

Signature:

Student Name: **Bakhtyar Nassih Najar**

Date: 3/6/2024

SUPERVISOR CERTIFICATE

This dissertation has been written under my supervision and has been submitted for the award of the degree of Doctor of Philosophy in Structural Engineering with my approval as supervisor.

Signature Name: Prof. Dr. Mereen Hassan Fahmi Rasheed

Date:

Signature Name: Asst. Prof. Dr. Bahman Omar Taha

Date:

I/We confirm that all requirements have been fulfilled.

Signature:

Name: Asst. Prof. Dr. Bahman Omar Taha

Head of the Department of Civil Engineering

Date:

I confirm that all the requirements have been fulfilled.

Postgraduate Office and Scientific Affairs

Signature:

Name: Mr. Bayad Abdulqadir Ahmad

Date

EXAMINING COMMITTEE CERTIFICATION

We certify that we have read this Dissertation: **Behavior and Strength of Steel Fiber Reinforced Concrete Columns Using Recycled Aggregate** and as an examining committee examined the student (Bakhtyar Nassih Mohammed) in its content and what related to it. We approve that it meets the standards of a dissertation for the degree of Doctor of Philosophy in Structural Engineering.

Signature:
Asst. Prof. Dr. Mezgeen Sisen Ahmed
Member of the committee
Date:

Signature:
Asst. Prof. Dr. Najmadeen Mohammed Saeed
Member of the committee
Date:

Signature:
Prof. Dr. Serwan khurshid Rafiq Al-Zahawi
Member of the committee
Date:

Signature:
Prof. Dr. Sinan Abdulkhaleq Yaseen
Member of the committee
Date:

Signature:
Asst. Prof. Dr. Bahman Omar Taha
Supervisor
Date:

Signature:
Prof. Dr. Mereen Hassan Fahmi Rasheed
Supervisor
Date:

Signature:
Prof. Dr. Ayad Z. Saber
Head of the committee
Date:

Signature:
Prof. Dr. Ayad Z. Saber
Dean of Erbil Technical Engineering Collage
Date:

DEDICATION

TO

My late father

My mother

My wife, Dr. Sundis Ahmed

My sons: Bawan, Blund and Aaran

Bakhtyar

2024

ACKNOWLEDGMENTS

This dissertation would not have been possible without the support and guidance of many individuals. I would like to express my deepest gratitude to all who have contributed to this achievement.

Firstly, I extend my heartfelt thanks to my supervisors, Prof. Dr. Mereen Hassan Fahmi Rasheed and Asst. Prof. Dr. Bahman Omar Taha. Dr. Mereen, your expertise, patience, encouragement and constructive criticism pushed me to refine my ideas. Dr. Bahman, your meticulous attention to detail and profound knowledge in researches provided a strong foundation for this research. Your mentorship has been invaluable.

I am also grateful for the support of my colleagues, particularly Dr. Zrar Siddiq Othman, Miss. Shina Jabar Abdulkarim, Dr. Fikrat Latif Hamid, and Mr. Muhasin khalid. Your friendship, insightful discussions, and collaborative spirit were instrumental in keeping me motivated and focused.

A special thank you to my wife, Dr. Sundis Ahmad, for your unwavering support and understanding. You have been my rock, always ready to offer a word of encouragement and make countless sacrifices to help me achieve my goals.

To my boys Bawan, Blund and Aaran, thank you for being my inspiration and motivation. Your smiles and laughter have been a constant reminder of the joys of life and the importance of perseverance.

In conclusion, I thank everyone who has been a part of this journey. Your support has been instrumental in the completion of this dissertation. This accomplishment is a shared success with all of you. Thank you.

ABSTRACT

This research study includes an experimental and analytical study of steel fiber-reinforced concrete columns using natural and recycled aggregate (RA). To improve the structural application of recycled aggregate and to protect the environment and preserve natural resources, it is crucial to use recycled aggregate in construction. The recycled coarse aggregate reinforced concrete columns with the addition of steel fiber subjected to concentric and eccentric loadings for short and slender columns are examined experimentally and analytically in this research. Forty two column specimens were cast to examine the impact of steel fiber, recycled aggregate, slenderness, and eccentricity on the behavior of reinforced concrete columns. In addition to concentrically loaded columns, columns were loaded at 50% and 100% eccentricity, corresponding to e/h ratios of 0.5 and 1.0. Three different slenderness ratios were selected to examine the effects of height: 17.24 for short columns, 26 for moderately slender columns, and 34.5 for highly slender columns. The research examined the failure mode, maximum load-carrying capacity, strain in the concrete, and strain in the reinforcement, mid-height lateral displacement, vertical displacement and ductility. Based on the results of the current study, it can be concluded that employing recycled concrete aggregate is a potential approach that can meet design codes. Columns produced with recycled concrete aggregate behaved similarly to columns made with natural aggregate (NA). The addition of 1% steel fiber effectively prevented concrete from crushing and spalling. Steel fiber, however, improved the columns' ductility and strength. According to experimental results, the steel fiber addition narrowed the crack width which visually observed and had a comparable effect on columns constructed with recycled aggregate and

columns constructed with natural aggregate. The experimental test maximum load carrying capacity agreed well with the results using ACI-318-19 equations. Furthermore, a model has been proposed for columns with both natural and recycled aggregate and accounts for eccentricity and slenderness to forecast the load-carrying capability. Additionally, the second-order effect due to the intentional such as given eccentricity and unintentional eccentricity such as alignment errors was investigated. The second-order effect is considered an excellent theoretical method to examine the behavior of columns. Using this method theoretical load path was drawn for each column tested as well as an experimental load path for comparison, later, using the same method, an axial load bending moment interaction diagram was plotted for all the tested columns. The outcomes demonstrated that the design principles were met well. Plots of load-moment interaction diagrams for short, slender columns prepared using the ACI-318-19 equations, 2^{nd} order effect method, and proposed method. The experimental findings were added to the interaction diagrams for comparison.

Finally, it needs to be mentioned that recycling concrete waste cubes and other recycled materials decreases the amount of waste sent to landfills. This practice helps avoid the consumption of natural resources, thereby preventing their quick depletion and cutting down on the expenses and distractions linked to their extraction. Utilizing sustainable materials and creating a new pathway for their reuse, such as incorporating recycled aggregates, can reduce waste and conserve natural resources.

CONTENTS

LIST OF FIGURES

LIST OF TABLES

NOTATIONS

Notation	Meaning
a	Height of the equivalent rectangular block stress of concrete, mm
A_c	Area of the equivalent rectangular block stress of concrete, mm^2
Ag	Gross cross sectional area of column, mm^2
b	Width of the rectangular cross-section, mm
c	Distance from top compression fiber to neutral axis, mm
C_c	Internal compression force developed in concrete
C_m	Factor relating actual moment diagram
d	Effective depth, the distance from top compression fiber to centroid of steel, mm
e	Eccentricity of the load, mm
E_c	Elastic modulus of concrete, GPa.
E_s	Elastic modulus of steel bar, GPa
$EI_{Eff.}$	Effective flexural stiffness, $N.m^2$
f'_c	Maximum concrete compressive strength, MPa
f_{ct}	Splitting tensile strength, MPa
f_r	Modulus of Rupture of concrete, MPa
f_y	Yield tensile strength of steel rebars, MPa
I_g	Moment of inertia of gross concrete
h	Cross-section dimension in bending direction
lu	Effective length of column, mm
Mc	the magnified moment for the column

M_2	Larger ends moment
M_1	Lesser ends moment
Mn	Nominal bending capacity of the column, kN.m
n	Modular ratio
Pc	Critical buckling load, kN
Pn	Nominal axial capacity of the column, kN
$P_{Exp.}$	Experimental axial load at failure, kN
P_{Theo}	Theoretical nominal axial capacity, kN
P_u	Factored axial load
R^2	Coefficient of determination
r	Radius of gyration of cross section, mm
S_2	Stress corresponding to 40% of ultimate load, MPa
S_1	Stress corresponding to a longitudinal strain of 0.000050, MPa
α	Coefficient for reducing the concrete flexural stiffness
β_1	Sectional factor in ACI 318-19
β_d	Reduction of stiffness of columns due to sustained axial loads
γ	Reduction factor of concrete compressive strength
δ	Moment magnifier
Δ	Displacement, mm
ϵ	Strain mm/mm

LIST OF ABBREVIATIONS

Abbreviations	Expanded form
CDW	Construction Demolition Waste
CFRP	Carbon Fiber Reinforced Polymer
COV	Coefficient of Variation
GFRP	Glass Fiber Reinforced Polymer
HSSCC	High Strength Self Compacting Concrete
LVDT	Linear Variable Differential Transformer
NA	Natural Aggregate
NAC	Natural Aggregate Concrete
RA	Recycled Aggregate
RAC	Recycled Aggregate Concrete
RCA	Recycled Concrete Aggregate
RC	Reinforced Concrete
SCC	Self-Compacting Concrete
SD	Standard Deviation
SF	Steel Fiber
SSD	Saturated Surface Dry

CHAPTER ONE

INTRODCTION

CHAPTER ONE
INTRODUCTION

1.1 OVERVIEW AND PROBLEM STATEMENT

The utilization of recycled aggregates reduces the demand for natural aggregates, redirects construction and demolition waste from landfills, and helps mitigate environmental pollution. The researches indicate that recycled aggregates meet or exceed the performance standards for various structural applications, ensuring safety and dependability. The establishment of guidelines and standards ensures consistent quality and performance. The promotion of recycled aggregates aligns with global sustainability objectives and encourages environmental responsibility in green building practices. The effective research and application can influence policies mandating the use of recycled materials in construction. Increased adoption also raises public awareness of sustainable construction, fostering greater demand and acceptance. Recycled aggregates find application in concrete for structural elements such as beams, columns, slabs, and foundations. Furthermore, they are used in bridges, tunnels, and other significant infrastructure projects, supporting sustainable urban development Tabsh and Abdelfatah (2009).

The ongoing research aids in understanding how recycled aggregates respond to different loads and environments, ensuring their structural durability and longer service life. In essence, incorporating recycled aggregate in structural applications holds substantial promise for promoting sustainable construction practices, mitigating environmental impact.

1.2 RECYCLED COARSE AGGREGATES

As urbanization and construction activities rapidly expand, the demand for natural aggregates continues to grow, driving increased concrete production. However, extracting these aggregates from natural sources can cause significant environmental harm. Additionally, the demolition of outdated buildings and structures generates substantial amounts of construction debris, posing a growing disposal challenge. A promising solution to these issues is the use of construction and demolition waste as a substitute for natural aggregates in concrete, known as recycled concrete aggregates. This method not only addresses waste management concerns but also has been a recognized and effective practice in infrastructure projects worldwide for many years. Surya et al. (2013)

Rampit et al. (2020) explained that the expansion of the global population, extensive urbanization, and the economic status of developing nations have significantly accelerated the growth of the construction industry. Consequently, there is a notable increase in the demolition of old structures to make room for new buildings. This widespread demolition activity results in a substantial amount of debris worldwide, leading to significant environmental pollution and disposal challenges. Recent reports indicate that the European Union produces around 850 million tonnes of construction and demolition waste (CDW) annually, comprising 31% of total waste generation. De Brito and Saikia (2012) stated that recycling construction and demolition waste (CDW) in new construction extends the lifecycle of construction materials. Some countries have enacted governmental laws and regulations to increase CDW recycling rates, resulting in levels as high as 90% in certain regions. CDW can serve as aggregate in new concrete production, similar to

natural aggregate (NA), and is characterized using comparable methods. Since aggregate typically occupies over 75% of the concrete mix volume, it's crucial to thoroughly evaluate the properties of CDW aggregates, especially given their diverse origins. BS 8500 (2002) shows two categories of CDW aggregates: recycled concrete aggregate (RCA), containing a minimum of 95% crushed concrete, and recycled aggregate (RC), comprised entirely of crushed masonry-based material, recycled aggregate that made of masonry.

Shatarat et al. (2019) concluded that substituting Natural Aggregate (NA) with Recycled Coarse Aggregate (RCA) in concrete offers significant environmental benefits by reducing the reliance on non-renewable natural resources like NA and minimizing landfill areas, thus decreasing pollution.

Shi et al. (2016) explained that numerous studies have investigated the impact of using RCA in concrete, with most findings indicating that RCA properties depend on the original concrete source and often exhibit lower quality than NA due to higher water absorption, surface cracks, remaining mortar particles and differences in strength. These factors can negatively affect concrete workability, durability, and mechanical properties. To address these challenges, various studies have explored treatment methods to enhance RCA performance. The recent researches have also focused on examining the structural behavior of large-scale elements using RCA.

Choi and Yun (2012) investigated the compressive behavior of RC columns utilizing RCA and suggested presoaking aggregates to mitigate high water absorption without the need for additional water. This way water- cement ratio

stays under control by adding water only for the mix without additional water for the recycled aggregate.

McNeil and Kang (2013) after the demolition of old roads and buildings, the resulting concrete is often discarded as waste. However, by collecting and processing this concrete, recycled concrete aggregate (RCA) is produced. The use of RCA in new construction is a relatively recent practice. The origins of RCA traced back to the end of World War II when the massive demolition of buildings and roads created a surplus of waste material and a pressing need for reconstruction in Europe. Although the immediate demand for recycled concrete declined after the war, the practice saw a resurgence in the 1970s in the United States, where RCA began to be used for non-structural purposes such as fill material, foundations, and base courses. Since then, research has explored the potential of RCA as a replacement for natural aggregates (NA) in structural concrete.

In the city of Erbil, there are several landfills which contains construction and demolition waste material that can be used in manufacturing recycled aggregate and help clean the environment. Figure 1.1 shows the land fill near the southern industrial area in Erbil.

Figure 1.1 Construction and demolition waste disposal in a landfill (Erbil).

1.3 RESEARCH OBJECTIVE

This study's primary objective is to investigate the behavior of RCA slender columns compared to short columns, an area not previously explored in combination. Additionally, it examines the performance of these columns under varying levels of eccentricity, subjected to both axial and eccentric loads. It also assesses the feasibility of entirely replacing natural aggregate (NA) with RCA, as well as partial replacement, in forty-two reinforced concrete columns by analyzing the effects of steel fiber on samples made from both RCA and NA. The study further investigates aspects such as slenderness, eccentricity, ductility, strain in concrete and steel, and the axial and vertical displacement of the columns. While recent studies have addressed some aspects of column behavior, including either slender or short columns made with RCA, they have not covered the other parameters. Therefore, there is a significant need for further research in this area.

1.4 DISSERTATION LAYOUT

This dissertation consists of six chapters:

Chapter 1: This chapter provides an overview of the problem and the purpose of this study, introducing recycled concrete aggregate.

Chapter 2: This chapter reviews the literature on the characteristics of RC columns, providing a historical overview of previous researches on recycled aggregate concrete columns along with their results and recommendations. It also examines the main factors influencing the axial behavior of eccentrically

loaded RC members, studies the effect of column height, and explores the impact of steel fiber in concrete on the columns.

Chapter 3: This chapter outlines the experimental work program, providing details on the specimens, materials and their properties, preparation and curing processes, fabrication methods, setup, testing procedures, and the machinery and equipment utilized.

Chapter 4: This chapter presents the experimental test results for all the tested reinforced concrete columns. The discussions cover the modes of failure, load-carrying capacity, displacements, concrete strain, reinforcement strain, ductility, and the effects of various test parameters such as eccentricity, slenderness ratio, recycled aggregate, and steel fiber.

Chapter 5: This chapter details the methods used to predict the strength of the columns examined in this study, utilizing equations of equilibrium and strain compatibility. It verifies the experimental test results using ACI-318-19 code provisions, considers second-order effects, and assesses proposed models. Additionally, the axial load and moment interaction diagrams are plotted for each method to compare with the experimental test results. The verification of strain and displacements is also addressed from the calculations of moment-interaction diagrams.

Chapter 6: This chapter comprises the conclusions drawn from the study, integrating both its experimental and theoretical results. Additionally, it includes recommendations and suggestions for future research endeavor.

CHAPTER TWO

LITERATURE REVIEW

CHAPTER TWO
LITERATURE REVIEW

2.1 INTRODUCTION

This chapter presents a comprehensive literature review on the effect of recycled aggregate and steel fibers on the structural behavior of concrete columns. It examines factors such as column size, slenderness ratio, loading eccentricity, and second-order effects. The environmental impact of using RCA is also covered, as the scarcity of natural resources and the environmental impact of construction demolition waste (CDW) have become major concerns in the construction industry. Utilizing RCA in concrete products is considered a promising approach to conserving natural resources and mitigating the environmental effects of CDW.

Numerous research efforts have been made to mitigate the negative impacts of recycled aggregates on the structural behavior of columns, beams, and other structural members, to promote their adoption in the construction industry. Researches on columns made of (RCAs) has been notably limited compared to beams. These research findings can serve as a basis for establishing criteria and guidelines for the design and construction of resilient and durable slender concrete columns utilizing recycled aggregates.

Concrete is among the most extensively utilized cement-based inorganic materials, with aggregates making up roughly 70%–80% of its mass (Verian et al., 2018). Knowing that the construction industry's recent surge in mining and consuming natural resources is rapidly consuming these materials. For example, global aggregate production escalated from approximately 21 billion

tons in 2007 to over 50 billion tons in 2017 Lima et al. (2021). Considering using recycled aggregate became an extreme need. The most recent data available in 2024, the Global Cement and Concrete Association (GCCA) and other industry sources, global aggregate production is estimated to be around 60 to 70 billion tons annually.

Thus, the primary objectives of the present research are vital: to examine behavior of concrete columns, experimentally and analytically, short and slender, subjected to axial and eccentric loading, and using recycled concrete aggregate as well as steel fiber.

2.2 THE ACI COMMITTEE 318-19 RECOMMENDATIONS:

ACI-318-19 (2019) established the formula for determining the nominal compression capacity (P_{no}) of a reinforced concrete column under concentric loading as follows:

$$P_{no} = 0.85\, f_c'\left(A_g - A_{st}\right) + f_y A_{st} \quad \text{---------- (2.1)}$$

Where:

f_c' : Concrete compressive strength.

A_g : Concrete section gross area

A_{st} : Steel reinforcement area

f_y : Yield strength of steel reinforcement.

Several experimental programs on reinforced concrete columns suggested a value of 0.85 for kc (Lyse and Kreidler, 1932). The occurrence of eccentricity in column sections, due to end conditions and material property variations, prompted ACI 318-19 to introduce reduction factors of 0.80 and

0.85 in the maximum nominal load capacity (Pno) for spiral and tied columns, respectively.

For spiral columns:

$$P_n = \phi P_{no} = 0.85\phi\left[0.85f_c'\left(A_g - A_{st}\right) + f_y A_{st}\right] \text{---------- (2.2)}$$

For tied columns:

$$P_n = \phi P_{no} = 0.80\phi\left[0.85f_c'\left(A_g - A_{st}\right) + f_y A_{st}\right] \text{---------- (2.3)}$$

Where Φ is a strength reduction factor of 0.75 for spiral columns and 0.65 for tied columns. Additionally, ACI 318-19 proposed a minimum and maximum ratio of longitudinal reinforcement area to column cross-section area between minimum of 1% and maximum of 8%.

2.3 REINFORCED CONCRETE COLUMNS USING RECYCLED AGGREGATE.

Choi and Yun (2012) conducted experimental tests on seventeen square columns constructed from recycled aggregate. Specimens, were fabricated with replacement percentages of recycled coarse aggregate of 0%, 30%, 60%, and 100%. They examined the failure mode, compressive strength, and ductility of these columns. The findings suggested that recycled concrete aggregate meets the ACI design strength criteria. Similar cracking patterns were noted. As the percentage of recycled aggregate replacement increased, the maximum axial load capacity decreased by approximately 7% compared to columns using natural aggregate. Overall, the axial behavior in columns using recycled aggregate aligns with that observed in conventional reinforced concrete columns made with natural aggregate.

Quang et al. (2022) studied square-reinforced concrete columns that were subjected to concentric compressive loads in a series of tests. Different replacement levels of natural aggregate with recycled aggregate (0%, 50%, and 100%) were examined. Various parameters including load, deformation, cracking load, cracking width, and compressive strain were analyzed. The results indicated that increasing the proportion of recycled aggregate decreased the strength of the columns by 6.33% for 50% replacement and 7.67% for 100% replacement. However, the mechanical behavior of columns containing recycled aggregate exhibited only a minor variation and did not significantly alter the behavior of the columns, suggesting the feasibility of using recycled aggregate concrete (RAC) in concrete structures. The recycled aggregate was sourced from construction demolition waste of a 20-year-old building. The failure mode observed in RAC columns was similar to that of columns using natural aggregate (NAC).

Ali et al. (2023) tested eight slender reinforced concrete columns with circular cross-sections to explore the influence of slenderness and recycled aggregate on column behavior, utilizing two primary types of transverse reinforcement: ties and spirals. The columns were modeled with RCA replacement percentages of 25%, 50%, and 100%, and subjected to axial concentric loading. The results indicated that substituting natural coarse aggregate (NCA) with recycled concrete aggregate (RCA) at 25%, 50%, and 100% led to reductions in the ultimate capacity of tied reinforced concrete (RC) columns by 13.41%, 14.07%, and 23.33%, respectively. Recycled concrete cubes and cylinders, with compressive strengths ranging from approximately 15 to 35 MPa, were obtained from the laboratory to produce the RCA, with a maximum particle size of 10 mm. Introducing RCA as a replacement material in the

concrete columns reduced the peak load compared to columns with NA. However, using spiral reinforcement in RCA columns resulted in a stiffer response to external loads and a higher peak load compared to square RC columns. The post-peak behavior of the load-displacement curve in both tied and spiral-reinforced RCA columns exhibited a sudden drop in load, indicating a brittle failure mode.

Ridzuan et al. (2005) Crushed waste concrete cubes that were initially tested for compressive strength, later reused as recycled coarse aggregate. Due to minimal information available regarding their origin and strength, the waste concrete was utilized to simulate real-life conditions. After 28 days, the compressive strength of the recycled aggregate concrete (RAC) mixes was found to be 3-16% higher than that of the corresponding natural aggregate concrete (NAC) mixes. The reason behind the RAC mixes' increased compressive strength could be traced back to the recycled concrete aggregates' high water absorption. This led to a decrease in the RAC mixes' effective water-cement ratio, which in turn produced a higher compressive strength than the similar NAC mixes. Nevertheless, the difference in compressive strength between the RAC and NAC mixes decreased as the water-cement ratio was reduced. This phenomenon could be explained by the fact that at higher design strengths, the recycled aggregate may fail earlier than the cement paste due to its limited strength, resulting in less resistance to crushing loads.

Khafaga and Sayed (2011) tested ten reinforced concrete columns in an experimental study, each incorporating varying percentages of recycled aggregate. The recycled aggregate used in the experiment was manufactured

and prepared in the laboratory from four distinct types of parent concrete mixes. The study aimed to comprehend the impact of the parent concrete and the mortar quality inside the parent concrete, and the replacement percentage of recycled aggregate. The results revealed that columns utilizing recycled aggregate exhibited 6.6% to 26.0% lower ultimate carrying capacities compared to columns using natural aggregate. Interestingly, employing parent concrete with high-quality mortar did not significantly affect the maximum strength of the columns tested. Moreover, it was observed that a higher grade of parent concrete used in the recycled aggregate contributed to a lesser reduction in the initial stiffness of the tested columns. Furthermore, incorporating a higher quality of mortar in the parent concrete mix of the recycled aggregate concrete not only mitigated the reduction in initial stiffness but also decreased the reduction in ultimate load carrying capacity observed in the tested columns.

Knaack and Kurama (2020) examined the impact of varying proportions of coarse recycled aggregate on the time-dependent vertical deflections of reinforced concrete columns enduring sustained service loads. The study evaluated deflections for both concentric and eccentric columns across different percentages of coarse aggregate replacement, concrete strength, column dimensions, longitudinal reinforcement ratios, shrinkage strain, and creep coefficient. Additionally, the study assessed the quality of RAC concerning various water absorption ratios. The findings of the research indicated that high-quality RAC with minimal porosity yielded deflections comparable to those of natural aggregate concrete columns. The increase in deflection attributed to recycled coarse aggregate was more pronounced in columns with higher concrete strength and larger cross-sectional dimensions,

as well as with lower longitudinal steel ratios. Moreover, the deflection was notably higher in concentric columns compared to exterior columns.

Ajdukiewicz and Kliszczewicz (2007) tested five series of columns. The objective was to analyze and present the differences in the behavior between simple reinforced concrete elements constructed with RCA, featuring various proportions of recycled aggregates, and those composed from concrete containing purely natural aggregate under compression. The results of the study were analyzed, the load-bearing capacities were comparable among the elements, yet substantially greater deformations were observed in the concrete of RCA specimens. In column tests, no observable difference was noted in behavior under load until failure; however, the failure occurred at a slower pace in columns fabricated with RCA, a consequence of the increased ductility observed in RCA specimens.

Deresa et al. (2020) offered a comprehensive evaluation of the structural behavior of reinforced RAC columns, based on experimental test. The findings from this analysis clearly demonstrate that reinforced RAC columns, with varying ratios of recycled concrete aggregate replacement, exhibit structural performances comparable to or marginally lower than those of reinforced natural aggregate concrete counterparts, highlighting the viability of recycled concrete aggregate for structural purposes.

It was also concluded that RAC columns exhibit similar crack progression and failure patterns as NAC columns under both concentric and eccentric loading conditions. The maximum axial load capacity showed a slight decrease with the increase in the replacement ratio. The concrete strain in RA columns surpasses that of NC columns, indicating a reduction in stiffness for RAs.

However, RA columns performance remains comparable to that of NA columns under eccentric loading, although with a decrease in the maximum axial load capacity with the increase in eccentricity. Furthermore, it was determined that in terms of seismic behavior under cyclic loads, the overall performance of RA columns is comparable with NA columns. While the lateral load capacity of RAC columns is marginally lower than that of equivalent NAC columns, RAC columns exhibit slightly higher rotation and lower ductility under cyclic loading compared to their NAC counterparts.

Asad-ur-Rehman Khan (2019) studied the performance of reinforced concrete columns constructed with recycled coarse aggregate under uniaxial loading. Various aspects were examined, including the percentage replacement of recycled aggregate (30%, 50%, 70%, and 100%) and curing for 28 days with a constant water-to-cement ratio of 0.43. The utilization of recycled aggregate resulted in a slight decrease in strength outcomes. It was noted that the load-carrying capacity of columns followed a similar trend to compressive strength, with columns featuring 0% replacement achieving maximum load-carrying capacity and a decrease observed with 100% replacement. Table 2.1 illustrates the decrease in load carrying capacity of the column as the replacement ration increases.

Table 2.1: Summary of Average Test Results Asad-ur-Rehman Khan (2019)

Replacement Ratio of RA	Loads (KN)	Percentage decrease
0%	1167	0
30%	1019	12.68%
50%	950	18.59%
70%	988	15.33%
100%	750	35.73%

2.4 REINFORCED CONCRETE COLUMNS UTILIZING STEEL FIBER AND RECYCLED AGGREGATE.

Paultre et al. (2010) tested large-scale square columns of high-strength concrete (HSC) reinforced with steel fibers under concentric compression loads. The study aimed to examine the effects of the steel fiber volumetric ratio on the behavior of these columns under axial compression. Additionally, the joint impact of the transverse steel reinforcement and steel fibers on the confinement was investigated. Results showed that adding discrete fibers to HSC mixtures in reinforced concrete columns improved the strength and the ductility while reducing premature spalling of the concrete cover.

Gao et al. (2021) evaluated thirteen concentrically loaded steel fiber reinforced recycled aggregate concrete short column specimens with slenderness ratio of 8.3 and height of 500 mm to examine the impact of stirrup spacing, recycled aggregate replacement ratio, and steel fiber volume fraction on the compression performance. Later presented an experimental and analytical investigation on recycled aggregate concrete columns reinforced with steel fibers under axial compression. Results indicated that steel fibers and stirrups enhance the strength and ductility of these columns, while RA had a negligible impact. Steel fibers improved the mechanical properties of the concrete and controlled cover spalling. Additionally, the combined effect of steel fibers and RA on column strength was quantified, and an equation for predicting the replacement effect of steel fibers on stirrups was proposed. It was found that 1% steel fibers could fully replace NA with RA and substitute 34–56% of transverse stirrups. Figure 2.1 illustrates the waste concrete cubes used to produce recycled aggregate and the jaw crusher used for crushing the concrete into recycled aggregate.

Figure 2.1 Waste concrete blocks (Right) and jaw crusher (left) Gao et al. (2021)

Nematzadeh et al. (2021) fabricated eighteen reinforced concrete columns, utilizing both plain concrete and fiber-reinforced concrete, with and without confinement using CFRP sheets. The columns had length-to-width ratios (L/h) of 4.2 and 8.3, and load eccentricity ratios (e/h) of 0.29, 0.46, and 0.63. They were subjected to testing under eccentric compressive loading. The results revealed that CFRP sheets enhanced the loading strength of the RC columns. The presence of steel fibers had minimal impact on the strength capacity of RC columns, with or without CFRP wrapping. Moreover, with the increase in the eccentricity from e/h = 0.29 to e/h = 0.46 and then e/h = 0.63, the slender column strength decreased significantly (by approximately 30–65%). This reduction wasn't notably compensated by CFRP wrapping and steel fibers. Additionally, the increase in the eccentricity led to a higher ultimate deflection for all RC columns, regardless of the wrapping. As the column length decreased, the ultimate loading capacity increased, especially pronounced for higher eccentricities. At e/h = 0.46 and e/h = 0.63, the ultimate loading capacity experienced an increase of 10–25% and 40–50%, respectively, relative to the slender columns.

Ragab and Eisa (2015) conducted an experimental study to assess the incorporation of steel fibers in high-strength self-consolidating concrete (SFRHSCC) reinforced with Glass Fiber Reinforced Polymers (GFRP) bars in both longitudinal and transverse directions. All columns were tested under concentric axial compressive loads. Seven square columns in three groups were tested. Group one served as the reference and consisted of two columns: group one columns poured with conventional concrete. Group two consisted of two columns cast with self-consolidating concrete, one with no addition of steel fibers (volume fraction of 0.0%) and the other column with addition of 0.75% of steel fibers, both reinforced with GFRP bars. Group three included three columns cast with high-strength self-consolidating concrete, featuring steel fibers volume fractions of 0.0% (none), 0.75%, and 1.5%, all reinforced with GFRP bars. The study revealed that the incorporation of steel fibers in high-strength self-consolidating concrete (SFRHSCC) enhanced ultimate load capacity, cover spalling load, ductility, and energy absorption capacity. However, it was shown that the compressive strength was lowered when steel fibers were added to the SCC or HSCC, suggesting a caution in their use within concrete columns. Experimental results were compared to the axial compression design loads provided by ACI 318-11 Building Code and Canadian Standards Association's Standard S806-02 (CSA S806-02). It was concluded that the experimental results aligned better with those calculated by CSA S806-02 rather than those from the ACI Code.

Tokgoz et al. (2012) fabricated a total of 32 square-section specimens with steel fiber volume fractions ranging from 0% to 1.0% to investigate the influence of steel fibers on column behavior. These specimens consisted of both reinforced concrete and composite columns. The experimental behavior

of the composite columns was assessed under conditions nearly identical to those of the reinforced concrete columns. The results indicated that the addition of steel fibers, within the range of 0.75% to 1.0% volume percentage, notably enhanced the confinement and ductility properties of the high-strength reinforced concrete and composite columns. Furthermore, steel fibers effectively prevent the crushing of the concrete core, spalling of the cover, and buckling of reinforcing bars. Additionally, the buckling in both types of reinforced concrete is mitigated by the presence of steel fibers.

Al-Taan and AlDoski (2020) investigated the influence of steel fiber weight on the behavior of reinforced high-strength concrete columns by subjecting twenty square columns, measuring 125 x 125 x 710 mm, to concentric and eccentric compression loads. Each column was reinforced with steel ties spaced 64 millimeters apart and four 10 mm diameter steel bars serving as longitudinal reinforcement. The experimental variables included the steel fibers of (0%, 1.2%, 2.4%, and 3.6%), The amount of steel fiber in the concrete mix was determined by calculating its volume as a percentage of the total concrete volume and then converting this volume to weight using the density of the steel fiber, and eccentricity values (0, 16, 32, 48, and 64 mm). The test results demonstrated that incorporating steel fibers into high-strength concrete mixes in reinforced concrete columns enhanced the strength of both eccentrically and axially loaded columns while also delaying an early spalling of the concrete cover. At the same load level, the inclusion of steel fibers reduced the stresses both in the steel and the concrete.

2.5 STRUCTURAL PROPERTIES FOR RECYCLED AGGREGATE CONCRETE.

Malešev et al. (2010) provided a comparison of experimental findings on the properties of fresh and cured concrete, focusing on different ratios of natural to recycled coarse aggregate replacement. The recycled aggregate was obtained by crushing leftover concrete from precast columns and laboratory test cubes. Three concrete mixtures were tested: one composed entirely of natural aggregate serving as the control (R0), and two incorporating natural fine aggregate with varying levels of recycled coarse aggregate replacement ratios of 50% and 100%, (R50 and R100). Ninety-nine specimens were produced to assess the fundamental characteristics of hardened concrete. Table 2.2 displays the results of the test as well as the standard deviation from mean. Recycled aggregate concrete demonstrated satisfactory performance across all replacement ratios, showing minimal deviation from the performance of control concrete.

Table 2.2: Concrete compressive strength at different ages. Malešev et al. (2010).

	Concrete age (days)			Standard deviation
Concrete Type	2	7	28	(MPa)
R0 (MPa)	27.55	35.23	43.44	1.577
R50 (MPa)	25.74	37.14	45.22	1.209
R 100 (Mpa)	25.48	37.05	45.66	3.502

Recycled Concrete Aggregates consist primarily of two distinct components: natural aggregate and adhering mortar. Consequently, RCAs often exhibit a considerable level of heterogeneity compared to their natural counterparts, in another word, recycled concrete aggregate vary more in composition and

properties than natural aggregate. This variability poses challenges to the RCA reutilization in concrete, as it introduces uncertainties regarding their performance. To identify the impact of the attached paste volume on the RCA characteristics, a unique methodology was used wherein RCA from a single source was segregated using a water jig which is a specialized apparatus based on particle density. This innovative approach mitigates potential confounding factors in data analysis, such as variations in paste or natural aggregate properties commonly encountered in the literature that aggregate RCA from diverse sources. The RCA utilized in the study comprised of a specific granular fraction (10–14 mm). Following the sorting process, the segregated RCA subjected to a comprehensive characterization, encompassing density measurement, water absorption analysis, particle size distribution assessment, evaluation of particle morphology, and determination of adhered mortar content. The findings revealed considerable disparities in density and water absorption, even within a narrow granular fraction, attributable to variations in the content of adhered mortar within the RCA Mazhoud et al. (2022).

Ozbakkaloglu et al. (2018) examined the mechanical and durability characteristics of concretes incorporating recycled aggregates of varying sizes and proportions. Fourteen batches of Recycled Aggregate Concrete (RACs) were produced and subjected to comprehensive testing, including assessments of compressive strength, elastic modulus, flexural strength, splitting tensile strength, workability, drying shrinkage, and water absorption. The study investigated how factors such as the ratio of recycled aggregate replacement, coarse aggregate size, and mixing method influenced the properties of the concrete. Contrary to common belief, the findings suggested that compressive strength alone does not determine the mechanical and durability attributes of

RACs. Instead, the size and proportion of coarse aggregates play a significant role in determining the properties of RAC mixes with similar compressive strengths.

2.6 DUCTILITY OF STRUCTURAL MEMBERS USING RECYCLED AGGREGATE.

Zhang et al. (2023) Conducted and experimental investigations to assess the ductile performance of concrete columns reinforced with high-strength steel under eccentric compression. Numerical models were constructed and validated for reliability. Utilizing these models, a parameter analysis was conducted, examining eccentricity, concrete strength, and reinforcement ratio to systematically explore the ductility of concrete column sections reinforced with high-strength steel. The findings indicated that under eccentric compression, the ductility of the section increased with the increase of the concrete strength and eccentricity. Moreover, the failure modes observed in concrete columns reinforced with high-strength steel under eccentric loading resembled those observed in reinforced columns with steel bars. The yield curvature was determined using load-displacement curve.

Sezen and Moehle (2004) conducted tests on four full-scale reinforced concrete columns subjected to constant and varying axial loads, as well as cyclic lateral loads. These columns, with nominally identical properties, featured design details typical of low seismic regions. Designed to experience significant stiffness and strength degradation from shear failure after flexural yielding, the study examined deformations from flexure, longitudinal bar slip,

and shear. All columns experienced shear failure, though the failure modes varied with axial and lateral loading histories. Significant lateral displacements were observed from flexure, bar slip, and shear, with bar slip and shear deformations notably affecting total displacement. A shear strength model was also proposed, incorporating the effects of transverse reinforcement and concrete, and addressing shear strength degradation through a factor related to displacement ductility.

Samani et al. (2015) reviewed the ductility index for reinforced concrete columns and utilized an analytical model to predict the ductility of various practical columns designed according to the Australian Concrete Standard. The parametric study revealed that columns detailed per the standard may not achieve the ductility index assumed by the code. Additionally, premature spalling of cover concrete is a noted issue in high-strength concrete columns. The Australian Concrete Standard addresses this by applying a reduction factor to the concrete strength when calculating the squash load. However, the study finds that this reduction factor, intended to cover multiple issues, is too conservative, especially for large columns with a small cover-to-core ratio. The code equations for typical reinforced concrete columns are also found to be overly conservative, suggesting a need for updates to incorporate core confinement, which can be crucial in determining the squash load.

Wang et al. (2004) conducted experimental study for 16 composite columns. They investigated the strength and ductility of composite columns subjected to axial compressive loads. The main test parameters were the concrete strength, the confinement index, the structural steel index, and the length-to-diameter ratio. The results showed that composite columns had very high

strength, ductility, and capacity for energy absorption because of the interaction between the steel tube, steel section, and concrete.

2.7 ECCENTRICALLY LOADED COLUMNS

Li et al. (2021) conducted compression tests with varying eccentricities on six reinforced high-ductility concrete (R/HDC) columns, highly ductile fiber–reinforced concrete (HDC) is characterized by a tensile strain–hardening behavior and high compressive toughness, which is expected to alleviate the cracking and durability problems induced by the brittleness of high–strength concrete (HSC), and two reinforced high-strength concrete (R/HSC) columns. The geometric and steel details illustrated in Figure 2.2. The study included crack patterns, failure modes, lateral deflection curves, load-displacement curves, and concrete and rebar strains. The findings demonstrated that R/HDC columns exhibited superior failure modes and crack patterns compared to HSC columns. A productive interaction between HDC and rebar notably enhanced the longitudinal rebar utilization. Additionally, a calculation method for R/HDC column bearing capacity was proposed, showing good agreement with the experimental results. P-M interaction diagrams of R/HDC columns computed and plotted. Furthermore, parametric analysis explored the impacts of HDC compressive and tensile strengths, reinforcement strength, and longitudinal reinforcement ratio on R/HDC column bearing capacity. The results suggested that high tensile strain ensures efficient utilization of HDC's tensile strength.

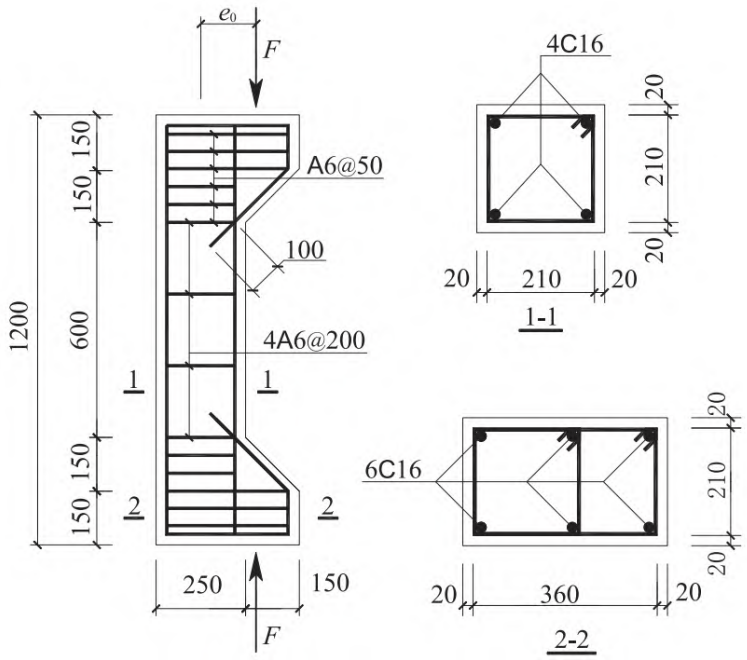

Figure 2.2. Cross-section and reinforcement details of specimens Li et al. (2021)

Li et al. (2019) conducted an experimental study on the large eccentric compression behavior of eight steel fiber reinforced concrete with recycled aggregate (SFRC-RA) columns. The columns, illustrated in Figure 2.3, had cross-sections of 150 mm × 300 mm and a length of 2.0 m, with an initial eccentricity (e0) of 200 mm. The primary variables were the strength of the SFRC-RA and the volume fraction of the steel fiber. The ultimate loads of the SFRC-RA columns under large eccentric compression were determined, considering second-order effects.

Throughout the loading process up to the ultimate state, the plane section of the SFRC-RA columns remained unchanged. However, failure occurred near the mid-height of the columns, indicated by vertical macroscopic cracks in the SFRC-RA compressive zone. The higher load-bearing capacity after reaching the ultimate load led to superior ductility in the SFRC-RA columns, which exhibited significant lateral displacement. There is a direct correlation between the tensile strength of SFRC-RA and the reduction in cracking of

SFRC-RA columns. For reinforced SFRC-RA columns, the appropriate tensile strength of SFRC-RA was substituted in the calculations for reinforced conventional concrete columns. Steel fiber presence led to a decrease in the crack spacing due to the uniform distribution of SFRC-RA strains, and reduced crack width owing to lower tensile stress in the longitudinal steel bars. Predictive formulas for crack spacing, average crack width, and maximum crack width was proposed based on bond stress-slip theory and principles linking reinforced conventional concrete columns. The bearing capacity of the test columns is significantly influenced by the strength of the SFRC-RA, with additional benefits provided by the steel fibers. Recommended formulas for the axial force at the bearing capacity state were proposed. The satisfactory accuracy of these predictions regarding key design characteristics highlights the suitability of SFRC-RA for structural applications.

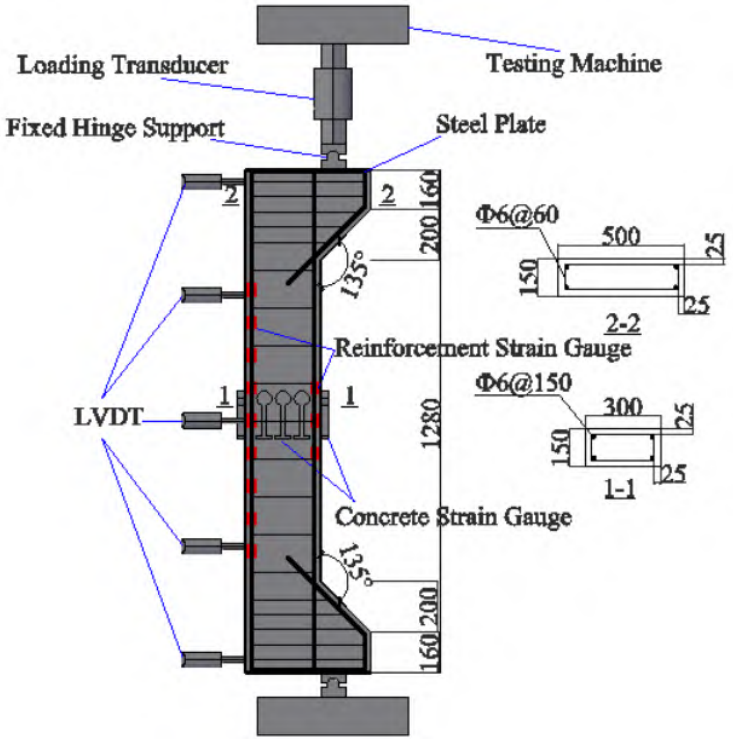

Figure 2.3: The details of the specimens Li et al. (2019)

2.8 REINFORCED CONCRETE SLENDER COLUMNS

El-Gohary (2005) conducted eccentric compression tests on fifteen columns. Each specimen had a cross-section of 10 cm × 20 cm and varied lengths to achieve different slenderness ratios. The lengths were 2.5 m, 3.0 m, and 3.5 m, corresponding to slenderness ratios of 25, 30, and 35, respectively. The ratio of 25 was chosen to comply with code limits, 30 represented the code limit, and 35 exceeded it. The columns were reinforced with four longitudinal bars of 10 mm diameter and rectangular lateral ties made of 6 mm diameter plain bars spaced at 10 mm intervals. The ties were placed 5 cm from both ends of the specimens over a distance of 30 cm to prevent end failure. Additionally, bolted steel end caps were used to confine the ends. The test specimens were cast horizontally in timber molds in the laboratory, removed after 24 hours, and cured for 28 days before testing. The dimensions of the test specimens are illustrated in Figure 2.4. The study focused on concrete strength, slenderness ratio, and imposed load's first time eccentricity as the primary factors. Their influence on failure load and specimen deformation was examined. The failure mode of normal-strength concrete columns varied depending on initial eccentricity and slenderness ratio. For small eccentricities and lower slenderness ratios, concrete compressive strength determined the failure. Conversely, for larger slenderness ratios and equivalent eccentricities, failure was controlled by the yielding of steel bars on the tension side.

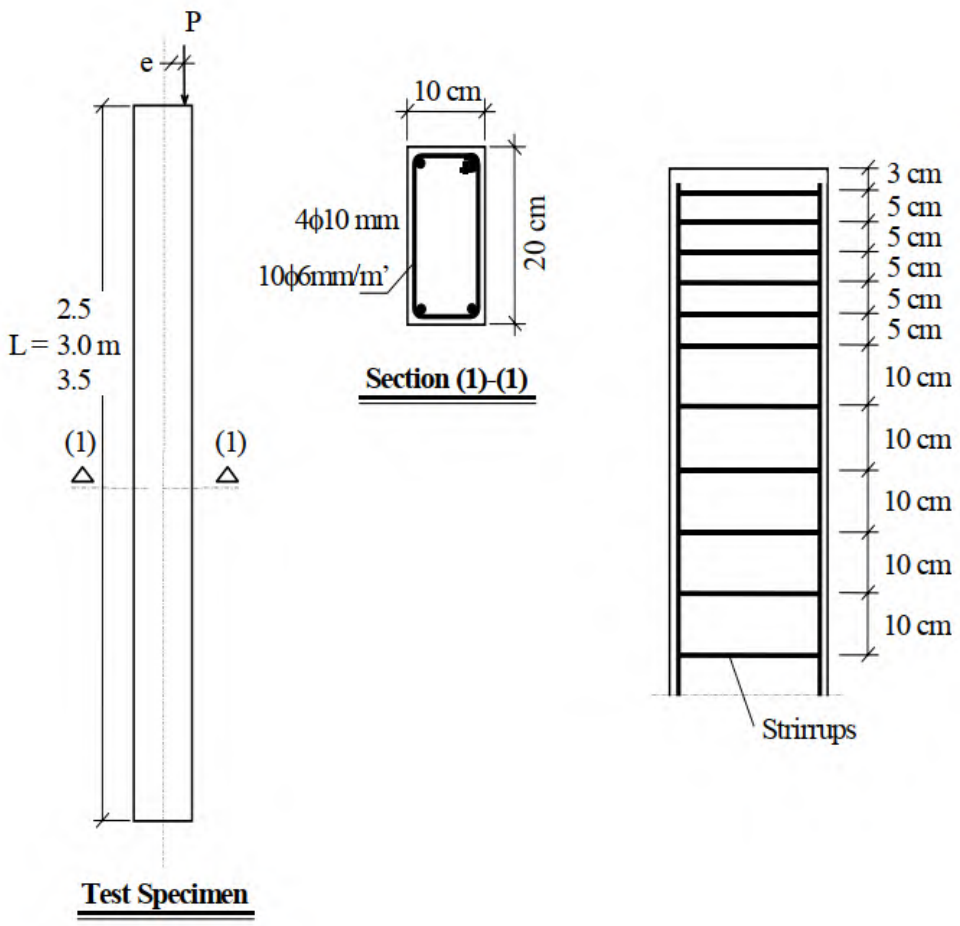

Figure 2.4: Details of test specimens El-Gohary (2005)

Ren et al. (2021) examined the impacts of various factors, including FRP confinement level, load eccentricity, column height, and the replacement ratio of recycled coarse aggregate (RCA), on the second-order bending moment and ultimate load-carrying capacity. Nine column specimens were subjected to eccentric load tests, considering the replacement ratio of RCA, the thickness of the GFRP tube, load eccentricity, and column height. The results indicated that the replacement ratio of RCA had minimal effect on the buckling behavior of slender columns, except for its influence on the ultimate load-carrying capacity, which was primarily governed by load eccentricity.

2.9 SIZE EFFECT IN AXIALLY LOADED REINFORCED CONCRETE COLUMNS

Şener et al. (2004) conducted a study investigating the size effect on axially loaded reinforced concrete columns. The specimens included pin-ended concrete columns of different sizes, maintaining geometric similarities to have a scale of 1:2:4. This resulted in slenderness ratios of 9.7, 18.0, and 34.7. The columns had square cross-sections with side lengths of 50 mm, 100 mm, and 200 mm, and lengths ranging from 0.14 m to 2.08 m. The observations revealed that irrespective of slenderness ratios, failure loads exhibited a size effect wherein the nominal stress at maximum load (failure load divided by cross-sectional area) decreased with the increase in the column size. This contradicts current design codes, indicating that failure is governed by fracture mechanics. Imperfections introduced by the loading arrangement were analyzed using the South well plot method (The South well plot method is a technique used to analyze imperfections introduced by loading arrangements in structural testing), demonstrating that larger columns exhibited greater imperfections. Imperfection could have been deviations or irregularities in the columns due to the loading arrangement and experimental setup, such as geometric misalignments or uneven load application, which can impact column behavior and test results. The columns were simply supported at both ends, and the axial load (P) was applied. Spherical seating supports were used to minimize the eccentricity of loading, ensuring axial application of the imposed load. Test specimens (Figure 2.5) were reinforced concrete columns with square cross sections. The maximum column length for each size was determined by the available space in the testing machine. Consequently, effective lengths corresponding to the smallest cross-section were 145, 270, and 520 mm; for the middle section size, they were 290, 540, and 1,040 mm;

and for the largest cross-section, they were 580, 1,080, and 2,080 mm. Columns within each slenderness ratio group exhibited geometric similarity despite varying in size. Table 2.3 displays the result and the effect of slenderness ratio.

Table 2.3: Measured Axial Peak Load P and Calculated Nominal Stress $\sigma_N = P/D^2$ for Various Column Slenderness λ and Cross Section Sizes D. Şener et al. (2004)

Column number	D (mm)	L (m)	λ	P (kN)	σ_N (N/mm^2)
RS1	50	0.52	34.7	98	39.2
RS2	50	0.52	34.7	104	41.6
RS3	50	0.52	34.7	107	42.8
RS4	50	0.27	18.0	110	44.0
RS5	50	0.27	18.0	101	40.4
RS6	50	0.27	18.0	106	42.4
RS7	50	0.145	9.7	85	34.0
RS8	50	0.145	9.7	76	30.4
RS9	50	0.145	9.7	88	35.2
RM1	100	1.04	34.7	400	40.0
RM2	100	1.04	34.7	383	38.3
RM3	100	1.04	34.7	398	39.8
RM4	100	0.54	18.0	366	36.6
RM5	100	0.54	18.0	371	37.1
RM6	100	0.54	18.0	405	40.5
RM7	100	0.29	9.7	322	32.2
RM8	100	0.29	9.7	379	37.9
RM9	100	0.29	9.7	354	35.4
RL1	200	2.08	34.7	1,248	31.0
RL2	200	2.08	34.7	1,308	32.7
RL3	200	2.08	34.7	1,315	32.9
RL4	200	1.04	18.0	1,306	32.7
RL5	200	1.04	18.0	1,296	32.4
RL6	200	1.04	18.0	1,411	35.3
RL7	200	0.58	9.7	1,290	32.3
RL8	200	0.58	9.7	1,263	31.6
RL9	200	0.58	9.7	1,288	32.2

Note: R indicates a reinforced concrete column; S, M, and L indicate small, middle, and large cross sections respectively; and 1→3, 4→6, and 7→9 indicate high, middle, and low slenderness ratios, respectively.

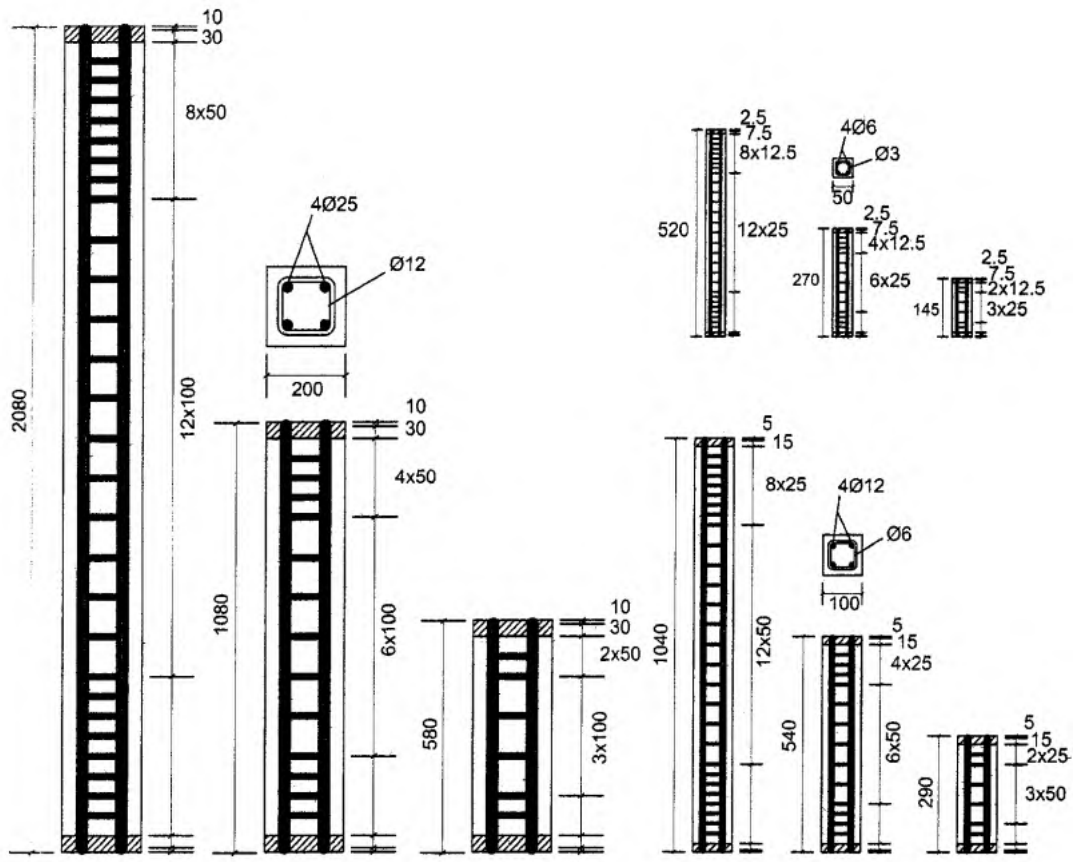

Figure 2.5: Test columns for different sizes (mm) Şener et al. (2004)

The findings illustrated the size effect observed in reinforced concrete columns, a phenomenon explained by fracture mechanics. These findings are consistent with the size effect law proposed by Bazant (1998). As the slenderness of the column increases, the magnitude of the size effect intensifies, leading to higher brittleness numbers. Higher brittleness numbers refer to a measure of how susceptible a column is to brittle failure as its size increases. Moreover, high slenderness columns exhibit more localized failure compared to their smaller counterparts. The imperfections in the testing setup were particularly significant, especially for the larger specimens utilized in the study.

Xu (2016) investigated the size effect in eccentrically loaded columns and examined how transverse reinforcement confinement impacts this effect. The study involved conducting a series of eccentric compression tests on 24 high-strength reinforced concrete (RC) columns, all geometrically similar but varying in size. The columns were scaled in a 1:2:4 ratio, with a constant slenderness ratio of 4.5. The study tested different eccentricities, with two values (e/h of 0.6 for large and 0.25 for small eccentricities) and two configurations of transverse reinforcement: columns with and without mid-length stirrups.

The columns had square cross-sections, ranging in width from 200 mm to 800 mm and in length from 900 mm to 3600 mm. The study analyzed the columns' behavior, including failure patterns, stress-strain relationships, ductility, nominal strength, and post-peak performance. Results confirmed a size effect in both large and small eccentrically loaded RC columns. Transverse reinforcement affected failure patterns, improved nominal strengths, and reduced brittleness in post-peak behavior. Columns without mid-length stirrups showed a more pronounced size effect and increased brittleness compared to those with stirrups. The nominal strengths observed aligned well with Bazˇant's proposed 'size effect law (SEL) Bažant et al. (2003) . Concrete cover thicknesses of 15 mm, 30 mm, and 60 mm were used for RC specimens with structural sizes of 200 mm, 400 mm, and 800 mm, respectively. Geometric similarity was maintained, including the dimensions and placement of steel rebar and stirrup diameters, scaled proportionally. Stirrup spacing was not considered significant for column strength in this study. Details are illustrated in Fig. 2.6.

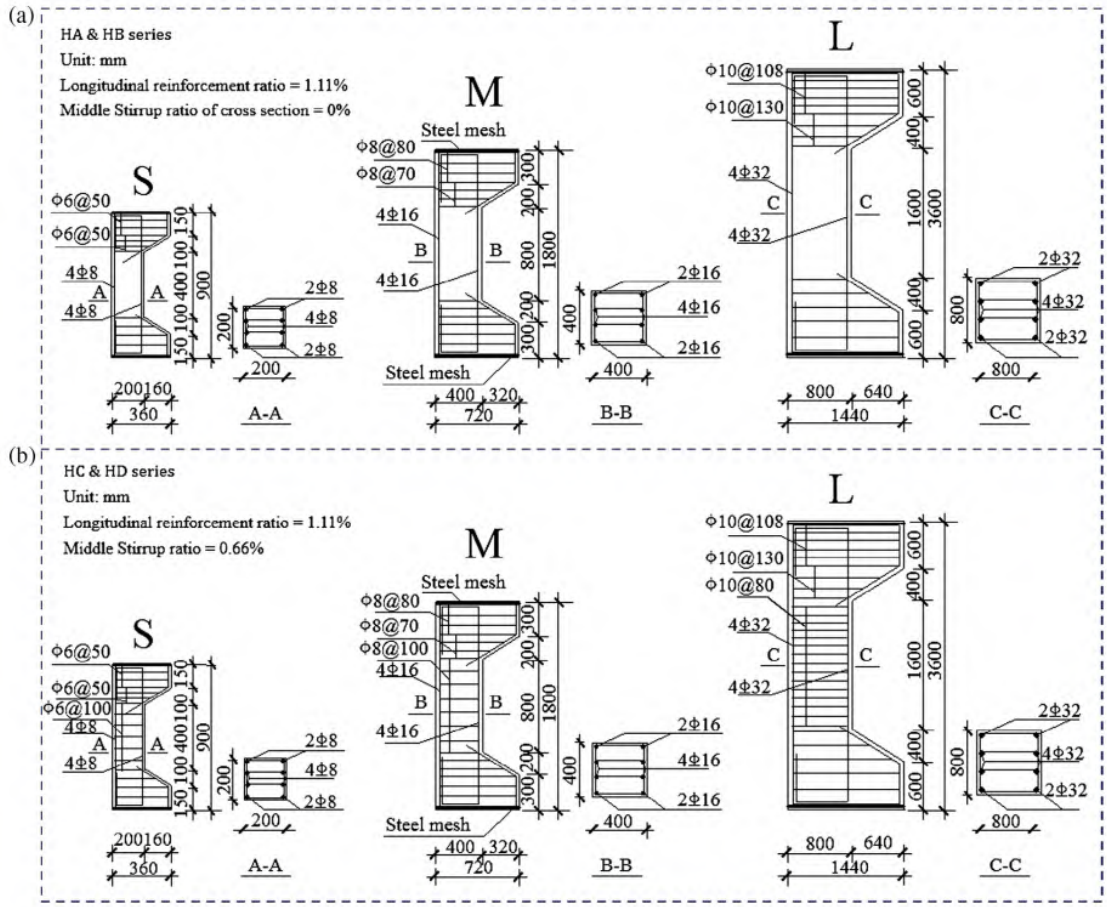

Figure 2.6. Details of the tested samples (Xu, 2016)

a. HA Series: without stirrups in the middle part of the RC columns.
b. HB Series: having middle stirrups with the stirrup ratio of 0.66%.

2.10 SUMMARY

• Most previous studies have focused on short columns using natural aggregate. In contrast, this study stands out by examining a broad range of variables and parameters within a single research framework.

• While most research on concrete columns has concentrated on short columns, this study aims to compare columns of varying heights, from short to slender.

• Previous research has typically investigated either concentrically or eccentrically loaded columns. This study, however, combines both loading types to assess their effects on columns.

• Research on columns made with recycled aggregate and steel fiber is limited. This study explores the performance of columns incorporating both recycled aggregate and steel fiber and compares them with columns made from natural aggregate.

• Research on the height effect of columns is scarce. This study will provide valuable insights by comparing columns of different heights.

• The literature review highlighted conflicting results regarding the behavior of recycled aggregate concrete. Further advanced research is needed to fully understand the structural behavior of reinforced concrete elements made with recycled coarse aggregate.

CHAPTER THREE

EXPERIMENTAL PROGRAM

CHAPTER THREE
EXPERIMENTAL PROGRAM

3.1 INTRODUCTION

This chapter outlines the preparation of materials including recycled aggregate, natural aggregate, fine aggregate, cement, steel reinforcement, strain gauges, and steel fiber. It involves studying the properties of these materials and comparing them to relevant standard specifications. Additionally, it introduces the tools and instruments utilized for preparing samples and conducting tests.

This chapter provides comprehensive insights into all practical activities conducted within and around the laboratory. The research program consisted of two primary components. The first part involved experimental work and testing, while the second part focused on presenting the results, comparing the effects of various variables in the tests, and comparison of the findings with suggested code analytical results, modified code equations, theoretical models, and proposed models discussed in subsequent chapters.

The experimental program was designed and executed to demonstrate the performance of reinforced concrete columns made with recycled coarse aggregate compared to those using natural aggregate. The study covered the behavior of columns with varying slenderness ratios. Samples were subjected to different eccentricity levels: concentric loading (e/h = 0), eccentric loading at e/h = 0.5, and high eccentric loading at e/h = 1.0. Additionally, the investigation explored the impact of steel fiber on columns with recycled and natural aggregate, considering both short and slender columns, as well as those loaded concentrically and eccentrically.

In this investigation, forty-two columns were produced and categorized into three categories. The first category was assigned to testing short columns, whose specimen names start with the letter (S), the second category focused on testing moderately slender columns whose specimen names start with the letter (T), and the third category was allocated to testing highly slender columns and the specimen names start with the letter (L). Each group comprised of columns loaded under both concentric and eccentric conditions, fabricated using both natural and recycled aggregates and with variations in the presence of steel fiber content.

3.2 MATERIALS

3.2.1 Cement

This research utilized Ordinary Portland cement. Table 3.1 presents the physical properties of the cement. Table 3.2 outlines its chemical compositions. The test results are following the specifications outlined in ASTM-C150/150M (2022)

Table 3.1 Physical properties of the cement (manufacturer)

Physical properties	Results	ASTM-C150 (2022)
Initial setting time	134 min.	Not less than 45 min.
Final setting time	169 min.	Not more than 375 min.
Three-day compressive strength	30.8 MPa	Not less than 12 MPa
Seven-day compressive strength	40.9 MPa	Not less than 19 MPa
Cement Modulus of Fineness cm^2/g	3471	Not less than 1600

3.2.2 Fine Aggregate

The study uses fine aggregate sourced from a nearby quarry. Table 3.3 details the particle size distribution of this fine aggregate and compares it against the ASTM standards ASTM-C33/C33M-18 (2018) for gradation. The analysis confirms compliance with the specified ASTM requirements. Figure 3.1 displays the fine aggregate particle size distribution.

Table 3.2 Chemical compositions of the cement (manufacturer)

Chemical compositions	Results	ASTM-C150 (2022)
Loss on ignition (%)	2.14	3.0%, Max.
Insoluble Materials (%)	0.43	1.5%, Max.
Al2O3 (%)	4%	
Fe2O3 (%)	4.50%	
MgO (%)	2.15%	6.0%, Max.
SO3 (%)	2.32%	3%, Max.
C3A (%)	0.88%	
Chloride	0.07	<0.1

Table 3.3 Grading of fine aggregate (Sand)

Sieve size (mm)	% Passing	Lower and upper limits of ASTM-C33,(2018)
9.52	100	100
4.75	99	95-100
2.36	82	80-100
1.18	65	50-85
0.6	44	25-60
0.3	12	5-30
0.15	2.2	0-10

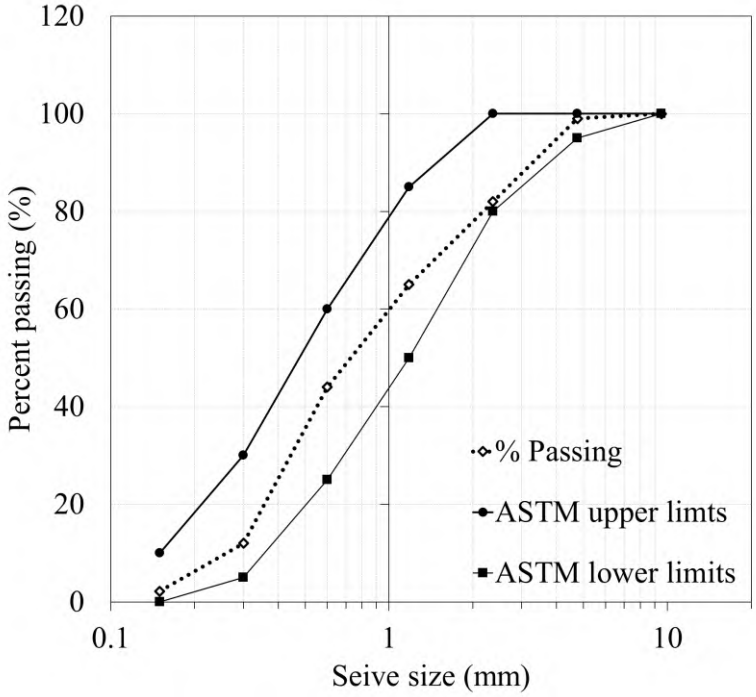

Figure 3.1: Fine aggregate particle size distribution

3.2.3 Natural Coarse Aggregate

The concrete mixes utilize locally obtained natural gravel as the coarse aggregate, with a maximum nominal size of 12.5 mm. Table 3.4 presents the grading values of the coarse aggregate both NA and RA, and compares them with the limits specified in ASTM standards ASTM-C33/C33M-18 (2018). The results demonstrate compliance with the ASTM-C33/C33M-18 (2018) requirements for particle size distribution. Figure 3.2 shows the particle size distribution and for both NA and RA.

3.2.4 Recycled Coarse Aggregate

The recycled aggregate is made from laboratory waste tested concrete cubes and cylinders, with a maximum particle size of 12.5 mm. Figure 3.3 shows

the process of preparation of the recycled aggregate. The RA with mostly mortar attached to its surface was observed. The results of sieve analysis were satisfactory to ASTM-C33/C33M-18 (2018) as shown earlier in Figure 3.2. Table 3.5 shows the physical properties of the coarse aggregate, where it was observed that the RA had much higher water absorption. The coarse aggregate, NA, and RA are shown in Figure 3.4 for comparison.

Table 3.4 Grading of coarse aggregate

Sieve size (mm)	% Passing NA	% Passing RA	Lower and upper limits of ASTM-C33,(2018)
12.5	100	100	100
9.5	96	98	90-100
4.75	52	58	40-70
2.36	0.1	1	0-15
1.18	0	0	0-5

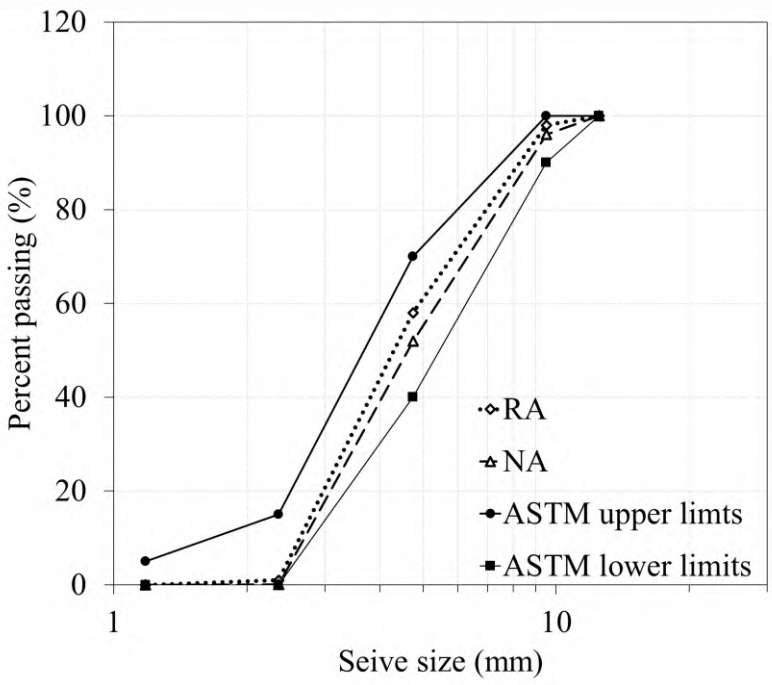

Figure 3.2: Coarse aggregate particle size distribution

(a) Collecting waste concrete

(b) Crushing of concrete

(C) Sorting recycled aggregate

(d) Collecting then washing RA

Figure 3.3: The process of preparing recycled aggregate in a local quarry.

(a) (b)

Figure 3.4: Coarse aggregate: (a) NA; (b) RA

Table 3.5: Physical properties of the coarse aggregate.

Aggregate Type	Apparent Density (kg/m^3)	Bulk Density (kg/m^3)	specific gravity (SSD)	Water Absorption (%)
NA	1591	1463	2.67 (2.68)	0.93
RA	1519	1417	2.55 (2.62)	2.61

3.2.5 Water

The drinking water is utilized in the washing, mixing, and curing processes of concrete samples.

3.2.6 Steel Reinforcement

10 mm diameter deformed steel rebar has been used as the main longitudinal reinforcement, 8 mm diameter deformed rebar as the tie reinforcement, and 12 mm diameter deformed steel rebar for the enlarged ends of the column specimen. Three samples of each rebar size were tested in tension, and the test average results are listed in Table 3.6. All specimens met the requirements outlined in ASTM-A615/A615M (2022).

Table 3.6: Mechanical properties of steel reinforcement (Tested in the EPU lab).

Type	Diameter (mm)	Area (mm^2)	Yield strength f_y (MPa)	Ultimate strength f_u (MPa)	Elongation
Longitudinal	10	78.53	530	762	17%
Ties	8	50.26	487	671	28%

3.2.7 CFRP sheet

The Carbon Fiber Reinforced Polymer (CFRP) sheet used in this study is the Sika Wrap-300C. It is used to reinforce the enlarged ends of the column specimens, mitigating premature failure risks. Sika Wrap®-300 C is a unidirectional woven carbon fiber fabric with moderate strength characteristics, suitable for both dry and wet application methods. Each sheet manufactured by Sika in 50 cm wide and 0.167 mm thick, the sheet was cut to five of 10 cm width sheets to wrap the end of the columns. Refer to Table 3.7 for detailed properties of the CFRP sheet, the specification sheet is in Figure I1 in appendix I. Figure 3.5 shows CFRP sheets cut in 10 cm width to wrap around the head of the column.

Table 3.7: Properties of Sika Wrap-300C (Appendix I)

Tensile strength, (MPa)	3500
Tensile modulus of elasticity, (GPa)	220
Elongation at failure, (%)	1.59
Density g/cm³	1.82

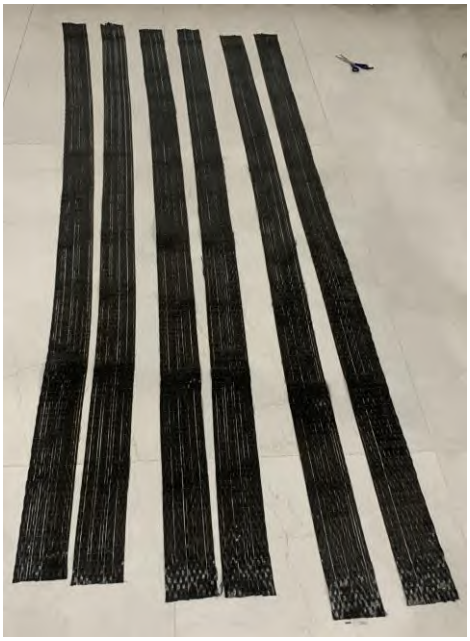

Figure 3.5: 10 cm width CFRP sheets to strengthen column ends

3.2.8 Epoxy

Sikadur-330 epoxy Figure 3.6, was utilized to bond the CFRP sheet of type Sikawrap-300C. Sikadur-330 is a two-part, thixotropic epoxy-based impregnating resin adhesive. Specification sheet is in Figure I2 in appendix I.

Figure 3.6: Sikadur-330 epoxy

3.2.9 Steel Fiber

A short discrete fiber, uniformly distributed and randomly oriented, was used in this experiment. The steel fiber was coated with copper, possessing a diameter of 0.20-0.25 mm and a length of 12-14 mm, with and aspect ratio of 56-60, having a 2850 MPa tensile strength, meeting the specifications outlined in ASTM-A820-01 (2001). A sample of the steel fiber is shown in Figure 3.7. The specification sheet is available in Figure I3 in appendix I.

(a) (b)

Figure 3.7: (a) Steel fiber; (b) Concrete mix with steel fiber distribution.

3.3 COLUMN SPECIMENS DETAIL

This experimental program comprised of forty-two reinforced concrete columns, divided into three categories based on their slenderness ratio. The first category, specimen name starts with the letter (S), consisted of fourteen short columns with a slenderness ratio (kl/r) of 17.24. The second category, specimen name starts with the letter (T), consisted of fourteen slender columns with a slenderness ratio of 26.0. The third category, specimen name

starts with the letter (L), and includes fourteen columns with a slenderness ratio of 34.5. Here, (k) represents the effective length factor, (l) denotes the height of the column, and (r) signifies the radius of gyration, which used in column analysis to predict buckling behavior. Following ACI 318-19 standards, columns with a slenderness ratio exceeding 22 are considered slender. Each column constructed with natural coarse aggregate is paired with an equivalent column made with recycled aggregate for comparative analysis. Columns without steel fiber reinforcement are compared with those containing a 1% steel fiber content. The columns are subjected to axial loading under three different eccentricities: concentric loading (e/h = 0), eccentric loading with e/h = 0.5 (e = 62.5 mm), and eccentric loading with e/h = 1.0 (e = 125 mm). Specimens are identified based on their composition and loading conditions, such as 'S-RA0Vf0E0.0' and 'L-RA100Vf0E0.0', respectively, 'RA0' and 'RA100' represent 100% natural aggregate and 100% recycled aggregate, 'Vf0' indicates without the content of steel fiber, 'Vf1' denotes 1% steel fiber content, and 'E0.0', 'E0.5', and 'E1.0' signify concentric and eccentric loading conditions. Further details are provided in Table 3.8.

The dimensions of the columns, including size and slenderness ratio, were determined by the specifications of the available testing machine in the laboratory. Additionally, the normal strength of concrete was selected based on the testing machine's capacity. The designed cross-section for all columns in this study measures 125 mm x 125 mm, with 25 mm concrete cover. The effective length of the short columns in Series S is 625 mm, with a total length of 1025 mm. slender columns in Series T have an effective length of 937 mm and a total length of 1337 mm, while those in Series L have an effective length of 1250 mm and a total length of 1650 mm.

The reinforcement for all columns kept constant throughout the study. Each column specimen is reinforced with four longitudinal 10 mm diameter steel bars, positioned at the corners of the cross-section, resulting in a reinforcement ratio of 2%. Transverse reinforcement is provided by steel ties of 8 mm diameter, which are spaced at 125 mm intervals, meeting the minimum spacing requirement set by ACI 318-19. 12 mm diameter steel bars used to strengthen the enlarged ends of the columns. The geometry, dimensions, and reinforcement arrangement are illustrated in Figure 3.8. To facilitate eccentric loading, all columns are enlarged at their ends to function as brackets. These enlarged ends are designed to be stronger than the actual height of the column, ensuring that they do not fail prematurely. This design feature results in a larger cross-section and a higher steel reinforcement ratio. Six concrete cylinders of (100 mm x 200 mm) were prepared to measure the concrete compressive strength (f_c') and concrete splitting strength (f_{ct}), three prisms of (100 mm x 100 mm x 400) mm cast to measure flexural strength (f_r), and three cylinders of (150 mm x 300) mm to measure modulus of elasticity (E_c). All of them were accompanied by the columns in the same batch of pouring and curing conditions.

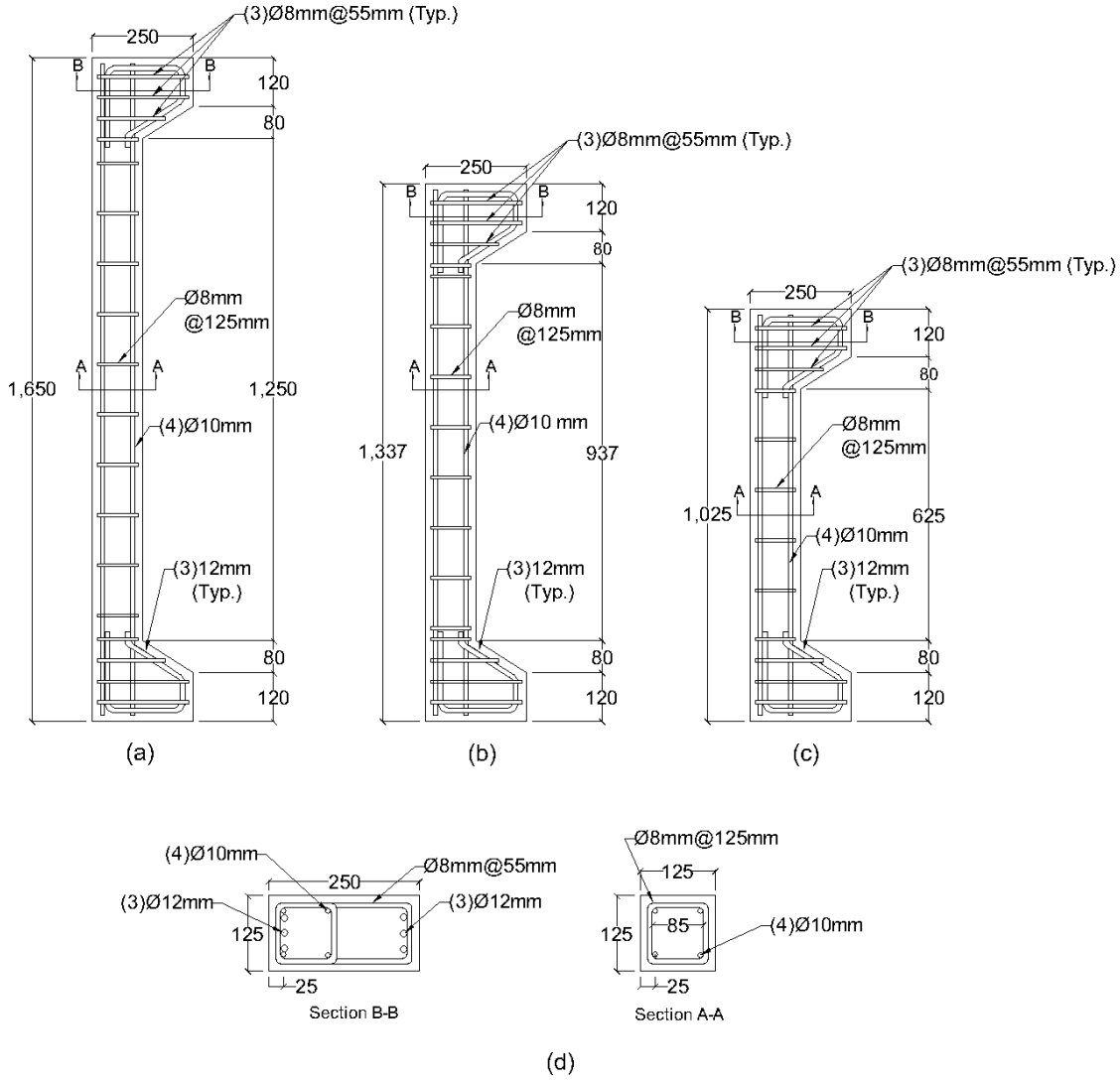

Figure 3.8: Reinforcement details (all dimensions are in mm): (a) Slender column of kl/r=34.5. (b) Slender column of kl/r = 26 (c) short column of kl/r=17.24 (d) cross-sections.

Table 3.8: Details of test specimens.

Specimen ID	kl/r	Vf%	e/h%	RA%
S-RA0Vf0E0	17.24	0	0	0
S-RA50Vf0E0	17.24	0	0	50
S-RA100Vf0E0	17.24	0	0	100
S-RA0Vf1E0	17.24	1	0	0
S-RA50Vf1E0	17.24	1	0	50
S-RA100Vf1E0	17.24	1	0	100
S-RA100Vf0E0.5	17.24	0	50	100
S-RA0Vf0E0.5	17.24	0	50	0
S-RA100Vf1E0.5	17.24	1	50	100
S-RA0-Vf1E0.5	17.24	1	50	0
S-RA100Vf0E1.0	17.24	0	100	100
S-RA0Vf0E1.0	17.24	0	100	0
S-RA100Vf1E1.0	17.24	1	100	100
S-RA0Vf1E1.0	17.24	1	100	0
T-RA0Vf0E0	26	0	0	0
T-RA50Vf0E0	26	0	0	50
T-RA100Vf0E0	26	0	0	100
T-RA0Vf1E0	26	1	0	0
T-RA50Vf1E0	26	1	0	50
T-RA100Vf1E0	26	1	0	100
T-RA100Vf0E0.5	26	0	50	100
T-RA0Vf0E0.5	26	0	50	0
T-RA100Vf1E0.5	26	1	50	100
T-RA0Vf1E0.5	26	1	50	0
T-RA100Vf0E1.0	26	0	100	100
T-RA0Vf0E1.0	26	0	100	0
T-RA100Vf1E1.0	26	1	100	100
T-RA0Vf0E1.0	26	1	100	0
L-RA0Vf0E0	34.5	0	0	0
L-RA50Vf1E0	34.5	0	0	50
L-RA100Vf0E0	34.5	0	0	100
L-RA0Vf1E0	34.5	1	0	0
L-RA50Vf1E0	34.5	1	0	50
L-RA100Vf1E0	34.5	1	0	100
L-RA100Vf0E0.5	34.5	0	50	100
L-RA0Vf0E0.5	34.5	0	50	0
L-RA100Vf1E0.5	34.5	1	50	100
L-RA0Vf1E0.5	34.5	1	50	0
L-RA100Vf0E1.0	34.5	0	100	100
L-RA0Vf0E1.0	34.5	0	100	0
L-RA100Vf1E1.0	34.5	1	100	100
L-RA0Vf1E1.0	34.5	1	100	0

3.4 CONCRETE MIX DETAILS

For this experimental test, a nominal compressive strength rating of 35 MPa was selected. Table 3.9 displays the concrete mix proportions determined through numerous trial mixes conducted in the laboratory by the researcher and consistently utilized throughout the experimental testing. The recycled aggregate replaced the natural aggregate by the same weight. Following ASTM-C127-15 (2015), Figure 3.9, shows both recycled aggregate (RA) and natural aggregate (NA) being washed and then immersed in room temperature water for 24 hours to produce saturated surface dry aggregate before being incorporated into the mixture. Subsequently, the surface moisture of the aggregate was dried using towels. Figure 3.10 illustrates the drying process. At this stage, both types of aggregate became saturated while remaining dry on the surface, which conforms to the definition of the saturated surface dry (SSD) condition. The water absorbed by both types of aggregate was not factored into the water-cement ratio. The same amount water added to the mixtures was sufficient for cement hydration within the concrete mixture

Table 3.9: The ingredients of $1m^3$ of the concrete mix

Material	cement	Natural fine aggregate (Sand)	Natural or recycled coarse aggregate (Gravel)	w	Steel Fiber
Weight (kg)	347	898	1041	166	1% or 0%

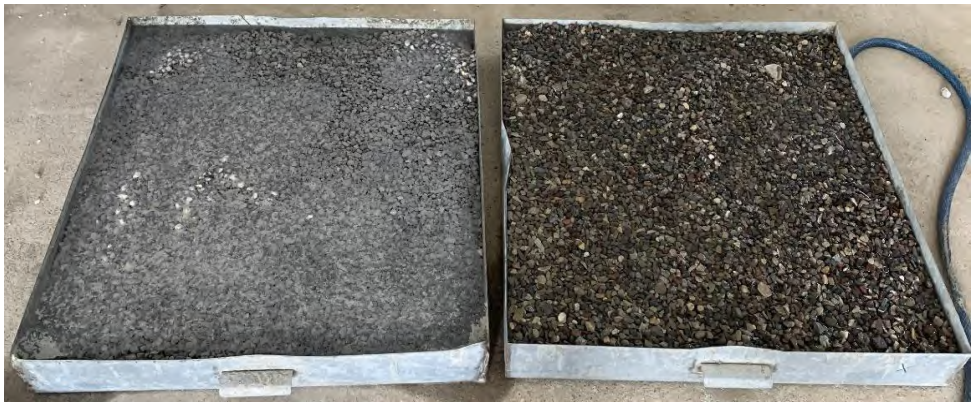

Figure 3.9: Coarse aggregate being submerged in water for 24 hours: RA (left) & NA (right)

Figure 3.10: Coarse aggregate drying process: RA (left) and NA (right)

3.5 SPECIMENS FORMWORKS

High-quality plywood sheets, 18mm thick, were utilized for constructing the formworks, imported and locally available. Molds were fabricated to the required dimensions at a local carpentry factory. Before use, the molds were thoroughly cleaned and treated with oil. Reinforcement cages were then carefully placed within the molds, with special attention given to protecting the wires of the strain cages. Sample images of these molds are depicted in Figure 3.11.

Figure 3.11: Column formworks for casting concrete

3.6 REINFORCEMENT CAGES

The steel reinforcements were cut to the required dimensions and assembled. Plastic spacers were used as concrete cover all around the reinforcement cage. Concrete cover of 25 mm from the edge of the formwork to the center of the steel bars has been provided longitudinally. Before the casting of concrete, the stability of the cages inside the wood molds was confirmed to stay stable during the casting and vibration process. Figure 3.12 shows a sample of the reinforcement cages placed in the wooden formworks and prepared for casting concrete in it.

Figure 3.12: Placement of steel cages within formworks

3.7 CASTING AND CURING

Four distinct concrete mixtures were used, all with the same ratio of materials. Two mixes utilized natural coarse aggregates, one without steel fiber content and the other with steel fiber content. Similarly, two mixes used recycled coarse aggregates, again with one mix lacking steel fiber content and the other including steel fiber. Laboratory temperature and humidity were maintained consistently for all mixes. The concrete was cast horizontally in two layers, with each layer compacted using an electrical vibrator. Control specimens, consisting of six cylinders and three prisms, were cast alongside the column specimens using the same concrete mix. To facilitate curing, the columns and control samples were covered with damp burlap at the laboratory environment, and the moisture of the burlap was maintained for a duration of 28 days, Figure 3.13 displays the process of curing, and Figure 3.14 shows the samples being cured and ready for testing.

Figure 3.13: Curing process for columns and control specimens in room temperature

Figure 3.14: Samples cured and ready for testing

3.8 STRENGTHENING THE ENLARGED HEAD

In order to avoid early damage at the column ends, they were enlarged and strengthened. This involved using larger reinforcement amounts with external confinement using CFRP (Carbon Fiber Reinforced Polymer). Sika Wrap-

300C was applied for confining around the enlargements, with the concentrically loaded columns wrapped with three layers and the eccentrically loaded columns being wrapped with two layers, reflecting the higher loads experienced by the former. The CFRP wrapping serves to prevent bearing failure at the ends. Sikadur-330 epoxy was used to adhere the 10 cm wide wraps to the concrete, facilitating axial load transfer and preventing failure at the column ends. Notably, the load is higher in concentrically loaded columns than in eccentrically loaded ones. Additionally, the surface of the enlarged ends of the columns was roughened by grinding to ensure proper adhesion of the epoxy when CFRP was applied. We ground the edges to remove sharpness, allowing the CFRP to adhere more effectively. Figure 3.15 shows the process of strengthening the enlarged ends of the columns.

(a) (b) (c)

Figure 3.15: Strengthening the columns ends:
(a) preparing the surface (b) CFRP wrapping (c) removing the excess epoxy.

All columns were painted white before testing to facilitate visualizing cracks during the tests (Figure 3.16).

Figure 3.16: The test samples being white painted

3.9 TEST MEAUREMENTS AND INSTUMENTATION

Four cameras were positioned at different angles to capture the loading process up to failure. Additionally, a screen recorder was utilized on the computer to document the data recordings. The computer's data read and recorded using a data recorder.

The load cell, strain gauges, and LVDT were connected to the data logger, which in turn was connected to the computer for recording and saving the readings. Figure 3.17 illustrates the workstation located adjacent to the testing machine. All necessary safety measures were implemented.

Figure 3.17: Equipment setup: computer, and data logger for sample testing

3.9.1 Load Measurement

A computerized compression apparatus with a 2000 kN nominal capacity housed in the laboratory of the Civil Engineering Department at Erbil Polytechnic University's Erbil Technical Engineering College has been used in the current study. The machine was paired with a load cell model (HC-200 t C3), sourced separately, with a capacity matching its nominal capacity of 2000 kN. The load cell was installed on the machine and connected to a data logger, allowing data to be read directly from the computer screen and recorded to the computer. Later the data was converted to an Excel worksheet to be used in the analysis in a later stage. Figure 3.18 displays the sketch of standardized test configuration for loaded column specimens. Figure 3.19 illustrates the column test setup being ready for testing. The laser was used for alignment, Load cell, LVDT, and chains were used for safety, and the crane was used to move the columns. Matching setup was done by Othman and Mohammad (2019).

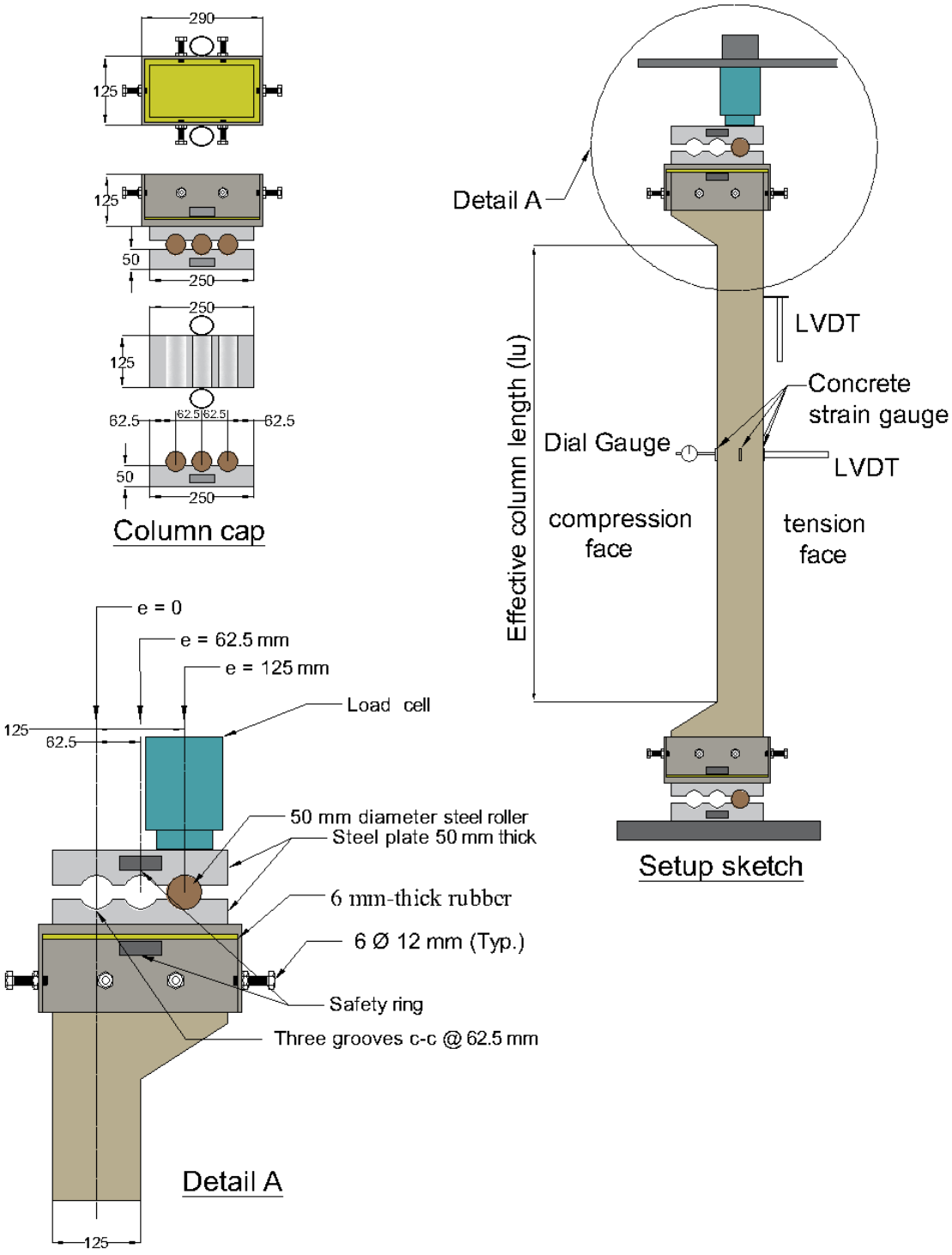

Figure 3.18: Sketch of standardized test configuration for loaded column

Figure 3.19: Standardized test configuration for loaded column specimens

3.9.2 Lateral and Axial Displacement Measurements

Lateral and axial displacements were measured using two Linear Voltage Displacement Transducers (LVDTs). One LVDT, connected to the data logger, was positioned horizontally against the column at mid-height of the sample to measure horizontal displacement, with a maximum allowable travel of 100 mm. Additionally, a dial gauge, optionally placed horizontally on the opposite

side for double checking the results, could be used to measure horizontal displacement, with an accuracy of 0.01 mm and a maximum travel of 30 mm. Second LVDT, connected to the data logger, was installed vertically at two-thirds of the column height to measure vertical displacement.

3.9.3 Concrete Strain

The strain of concrete was measured at the mid-height of the columns. For the concentrically loaded columns, four strain gauges were installed. One strain gauge on each face. For the eccentrically loaded columns, two strain gauges were installed one on the compression face and one on the tension face. The electrical strain gauge used with the model number BX120-80AA, manufactured by OASIS TECHNOLOGY (BEIJING) CO., LTD. The quality certificate is available in Figure I4 in appendix I of this thesis. Strain gauges were tested prior to its use. Figure 3.20 shows the concrete strain gauge being installed, after smoothening and cleaning the surface with proper material and proper method.

Figure 3.20: Concrete strain gauge installed on the column.

3.9.4 Longitudinal Reinforcement Strain

Electrical resistance strain gauges of type BX120-6AA were utilized to measure the strain in the longitudinal reinforcement of the columns. Each column, whether eccentrically or concentrically loaded, was equipped with two strain gauges: one on the compression face and the other on the tension face. However, in the case of concentrically loaded columns, both strain gauges were subjected to compression. These strain gauges are manufactured by OASIS TECHNOLOGY (BEIJING) CO., LTD. Strain gauges were tested prior to its use. Figure 3.21 shows the concrete strain gauge being installed. The quality certificate for this model is available in Figure I5 in appendix I of this thesis.

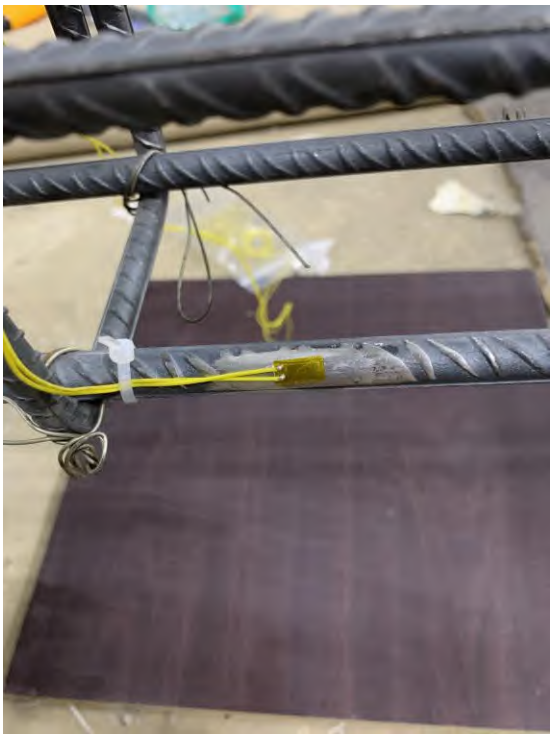

Figure 3.21: Steel strain gauge installed on tension and compression faces bars.

3. 9.5 Loading Cap

The loading caps illustrated in Figure 3.22 were installed at both heads of the columns, functioning as hinges to facilitate loading the sample at e/h=0, e/h=0.5, and e/h=1.0, representing concentric and two different eccentric loading levels. Each set consisted of two plates measuring 250 mm x 125 mm x 50 mm thick. A 6 mm-thick rubber was inserted inside the caps to ensure the load distributed uniformly from the machine to the column. Each plate was grooved with a semi-circular shape along the long side, featuring a diameter of 50 mm. The grooves were centrally positioned at 62.5 mm center to center. A 50 mm diameter roller was placed in the grooves between the upper and lower plates at both ends of the columns. One plate (the upper plate for the lower support) was welded with a 6 mm thickness and a height of 100 mm around its perimeter, forming a box for the column ends to rest in.

Figure 3.22: Pin support and laser used for alignment.

3. 10 TESTING PROCEDURE

The loaded column specimens were tested under axial compressive loading conditions. Two perpendicular lasers were utilized to align the columns in the center of the loading machine. Loading caps were installed at the bottom and top ends of the column to avoid premature failure and ensuring uniform distribution of the applied load across the cross-section.

The strain gauges were connected to the channels of the data logger, recording the strains of concrete and steel reinforcement, while LVDTs were installed and connected to the data logger, recording the vertical and lateral displacements. Initially, a small load was applied to the column, and the LVDT and strain gauge readings were monitored. Once the position of the specimen had been checked, the column was unloaded, and all the readings were set to zero. Subsequently, the load was reapplied at an average rate of 1.0 kN/sec.

During the testing process, the columns were monitored for cracks. The data logger recorded the progress of loads through the audio speaker of the computer, which could be heard in the lab. This auditory feedback assisted in precisely recording the first cracking load for the columns loaded eccentrically, with cracks marked on the tension side of the column as they propagated. Conversely, for concentrically loaded columns, all personnel inside the lab were required to keep a safe distance from the column, as this type of failure was sudden and explosive.

3.11 CONTROL SPECIMEN

The column specimens and their corresponding control specimens were both cast on the same day. After curing, they were both tested on the same day.

3.11.1 Cylinder Compressive Strength

Three cylinders of 100 mm diameter and 200 mm height, were cast for compression strength testing according to ASTM-C39/C39M-21 (2021). Capping was provided prior to the test. The tests were conducted using a Yuksel Kaya Makina hydraulic compression machine with a maximum capacity of 2000 kN. as depicted in Figure 3.23. The process was done under lab staff supervision.

Figure 3.23: Hydraulic compression machine used for the compressive strength

3.11.2 Splitting Tensile Strength

The splitting tensile strength test was conducted on three cylindrical samples, each measuring 200 mm in height and 100 mm in diameter, in accordance with the ASTM-C496-96 (1996) standard. The testing machine provides the required surface to distribute the load equally on the top and bottom line of the cylinder. The process was done under lab staff supervision. Three specimens were tested for each mix using a Yuksel Kaya Makina hydraulic compression machine with a maximum capacity of 2000 kN, as shown in Figure 3.24.

Figure 3.24: Hydraulic compression machine used for splitting tensile strength

3.11.3 Flexural Strength

Three concrete prisms, each measuring 100x100x400 mm, were subjected to two-point loading tests following the ASTM-C78-09 (2009) standard to determine their flexural strength. The tests were performed using a UTEST Hydraulic Compression Machine, as depicted in Figure 3.25. The process was done under lab staff supervision.

Figure 3.25: Hydraulic compression machine used for flexural strength of concrete.

3.11.4 Modulus of Elasticity

Concrete's elasticity modulus was measured by testing three samples for each mix, which were cylindrical with dimensions of 150x300 mm. The tests were conducted using two-ring apparatuses, as shown in Fig. 3.26. The testing procedure followed the (ASTM-C469/C469M-22, 2022) standard. This test measured the stress corresponding to a 0.000050 axial strain and the strain matching to 40% of the maximum load. The process was done under lab staff supervision.

Figure 3.26: Two-ring test apparatus used for measuring concrete modulus of elasticity.

CHAPTER FOUR

EXPERIMENTAL

RESULTS AND DISCUSSION

CHAPTER FOUR
EXPERIMENTAL RESULTS AND DISCUSSION

4.1 INTRODUCTION

The results of the experimental work are presented in this chapter. These results include mechanical properties such as compressive, splitting, and flexural strength. The load-carrying capacity, failure mode, lateral and vertical displacements, concrete and reinforcement strains, and ductility are presented and discussed. Additionally, the effects of the recycled aggregate and steel fiber are analyzed. The impacts of the slenderness ratio and loading at different levels of eccentricity are also examined. For comparison, the verification of strains and lateral displacement is analytically presented and compared with the experimental values.

4.2 MECHANICAL PROPERTIES OF CONCRETE

The following sections present the properties of the concrete used in casting the specimens.

4.2.1 Cylinder Compressive Strength of Concrete

Three concrete cylinders, each with dimensions of 100 x 200 mm, were tested in compression for each column, following ASTM-C39/C39M-21 (2021). The average compressive strength for the control specimens of each column is listed in Table 4.1.

4.2.2 Splitting Tensile Strength of Concrete

The splitting tensile test was performed on three cylinders, each with a diameter of 100 mm and a height of 200 mm, for each column. The test followed ASTM-C496-96 (1996). The average tensile splitting strength for the control specimens of each column is listed in Table 4.1.

4.2.3 Flexural Strength of Concrete

Table 4.1 presents the average results of the prism tests. Prisms measuring 100 x 100 x 400 mm were utilized, with three control specimens for each column tested under two-point loading in accordance with ASTM-C78-09 (2009)

4.2.4 Modulus of Elasticity of Concrete

Concrete cylinders with a diameter of 150 mm and a height of 300 mm were tested according to (ASTM-C469/C469M-22, 2022). This test was conducted to determine the modulus of elasticity. The modulus of elasticity was calculated using Equation 4.1, which is based on the stress corresponding to a 0.000050 axial strain and the strain corresponding to 40% of the ultimate load. The average modulus of elasticity for each column is presented in Table 4.1.

$$E = \frac{(S_2 - S_1)}{(\varepsilon_2 - 0.000050)} \quad \text{---------- (4.1)}$$

E = chord modulus of elasticity, MPa,

S_2 = stress corresponding to 40 % of the ultimate load, MPa

S_1 = stress corresponding to a longitudinal strain, ε_1 of 50 millionths MPa.

ε_2 = longitudinal strain produced by stress *S2*

4.3 FAILURE MODES

4.3.1 Concentrically Loaded Columns (e/h=0)

The concentrically loaded columns exhibited a brittle and sudden failure mode, as shown in Figure 4.1 for columns S-RA0Vf0E0 and S-RA100Vf0E0. The steel reinforcements were visibly exposed and buckled outward at failure, with no rupture in the ties. An unintentional eccentricity accompanied the sudden failure, causing mid-height movement in most samples, though this did not impact the results, as strains continued to increase until failure. The columns made with recycled aggregate demonstrated a similar failure process but in a more fragile manner, likely due to differences in drying shrinkage. Interestingly, these columns generally required higher loads for failure than those with natural aggregate. Although no vertical cracks were visible before failure, recorded videos revealed short, hairy vertical cracks near the corner edges milliseconds before reaching maximum load in most samples.

In all concentrically loaded columns, concrete crushed and steel buckled. The steel fiber helped resist some tension stresses, and even at the final stage of failure, much of the concrete cover contained steel fibers, likely contributing to the bearing capacity, despite some small pieces detaching from the surface. The slenderness ratio did not affect the mode of failure; all concentrically loaded columns failed in compression-controlled mode due to concrete crushing and steel yielding at maximum load, even with recycled aggregate. However, the sound of failure in the columns with steel fiber was dampened compared to those without.

Table 4.1: Mechanical properties of the concrete specimens

Specimen ID	f'_c MPa	f_{ct} MPa	f_r MPa	E_c MPa
S-RA0Vf0E0	35.26	2.90	4.71	31632
S-RA50Vf0E0	35.91	3.08	5.31	32056
S-RA100Vf0E0	38.61	3.15	5.08	32120
T-RA0Vf0E0	35.26	3.23	4.56	31007
T-RA50Vf0E0	36.09	3.37	4.62	32033
T-RA100Vf0E0	36.83	3.31	4.73	33230
L-RA0Vf0E0	35.50	2.97	4.62	30770
L-RA50Vf1E0	33.46	2.79	4.80	31945
L-RA100Vf0E0	37.40	3.05	4.86	32204
S-RA0Vf1E0	36.50	3.49	5.64	33763
S-RA50Vf1E0	35.90	3.47	5.83	33227
S-RA100Vf1E0	38.12	3.60	5.80	34464
T-RA0Vf1E0	35.46	3.46	5.76	31626
T-RA50Vf1E0	36.34	3.58	5.85	32299
T-RA100Vf1E0	37.68	3.64	6.23	33053
L-RA0Vf1E0	35.13	3.28	5.48	31273
L-RA50Vf1E0	33.27	3.15	5.27	30742
L-RA100Vf1E0	36.48	3.47	5.52	32760
S-RA100Vf0E0.5	34.33	2.75	4.31	31621
S-RA0Vf0E0.5	37.45	3.02	4.82	32312
T-RA100Vf0E0.5	33.14	3.16	4.08	31232
T-RA0Vf0E0.5	35.49	3.23	4.40	31608
L-RA100Vf0E0.5	34.33	2.74	4.40	29778
L-RA0Vf0E0.5	33.65	2.70	4.30	29331
S-RA100Vf1E0.5	35.93	3.48	5.86	32130
S-RA0-Vf1E0.5	35.25	3.38	5.42	31756
T-RA100Vf1E0.5	35.63	3.17	5.75	32139
T-RA0Vf1E0.5	34.49	3.15	5.75	31865
L-RA100Vf1E0.5	34.49	3.35	5.52	30844
L-RA0Vf1E0.5	35.34	3.40	5.78	30935
S-RA100Vf0E1.0	36.2.8	2.94	4.29	32551
S-RA0Vf0E1.0	34.84	2.83	4.23	31032
T-RA100Vf0E1.0	33.49	3.09	4.35	32605
T-RA0Vf0E1.0	35.63	3.33	4.78	33562
L-RA100Vf0E1.0	34.87	2.86	4.38	30834
L-RA0Vf0E1.0	32.85	2.69	3.90	29039
S-RA100Vf1E1.0	36.71	3.51	5.79	30973
S-RA0Vf1E1.0	35.42	3.37	5.88	36199
T-RA100Vf1E1.0	33.63	3.10	5.68	32435
T-RA0Vf1E1.0	34.32	3.23	5.49	30442
L-RA100Vf1E1.0	33.63	3.20	5.28	30486
L-RA0Vf1E1.0	32.71	3.07	5.09	28918

4.3.1.1 Short Columns (kl/r = 17.24)

In the four short column specimens of concentrically loaded columns (S-RA0Vf0E0, S-RA50Vf0E0, S-RA100Vf0E0, and S-RA50Vf1E0), failure primarily occurred due to compression. Figure 4.1 shows the samples at failure, with evident steel yielding and concrete crushing. Columns S-RA0Vf1E0 and S-RA100Vf1E0 failed under compression accompanied by shear, likely due to the inclusion of steel fiber. Shear forces acted on the upper and lower parts of the columns after core compression, leading to small cracks at the corners milliseconds before failure. Recycled aggregate columns exhibited a similar but more fragile failure process than natural aggregate. For example, S-RA100Vf0E0 showed a more explosive failure than S-RA0Vf0E0, possibly due to significant differences in drying shrinkage between the concrete cover and core. In contrast, the addition of steel fiber resulted in a ductile failure pattern. Notably, S-RA50Vf0E0, with 50% natural and recycled aggregate, behaved more like columns with recycled aggregate (Figure 4.2). In S-RA0Vf1E0, S-RA50Vf1E0, and S-RA100Vf1E0, most of the concrete cover remained intact, aiding bearing capacity despite some small surface detachment. S-RA100Vf0E0 showed no cracks before failure, while long vertical cracks and corner spalling developed during crushing. The steel reinforcements buckled locally between upper and lower ties, mainly at mid-height. In S-RA100Vf1E0, vertical cracks started from the corners toward the middle, similar to S-RA100Vf0E0 without steel fiber. The failure produced a significant sound but maintained structural integrity, with both S-RA100Vf1E0 and S-RA0Vf1E0 crushing at approximately similar loads. Figure 4.3 illustrates the failure patterns of the concentrically loaded short columns.

(a) S-RA0Vf0E0 (b) S-RA100Vf0E0

Figure 4.1: Columns at the time of failure (Explosion):

4.3.1.2 Slender Columns (kl/r = 26)

In the six concentrically loaded columns—T-RA0Vf0E0, T-RA50Vf0E0, T-RA100Vf0E0, T-RA0Vf1E0, T-RA50Vf1E0, and T-RA100Vf1E0—the entire cross-section failed under compression, with observed steel buckling and concrete crushing. Similar to the behavior observed in the short columns, all the six columns exhibited a brittle, sudden, and explosive failure mode, with steel reinforcements visibly exposed and buckling outward. Notably, no rupture in the ties was detected even after reaching failure load in any of the concentrically loaded columns. Figure 4.4 illustrates the failure pattern of the slender columns with kl/r = 26. T-RA50Vf0E0 failed near the top end of the column, followed by compression and steel reinforcement buckling. Despite the location of failure being near the top, the strain values matched those of samples failing near the mid-height of the columns. Similarly, T-RA100Vf0E0

also failed near the top, possibly due to the double curvature of the column. Interestingly, neither the addition of steel fiber nor the replacement of recycled aggregate had a significant effect on the failure location. Columns T-RA0Vf0E0, T-RA0Vf1E0, and T-RA50Vf1E0, with steel fiber addition, failed at the mid-height, while T-RA100Vf1E0 failed slightly at a higher zone, all in compression.

4.3.1.3 Slender Columns (kl/r = 34.5)

In the six concentrically loaded columns (L-RA0Vf0E0, L-RA50Vf1E0, L-RA100Vf0E0, L-RA0Vf1E0, L-RA50Vf1E0, and L-RA100Vf1E0) with the slenderness ratio of 34.5, the entire cross-section failed in compression. However, these samples failed at lower loads compared to the short columns (kl/r=17.24) and slender columns (kl/r=26) Referenced from mechanics of materials, short columns often fail under high loads due to crushing rather than buckling, as they reach their compressive strength limit quickly. In this six column group, all the columns failed near the mid-height by crushing the concrete and yielding of the steel, except for L-RA100Vf0E0, which crushed near the top end of the column. The concrete and steel strains of L-RA100Vf0E0 were comparable to those of the other columns. Figure 4.5 illustrates that columns L-RA0Vf0E0, L-RA50Vf0E0, and L-RA100Vf0E0 lost large pieces of concrete at failure, whereas L-RA0Vf1E0, L-RA50Vf1E0, and L-RA100Vf1E0 only had small pieces come off. This difference is likely due to the presence of the steel fiber. L-RA0Vf0E0, a long column without fiber, crushed suddenly with no visible warning or crack. In contrast, L-RA0Vf1E0, a slender column with fiber, developed cracks starting from the mid-height, extending vertically to the corners. Figure 4.2 shows after failure shape of the column.

Figure 4.2: S-RA50Vf0E0 after failure

Figure 4.3: Failure mode of concentrically loaded short columns

T-RA0Vf0E0 T-RA50Vf0E0 T-RA100Vf0E0 T-RA0Vf1E0 T-RA50Vf1E0 T-RA100Vf1E0

Figure 4.4: Failure mode of concentrically loaded slender columns (kl/r = 26)

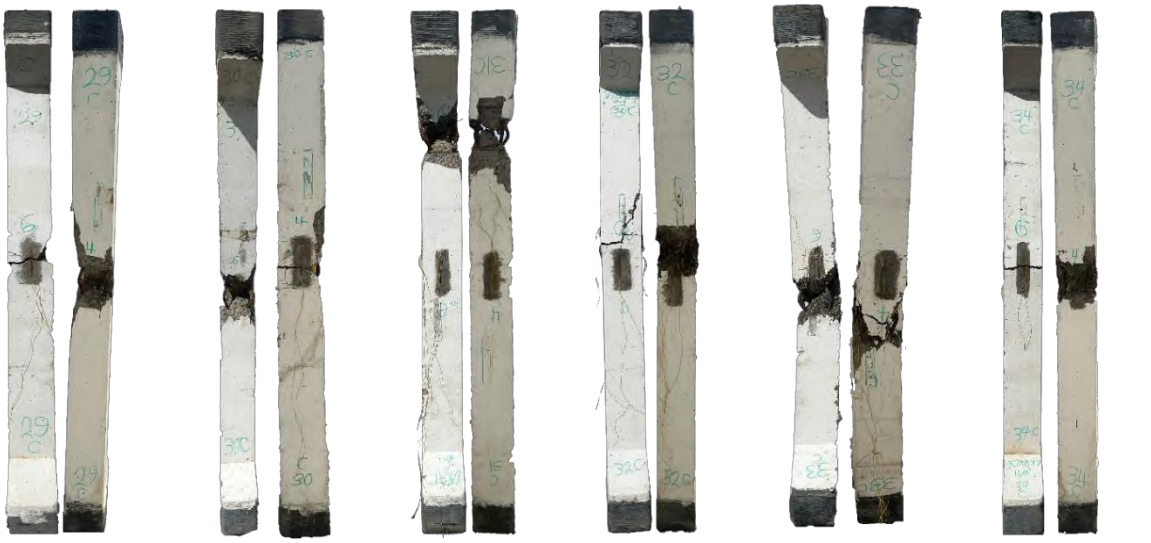

L-RA0Vf0E0 L-RA50Vf0E0 L-RA100Vf0E0 L-RA0Vf1E0 L-RA50Vf1E0 L-RA100Vf1E0

Figure 4.5: Failure mode of concentrically loaded slender columns (kl/r = 34.5)

4.3.2 Eccentrically Loaded Columns (e/h=0.5)

In all eccentrically loaded columns, the load was removed once it reached its maximum and began to decline. The number of cracks remained consistent before and after reaching maximum failure load, but their width and extension into the compression zone increased. Unlike concentric columns, the failure mode of eccentrically loaded columns was smoother and less abrupt. During loading, it was possible to closely approach the samples and mark crack locations from the early stages.

Due to the applied eccentricity, slender columns with an e/h ratio of 0.5 failed in a tension-controlled mode, with concrete crushing occurring after steel reinforcement yielded on the tension side. In short columns, however, the steel did not yield in tension. Steel strain levels were similar in both natural and recycled aggregate samples, but the inclusion of steel fiber resulted in higher steel strains at failure loads, albeit lower than in samples without steel fiber. In columns with steel fiber, cracks developed gradually during loading, spreading across the tension side. Figures 4.6, 4.7, and 4.8 visually illustrate the spacing and width of these flexural cracks. Additionally, the steel fiber restricted crack extension toward the compressive side, resulting in a greater effective depth of the compressive region at failure compared to columns without steel fiber. Tables 4.2 and 4.3 present cracking loads, cracking load as a percentage of failure load, and crack depth, calculated based on linear strain distribution. The crack depth was determined by subtracting the compression depth from the total section depth.

4.3.2.1 Short Columns (kl/r = 17.24)

The short columns, S-RA100Vf0E0.5 and S-RA0Vf0E0.5, cracked at the 54% and 45% of their maximum load capacity, respectively, the tension face, and the concrete crushed the compression face. Similarly, S-RA100Vf1E0.5 and S-RA0Vf1E0.5, loaded eccentrically at e/h = 0.5, cracked at the 53% and 58% of the failure load, respectively, followed by failure due to crushing of concrete on the compression face without yielding of the steel on the tension face. The cracks in S-RA0Vf0E0.5 started within the top two-thirds of the column's height and were unevenly spaced. With the sample S-RA100Vf0E0.5 being loaded to beyond the maximum failure capacity accidentally, the tension-side steel ruptured and the compression-side concrete spalled. At the absence of steel fiber, horizontal cracks formed at the mid-height of the column during loading, spreading outward and extending to both the top and bottom as the load increased, with the crack width widening at higher loading stages.

4.3.2.2 Slender Columns (kl/r = 26)

The specimens T-RA100Vf0E0.5 and T-RA0Vf0E0.5, both with a slenderness ratio of 26, cracked at 44% and 51% of the failure load, respectively, with the failure occurring after the steel yielded at the tension side and the concrete crushed on the compression face. The concrete strain on the tension face and the compression face readings showed 0.000266 and 0.000929, shown in Table 4.29, when the cracks appeared. Similarly, T-RA100Vf1E0.5 and T-RA0Vf1E0.5, were also loaded eccentrically at e/h = 0.5, cracked at 46% and 50% of the failure load, respectively, with the failure happening, with the

tension-side steel yielding and the compression-face concrete crushing. The strain levels were higher than the previous six samples in previous section of 4.3.2.1, as shown in the Table 4.29.

4.3.2.3 Slender Columns (kl/r = 34.5)

The specimens L-RA100Vf0E0.5 and L-RA0Vf0E0.5, both with a slenderness ratio of 34.5, exhibited a behavior similar to S-RA0Vf0E0 and S-RA50Vf0E0, with the tension-face concrete strain reaching 0.000978 and 0.000177, respectively. L-RA100Vf0E0.5 cracked at 35% of the failure load, while L-RA0Vf0E0.5 cracked at 45% of the failure load. Similarly, the columns L-RA100Vf1E0.5 and L-RA0Vf1E0.5, loaded eccentrically at e/h = 0.5, experienced compression-face concrete crushing and tension-face steel yielding, with higher strains indicated in the Table 4.29. L-RA100Vf1E0.5 cracked at 44% of the failure load, and L-RA0Vf1E0.5 cracked at 49% of the failure load.

Table 4.2 Cracking load for columns with e/h = 0.5 and Vf = 0

Specimen ID	Failure Load (kN)	Cracking Load (kN)	Cracking Load %	No. of cracks	Crack Depth (mm)
S-RA100Vf0E0.5	190	102.1	54%	7	66
S-RA0Vf0E0.5	210	95	45%	9	67
T-RA100Vf0E0.5	176	77	44%	14	70
T-RA0Vf0E0.5	172	83	51%	12	73
L-RA100Vf0E0.5	161	56	35%	19	71
L-RA0Vf0E0.5	158	69	45%	17	73

Table 4.3 Cracking load for columns with e/h = 0.5 and Vf = 1%

Specimen ID	Failure Load (kN)	Cracking Load (kN)	Cracking Load %	No. of cracks	Crack Depth (mm)
S-RA100Vf1E0.5	223	117.5	53%	10	62
S-RA0-Vf1E0.5	218	126.1	58%	9	64
T-RA100Vf1E0.5	186	86	46%	16	66
T-RA0Vf1E0.5	177	88	50%	14	69
L-RA100Vf1E0.5	163	72.3	44%	20	68
L-RA0Vf1E0.5	168	82	49%	19	70

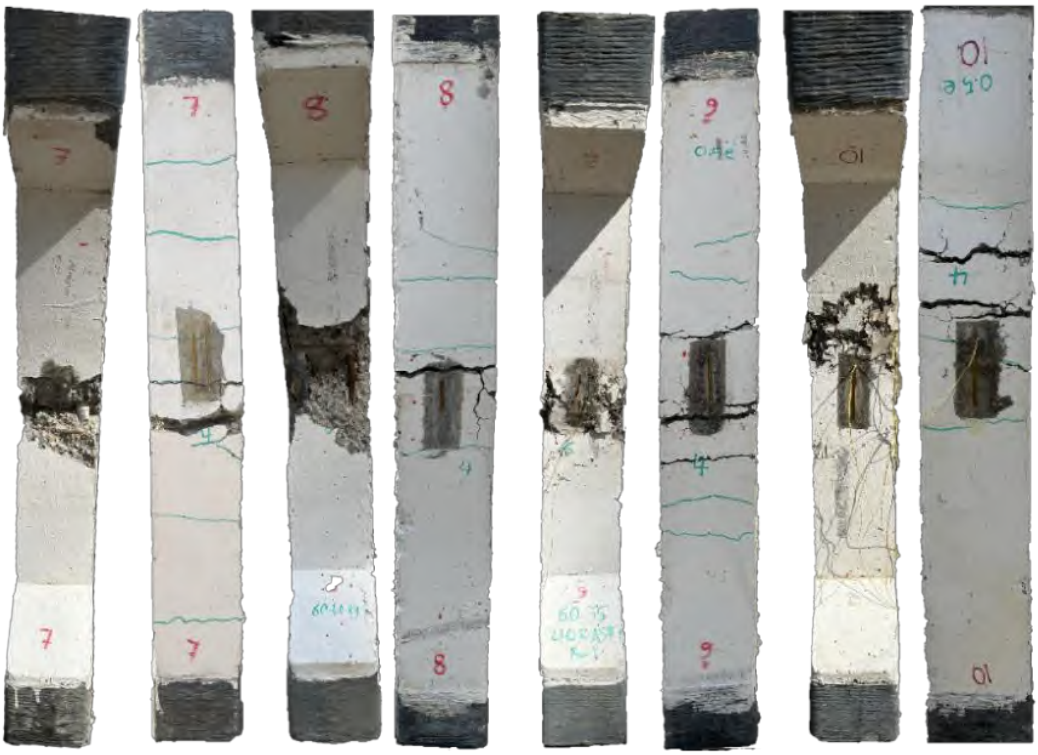

S-RA100Vf0E0.5 S-RA0Vf0E0.5 S-RA100Vf1E0.5 S-RA0Vf1E0.5

Figure 4.6: Failure mode of eccentrically loaded short columns (e/h = 0.5)

Figure 4.7: Failure mode of eccentrically loaded slender columns (Kl/r = 26, e/h = 0.5)

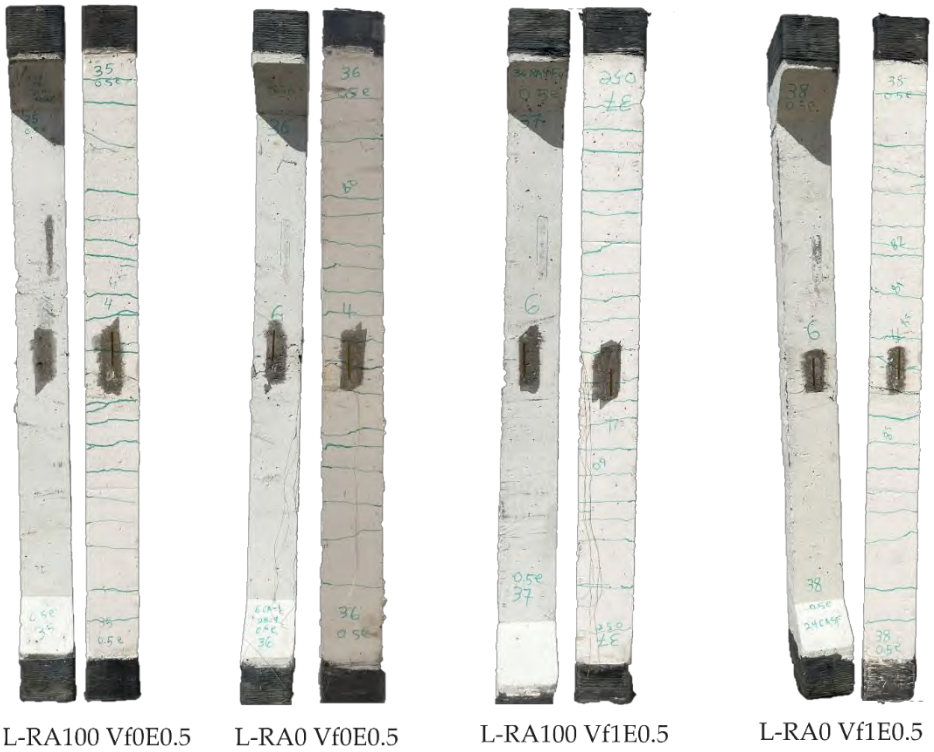

Figure 4.8: Failure mode of eccentrically loaded slender columns (Kl/r = 34.5, e/h = 0.5)

4.3.3 Eccentrically Loaded Columns (e/h=1.0)

The columns subjected to larger eccentricity (e/h=1.0) exhibited significantly greater lateral deformation and failed at smaller axial loads compared to those under smaller eccentricity (e/h=0.5). The crack distribution at failure is illustrated in Figures 4.9, 4.10, and 4.11, revealing slightly deeper cracks but at lower loads, indicating reduced compressive depth. As loading progressed, transverse crack density increased, extending to the compressive sides. Approaching failure, vertical micro cracks emerged at the compressive side, with rapid increases in crack width and lateral displacement. Columns with recycled aggregates showed no notable effect on failure mode across all replacement stages, while the addition of steel fiber significantly influenced the failure mode, resulting in higher ductility and a more gradual failure process. Generally, samples with steel fiber exhibited more transverse cracks compared to those without, and the spacing and width of flexural cracks were influenced by fiber bridging toward the compression face. In all columns of this group, steel reinforcement yielded on the tension side but not on the compression side, and the columns maintained their integrity after failure.

4.3.3.1 Short Columns (kl/r = 17.24)

Higher moment arms due to a larger eccentricity and lateral displacement caused early cracking in the columns. S-RA100Vf0E1.0 and S-RA0Vf0E1.0 cracked at 42% and 36% of the failure load, respectively, while those with steel fiber, S-RA100Vf1E1.0 and S-RA0Vf1E1.0, cracked at 46% and 38% of the failure load, respectively. The columns with steel fiber cracked at 4% higher loads than those without. Smaller loads induced higher lateral

displacement compared to columns with e/h=0.5 eccentricity. The column curvature was visible during loading, with the shear cracks appearing near the ends at around 80% of the failure load. The tension steel yielded at strains around 0.005, while the concrete crushed at strains ranging from 0.0029 to 0.0038. The compression steel did not yield indicating tension-controlled failure in bending. The recycled aggregate had no apparent effect on the failure modes, the steel while steel fiber significantly influenced them, resulting in smaller cracks width and better crack distribution.

Table 4.4 Cracking load for columns with e/h = 1.0 and Vf = 0

Specimen ID	Failure Load (kN)	Cracking Load (kN)	Cracking Load %	No. of cracks	Crack Depth (mm)
S-RA100Vf0E1.0	100	42	42%	10	80
S-RA0Vf0E1.0	105	38	36%	10	81
T-RA100Vf0E1.0	76.5	20	26%	15	87
T-RA0Vf0E1.0	80	18	23%	13	86
L-RA100Vf0E1.0	74.5	20	27%	18	88
L-RA0Vf0E1.0	73	19	27%	20	87

Table 4.5 Cracking load for columns with e/h = 1.0 and Vf = 1%

Specimen ID	Failure Load (kN)	Cracking Load (kN)	Cracking Load %	No. of cracks	Crack Depth (mm)
S-RA100Vf1E1.0	107	49	46%	12	79
S-RA0Vf1E1.0	112	43	38%	8	80
T-RA100Vf1E1.0	86.5	24	28%	18	82
T-RA0Vf1E1.0	87	21	24%	16	83
L-RA100Vf1E1.0	80.5	33	41%	21	85
L-RA0Vf1E1.0	76.5	26	34%	20	86

4.3.3.2 Slender Columns (kl/r = 26)

T-RA100Vf0E1.0 and T-RA0Vf0E1.0 cracked at 26% and 23% of the maximum load capacity, respectively. While the columns with the steel fiber, T-RA100Vf1E1.0 and T-RA0Vf1E1.0 cracked at 28% and 24% of the peak loads. The columns with the steel fiber cracked at 2% and 1% higher loads. Smaller loads caused higher lateral displacement compared to the columns tested at (e/h=0.5). The column curvature of the columns was obvious to rare eyes even before the failure during the loading process. The shear cracks appeared near the ends of the column around 70 - 80% of the maximum load. The reinforcement steel at the tension side yielded, obviously at high strain of 0.0046 – 0.0048, while the concrete crushed at a strain ranging between 0.0029 and 0.0035, shown in Table 4.30. The reinforcement steel at the compression side did not yield in the columns T-RA100Vf0E1.0, T-RA0Vf0E1.0, T-RA100Vf1E1.0, and T-RA0Vf1E1.0. This is identified as a flexural failure with a tension control behavior.

4.3.3.3 Slender Columns (kl/r = 34.5)

Similar to the other columns with 100% eccentricity but with different slenderness ratio, higher moment arms due to the eccentricity and higher lateral displacement caused the column to crack at an early stage of the test. L-RA100Vf0E1.0 and L-RA0Vf0E1.0 cracked at 27% of the failure load. The columns with steel fiber, L-RA100Vf1E1.0, and L-RA0Vf1E1.0 cracked at 41% and 34% of the failure load. The column L-RA100Vf1E1.0 with steel fiber cracked at a 14% higher load than L-RA100Vf0E1.0. The column L-RA0Vf1E1.0 with steel fiber cracked with a 7% higher load than L-

RA0Vf0E1.0. The steel reinforcement in the tension face yielded, obviously with a high strain of 0.0048 – 0.0050 while the concrete crushed at a strain ranging between 0.0029 and 0.0033, shown in Table 4.30. The steel reinforcement at the compression side did not yield in Columns L-RA100Vf0E1.0, L-RA0Vf0E1.0, L-RA100Vf1E1.0 and L-RA0Vf1E1.0. This is a Flexural failure with tension-controlled behavior.

It is observed that the crack depths of columns under the eccentricity of (e/h=1.0) were slightly larger than those under eccentricity (e/h=0.5), even at smaller loads. This is an indication that the larger eccentricity reduced the compressive depth of the concrete and increased the crack depth focusing on the mid-height of the columns.

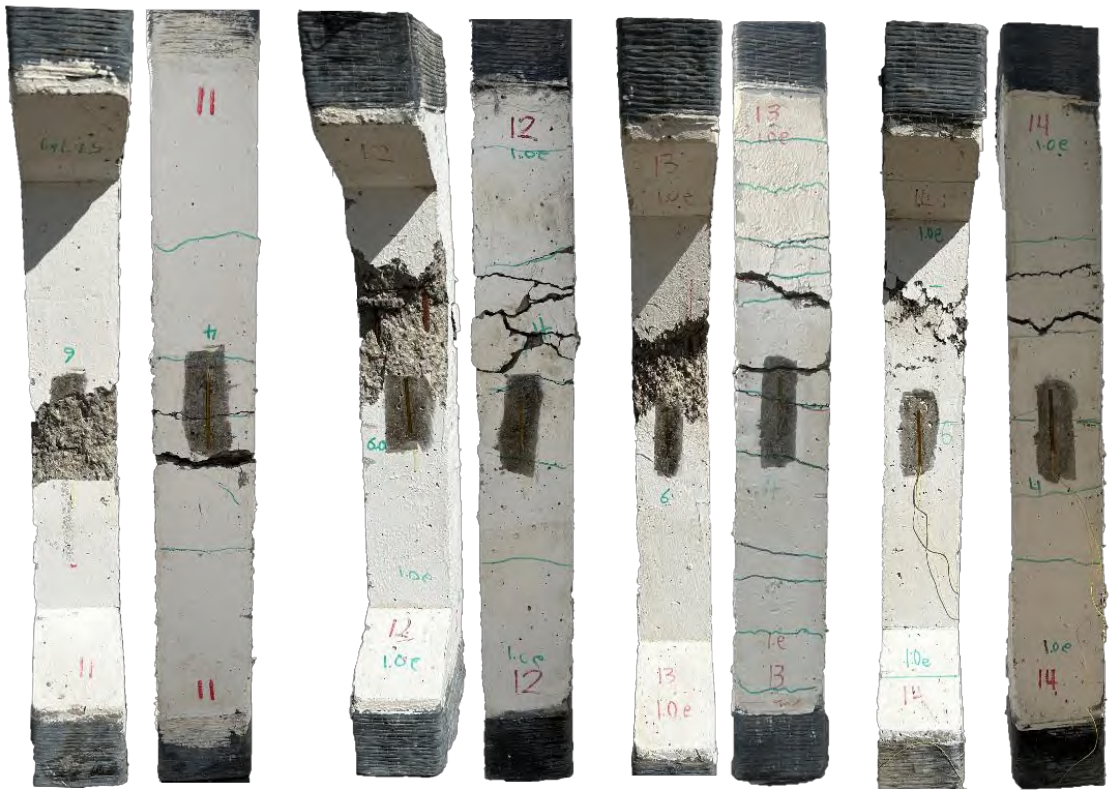

S-RA100Vf0E1.0 S-RA0Vf0E1.0 S-RA100Vf1E1.0 S-RA0Vf1E1.0

Figure 4.9: Failure mode of eccentrically loaded short columns (Kl/r = 17.24, e/h = 1.0)

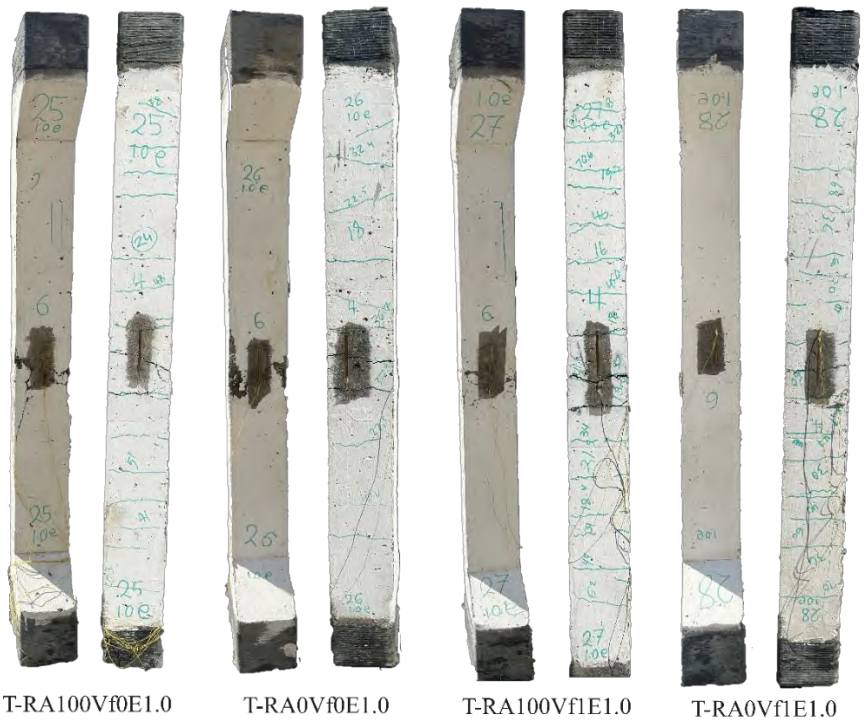

Figure 4.10: Failure mode of eccentrically loaded slender columns (Kl/r = 26, e/h = 1.0)

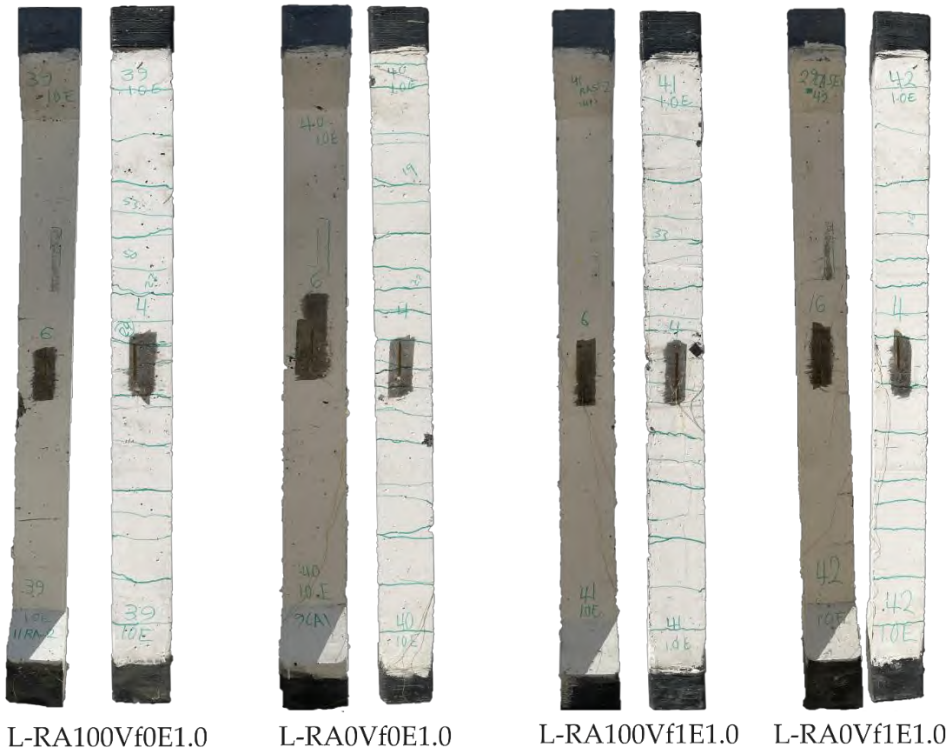

Figure 4.11: Failure mode of eccentrically loaded slender columns (Kl/r = 34.5, e/h = 1.0)

4.4 LOAD CARRYING CAPACITY

4.4.1 Concentrically Loaded Columns

The failure loads, as listed in Tables 4.6 and 4.7, demonstrate the varying influence of concrete mix types on the load-carrying capacity of columns, depending on the recycled aggregate replacement and steel fiber addition. In the concentrically loaded samples, the columns constructed with the recycled aggregate exhibited comparable strength to those made with the natural aggregate, and in most of cases, even withstood higher loads. Nonetheless, the differences were relatively small. The effect of the steel fiber on the concentrically loaded columns appeared to be insignificant; the addition of the steel fiber in compression is less effective than in tension. However, the primary determining factor remains the slenderness ratio, which had a moderate impact on capacity. It is important to emphasize that eccentricity is the predominant factor influencing the load.

4.4.1.1 Effect of Recycled Aggregate on Column Load Capacity

The failure loads are presented in Tables 4.6 and 4.7, demonstrating the influence of the recycled aggregate on the strength. In short columns (with the slenderness ratio of 17.24), a 4.4% increase in the strength was observed when 50% of the natural coarse aggregate was replaced by the recycled aggregate. The complete replacement of the natural aggregate with the recycled aggregate resulted in an 8.1% increase in the strength.

In long columns with the slenderness ratio of 26 (columns T-RA0Vf0E0, T-RA50Vf0E0, and T-RA100Vf0E0), a 6.2% and 8.5% increase in the strength was noted with 50% and 100% replacement of the natural aggregate by

recycled aggregate, respectively. Similarly, in columns L-RA0Vf0E0, L-RA50Vf1E0, and L-RA100Vf0E0 with the slenderness ratio of 34.5, the strength increased by 5.6% and 7.5% with 50% and 100% replacement of natural aggregate with recycled aggregate, respectively. The effect of replacing the natural aggregate with the recycled aggregate exhibited slightly different results with the addition of steel fiber. In the short columns, a 50% replacement in S-RA50Vf1E0 and 100% replacement in S-RA100Vf1E0 increased in the strength by only 2.2% and 4.8%, which is not significant.

The 4.4% strength increase with 50% recycled aggregate and 8.1% with full replacement indicates that recycled aggregates effectively support compressive loads in short columns, where material strength is more critical than stability.

In longer columns, the strength gains of 6.2% to 8.5% with 50% to 100% replacement arise from reduced lateral buckling risk. The improved confinement and mechanical interlocking of recycled aggregates enhance load-bearing capacity, mitigating the effects of increased slenderness. In long columns with a slenderness ratio of 26 (columns T-RA0Vf1E0, T-RA50Vf1E0, and T-RA100Vf1E0), replacing 50% and 100% of the natural aggregate with the recycled aggregate led to increases in strength by 8.0% and 11.6%, respectively. However, in long columns with the slenderness ratio of 34.5, adding 1% steel fiber resulted in varying outcomes. While a 50% replacement in L-RA50Vf1E0 increased the strength by 4.1%, a 100% replacement in L-RA100Vf1E0 led to a 5.4% increase in strength.

Columns made with recycled aggregates demonstrated higher load capacity compared to those made with natural aggregates. This may be due to the

greater density of recycled aggregates, which enhances load-bearing capacity Chan and Sun (2006), and the adhered cement paste that improves bonding with the new concrete, resulting in a stronger composite Kim et al. (2019). Additionally, the angularity and surface texture of recycled aggregates enhance mechanical interlock, increasing shear strength and overall load capacity Pacheco Torgal et al. (2011).

Moreover, the strength of the parent concrete from which the recycled aggregates are derived plays a role. This effect may also be linked to the use of the Saturated Surface Dry (SSD) condition, where aggregates are submerged in water for 24 hours prior to use. Furthermore, recycled aggregates generally exhibit higher porosity than natural aggregates, largely due to the old mortar that adheres to their surfaces.

Table 4.6.Effect of the recycled aggregate on column capacity (e/h=0, Vf 0%)

Specimen ID	RA%	Kl/r	Failure Load (kN)	Increase in strength
S-RA0Vf0E0	0	17.24	680	
S-RA50Vf0E0	50		710	4.4%
S-RA100Vf0E0	100		735	8.1%
T-RA0Vf0E0	0	26	645	
T-RA50Vf0E0	50		685	6.2%
T-RA100Vf0E0	100		700	8.5%
L-RA0Vf0E0	0	34.5	642	
L-RA50Vf1E0	50		678	5.6%
L-RA100Vf0E0	100		690	7.5%

Figure 4.12 illustrates the effect of the replacing recycled aggregate ratio on the failure load in the columns containing no steel fiber, while Figure 4.13 depicts the effect in columns containing 1% steel fiber.

Table 4.7.Effect of the recycled aggregate on column capacity (e/h=0, Vf 1%)

Specimen ID	RA%	Kl/r	Failure Load (kN)	Increase in strength
S-RA0Vf1E0	0	17	714	
S-RA50Vf1E0	50		730	2.2%
S-RA100Vf1E0	100		748	4.8%
T-RA0Vf1E0	0	26	678	
T-RA50Vf1E0	50		700	3.2%
T-RA100Vf1E0	100		723	6.6%
L-RA0Vf1E0	0	34.5	665	
L-RA50Vf1E0	50		692	4.1%
L-RA100Vf1E0	100		701	5.4%

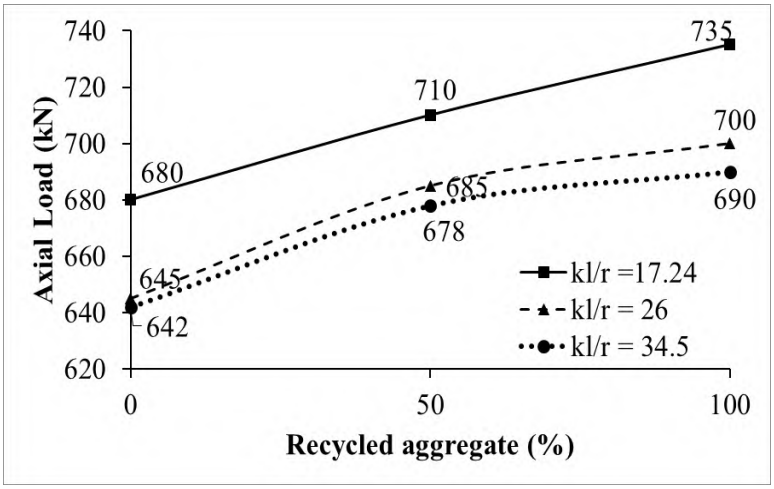

Figure 4.12 Effect of recycled aggregate on column capacity (e/h = 0, Vf = 0%)

4.4.1.2 Effect of Slenderness Ratio (kl/r)

The effect of the slenderness ratio on the column axial strength is presented in Tables 4.8 and 4.9. For columns with 100% natural aggregate, the strength decreased by 5.1% when transitioning from the slenderness ratio of 17.24 to 26, and by 5.6% when the ratio increased to 34.5. Similarly, in the columns with 50% natural and 50% recycled aggregate, the strength decreased by 3.5%

and 4.5%, respectively, with increasing slenderness ratio. Upon adding 1% steel fiber, the columns with 100% natural aggregate experienced a 9.2% decrease in the strength when the slenderness ratio increased to 26, and a 6.9% decrease at the slenderness ratio 34.5. For columns with 50% natural and 50% recycled aggregate, the strength decreased by 4.1% and 5.2%, respectively, with the increase in the slenderness ratio.

As the slenderness ratio (kl/r) increases, columns become more susceptible to buckling, which reduces their load-carrying capacity, especially beyond a critical threshold. For example, the 5.1% strength decrease in columns with 100% natural aggregate when moving from a slenderness ratio of 17.24 to 26 illustrates this effect. Higher slenderness ratios result in greater lateral deflections, further diminishing the column's effective load-bearing capacity. This is supported by (Wang et al., 2004).

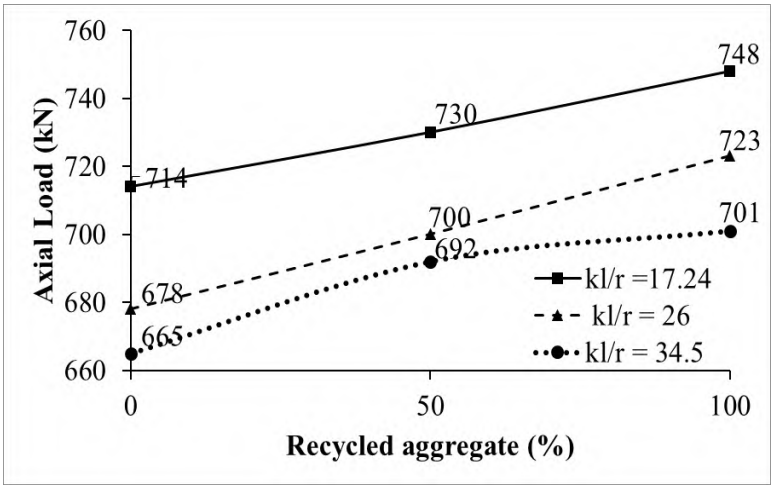

Figure 4.13 Effect of recycled aggregate on column capacity (e/h = 0, Vf = 1%)

For columns entirely made of the recycled aggregate and with 1% steel fiber, the strength decreased by 3.3% when the slenderness ratio increased from

17.24 to 26, and decreased by 6.3% when slenderness ratio increased to 34.5. Figures 4.14 and 4.15 illustrate these trends without and with the use of steel fiber, respectively.

Table 4.8. Effect of slenderness ratio on samples (e/h = 0, Vf = 0%)

Specimen ID	RA	Kl/r	Failure Load (kN)	Decrease in strength
S-RA0Vf0E0	0%	17.24	680	
T-RA0Vf0E0		26	645	5.1%
L-RA0Vf0E0		34.5	642	5.6%
S-RA50Vf0E0	50%	17.24	710	
T-RA50Vf0E0		26	685	3.5%
L-RA50Vf1E0		34.5	678	4.5%
S-RA100Vf0E0	100%	17.24	735	
T-RA100Vf0E0		26	700	4.8%
L-RA100Vf0E0		34.5	690	6.1%

Table 4.9. Effect of slenderness ratio on samples (e/h = 0, Vf = 1%)

Specimen ID	RA	Kl/r	Failure Load (kN)	Decrease in strength
S-RA0Vf1E0	0%	17.24	714	
T-RA0Vf1E0		26	678	5.0%
L-RA0Vf1E0		34.5	665	6.9%
S-RA50Vf1E0	50%	17.24	730	
T-RA50Vf1E0		26	700	4.1%
L-RA50Vf1E0		34.5	692	5.2%
S-RA100Vf1E0	100%	17.24	748	
T-RA100Vf1E0		26	723	3.3%
L-RA100Vf1E0		34.5	701	6.3%

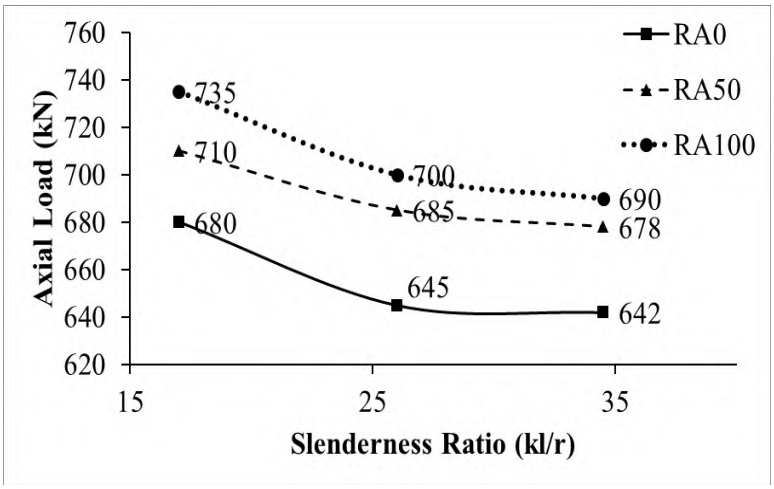

Figure 4.14. Effect of slenderness ratio on strength (e/h = 0, Vf = 0%)

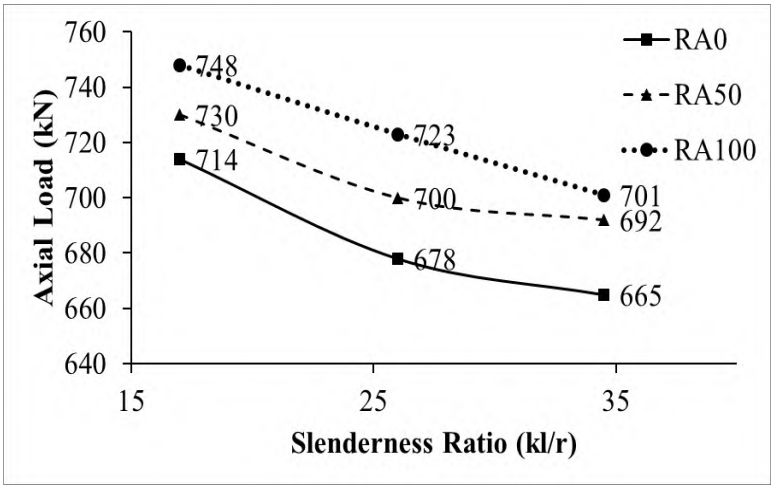

Figure 4.15. Effect of slenderness ratio on strength (e/h = 0, Vf = 1%)

4.4.1.3 Effect of Steel Fiber Content

The addition of 1% steel fiber to the concrete mixes modestly increased the strength of the columns, primarily due to the reinforcing effect at the compression zones. Table 4.10 presents the impact of the steel fiber in the concentrically loaded columns. Across all columns, the strength showed an improvement ranging from 0.5% to 5%. Figures 4.16, 4.17, and 4.18 illustrate the impact of the steel fiber.

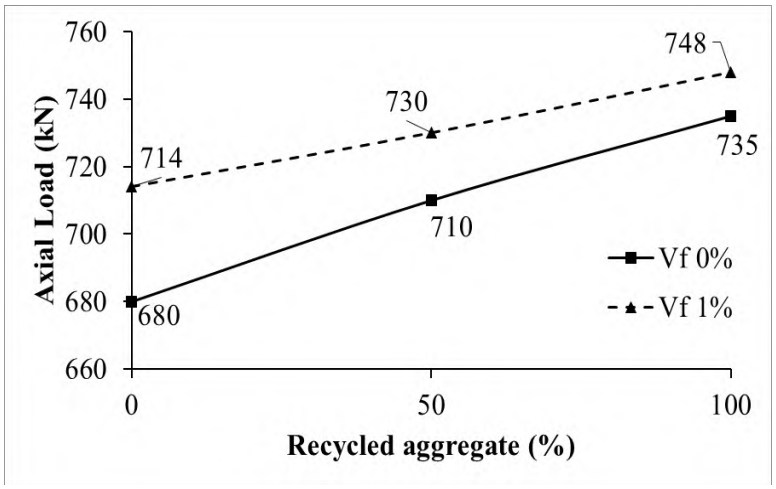

Figure 4.16: Effect of Vf on strength for different RA ratios (kl/r=17.24) (e/h =0)

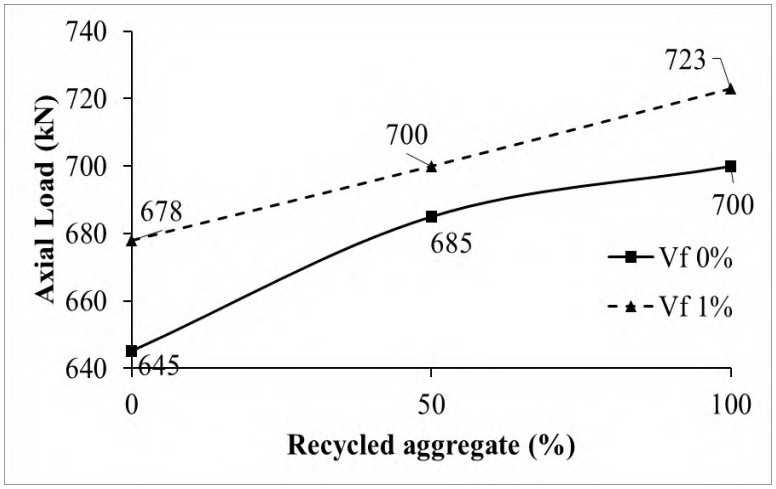

Figure 4.17: Effect of Vf on strength for different RA ratios (kl/r = 26) (e/h = 0)

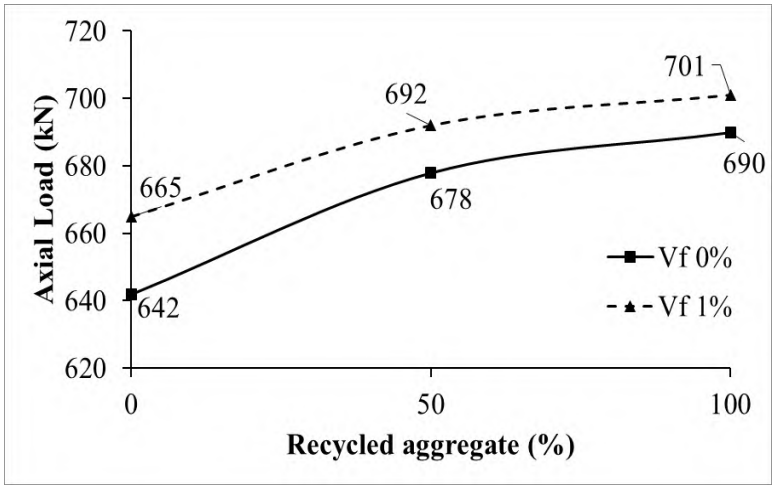

Figure 4.18: Effect of Vf on strength for different RA ratios (kl/r =34.5) (e/h = 0)

Table 4.10: Effect of the 1% steel fiber content on the column capacity (e/h = 0)

Specimen ID	Failure Load (kN)	Specimen ID	Failure Load (kN)	Increase in Strength
S-RA0Vf0E0	680	S-RA0Vf1E0	714	5.0%
S-RA50Vf0E0	710	S-RA50Vf1E0	730	2.8%
S-RA100Vf0E0	735	S-RA100Vf1E0	748	1.8%
T-RA0Vf0E0	645	T-RA0Vf1E0	678	0.5%
T-RA50Vf0E0	685	T-RA50Vf1E0	700	2.2%
T-RA100Vf0E0	700	T-RA100Vf1E0	723	3.3%
L-RA0Vf0E0	642	L-RA0Vf1E0	665	3.6%
L-RA50Vf0E0	678	L-RA50Vf1E0	692	2.1%
L-RA100Vf0E0	690	L-RA100Vf1E0	701	1.6%

4.4.2 Eccentrically Loaded Columns

4.4.2.1 Analysis of Columns Subjected to Eccentric Loading (e/h = 0.5)

4.4.2.1.1 Effect of Recycled Aggregate (RA) on Column Capacity

The strength of S-RA100Vf0E0.5 decreased by 9.5% compared to S-RA0Vf0E0.5 in short columns (kl/r = 17.24) when all-natural aggregate was replaced by recycled aggregate. Conversely, column T-RA100Vf0E0.5 exhibited a 2.3% strength increase compared to T-RA0Vf0E0.5 after replacing all-natural aggregate with recycled aggregate. For column L-RA100Vf0E0.5, the strength decreased by 1.9% due to natural aggregate replacement with recycled aggregate. After adding 1% steel fiber to the mix, the strength changes varied. S-RA100Vf1E0.5 showed a 2.3% increase compared to S-RA0Vf1E0.5, while T-RA100Vf1E0.5 saw a 5.1% increase after replacing the natural aggregate with the recycled aggregate. However, in slender columns,

the strength decreased by 3% when the natural aggregate was replaced with the recycled aggregate.

Table 4.11 compares the maximum strength after replacing the natural aggregate with recycled aggregate in eccentrically loaded samples with e/h = 0.5 eccentricity and no steel fiber in the mixture. Table 4.12 presents a similar comparison with the addition of steel fiber. Figures 4.19 and 4.20 illustrate the impact of the natural aggregate replacement by the recycled aggregate across three slenderness ratios, with the former depicting samples without steel fiber and the latter with the addition of steel fiber.

The strength variations observed highlight the mixed impact of recycled aggregates on column capacity. The 9.5% decrease in strength for the short column (S-RA100Vf0E0.5) suggests that recycled aggregates may not fully meet the demands of shorter columns, potentially due to lower bonding and compressive strength. Conversely, the 2.3% strength increase in the taller column (T-RA100Vf0E0.5) indicates that improved load distribution can enhance performance. The minimal decrease (1.9%) in the long column (L-RA100Vf0E0.5) suggests that recycled aggregates do not severely compromise strength. Adding 1% steel fiber results in strength increases for both short (2.3%) and tall (5.1%) columns, showing that fibers enhance ductility and mitigate weaknesses associated with recycled aggregates. However, the 3% decrease in slender columns emphasizes the ongoing influence of slenderness on performance. Kou and Poon (2013).

Table 4.11: Effect of recycled aggregate on column capacity (e/h=0.5, Vf=0%)

Specimen ID	RA%	Kl/r	Failure Load (kN)	Change in strength
S-RA0Vf0E0.5	0		210	
S-RA100Vf0E0.5	100	17.24	190	-9.5%
T-RA0Vf0E0.5	0		172	
T-RA100Vf0E0.5	100	26	176	2.3%
L-RA0Vf0E0.5	0		158	
L-RA100Vf0E0.5	100	34.5	161	-1.9%

Table 4.12: Effect of recycled aggregate on column capacity (e/h=0.5, Vf=1%)

Specimen ID	RA%	Kl/r	Failure Load (kN)	Change in strength
S-RA0-Vf1E0.5	0		218	
S-RA100Vf1E0.5	100	17.24	223	2.3%
T-RA0Vf1E0.5	0		177	
T-RA100Vf1E0.5	100	26	186	5.1%
L-RA0Vf1E0.5	0		168	
L-RA100Vf1E0.5	100	34.5	163	-3.0%

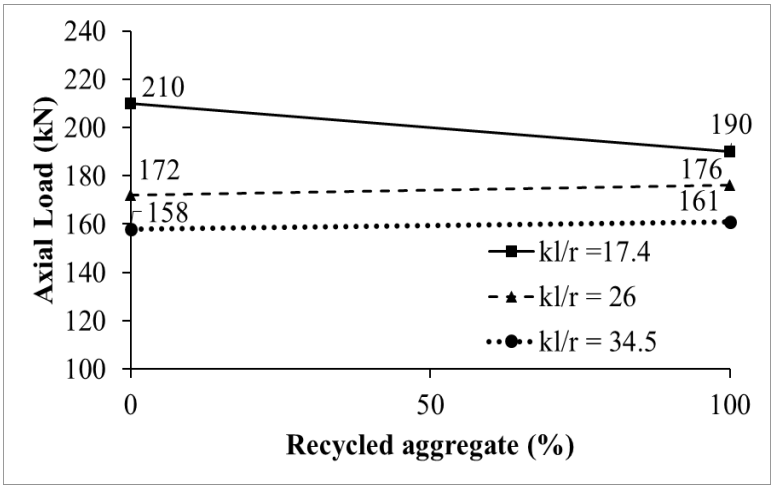

Figure 4.19: Effect of recycled aggregate on column capacity (Vf=0%, e/h=0.5)

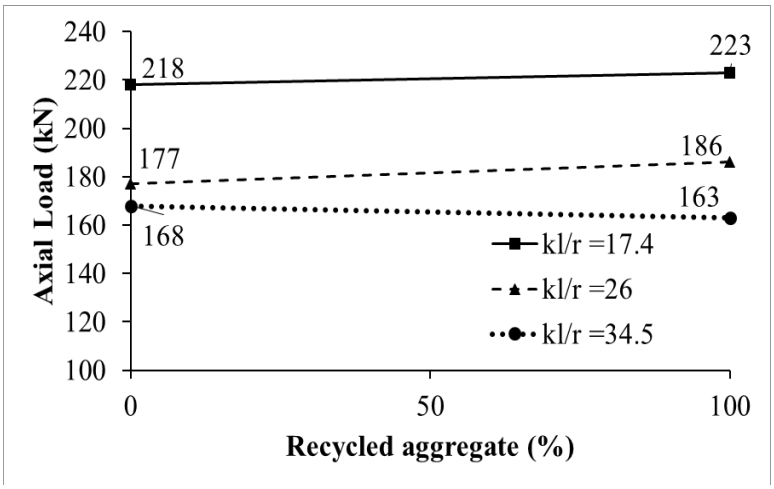

Figure 4.20: Effect of recycled aggregate on column capacity (Vf=1%, e/h=0.5)

4.4.2.1.2 The Effect of Slenderness Ratio (kl/r) on Column Capacity

Table 4.13 displays the effect of the slenderness ratio for the samples without steel fiber. The columns lost the strength once the slenderness ratio increased. As slenderness increases, columns become more susceptible to buckling, resulting in greater lateral deflections and reduced load-carrying capacity Reynolds and Steedman (2017). In this study, with e/h = 0.5 eccentricity, in the samples without steel fiber, the reduction in strength was 7.4% in T-RA100Vf0E0.5 compared to S-RA100Vf0E0.5 and the reduction was 15.3% in L-RA100Vf0E0.5 compared to S-RA100Vf0E0.5. In the columns with Natural aggregate, S-RA0Vf0E0.5 lost an 18.1% of its strength when compared to T-RA0Vf0E0.5, and, it lost s 24.8% when compared to L-RA0Vf0E0.5.

Table 4.14 displays the effect of the slenderness ratio for the samples with steel fiber. In these columns, the steel fiber was added and the coarse recycled aggregate was used, the reduction in the strength was 16.6% comparing S-RA100Vf1E0.5 to T-RA100Vf1E0.5.

Table 4.13: Effect of slenderness ratio on column capacity (e/h = 0.5) (Vf = 0%)

Specimen ID	RA (%)	Kl/r	Failure Load (kN)	Decrease (%)
S-RA100Vf0E0.5	100%	17.24	190	
T-RA100Vf0E0.5		26	176	7.4%
L-RA100Vf0E0.5		34.5	161	15.3%
S-RA0Vf0E0.5	0%	17	210	
T-RA0Vf0E0.5		26	172	18.1%
L-RA0Vf0E0.5		34.5	158	24.8%

However, the reduction was 26.9% when S-RA100Vf1E0.5 compared with L-RA100Vf1E0.5. The specimens made of 100% natural aggregate with the addition of steel fiber, S-RA0-Vf1E0.5 lost 18.8% in its strength compared to T-RA0Vf1E0.5. When compared S-RA0-Vf1E0.5 to L-RA0Vf1E0.5 the reduction in the strength was 22.9%. Figures 4.21 and 4.22 display the effect of the slenderness ratio graphically for samples with and without steel fiber. Each figure compares samples made of 100% natural aggregate to samples made of 100% recycled aggregate.

Table 4.14: Effect of slenderness ratio on column capacity (e/h = 0.5) (Vf = 1%)

Specimen ID	RA (%)	Kl/r	Failure Load (kN)	Decrease (%)
S-RA100Vf1E0.5	100%	17.24	223	
T-RA100Vf1E0.5		26	186	16.6%
L-RA100Vf1E0.5		34.5	163	26.9%
S-RA0-Vf1E0.5	0%	17.24	218	
T-RA0Vf1E0.5		26	177	18.8%
L-RA0Vf1E0.5		34.5	168	22.9%

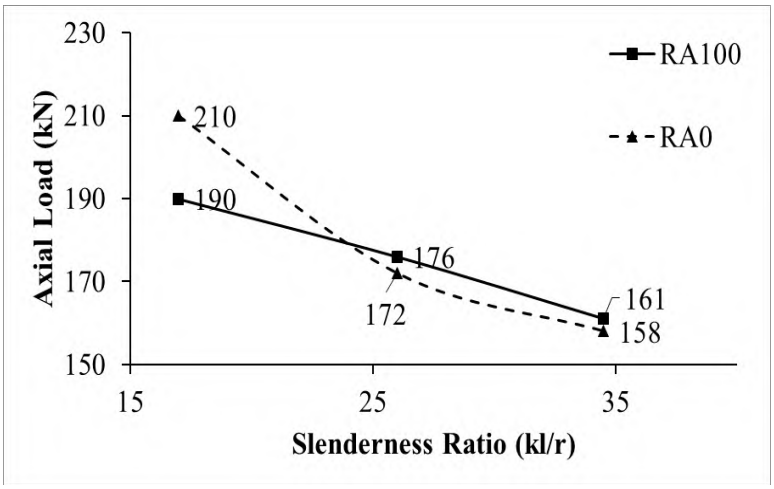

Figure 4.21: Effect of slenderness ratio on column capacity (e/h=0.5) (Vf=0%)

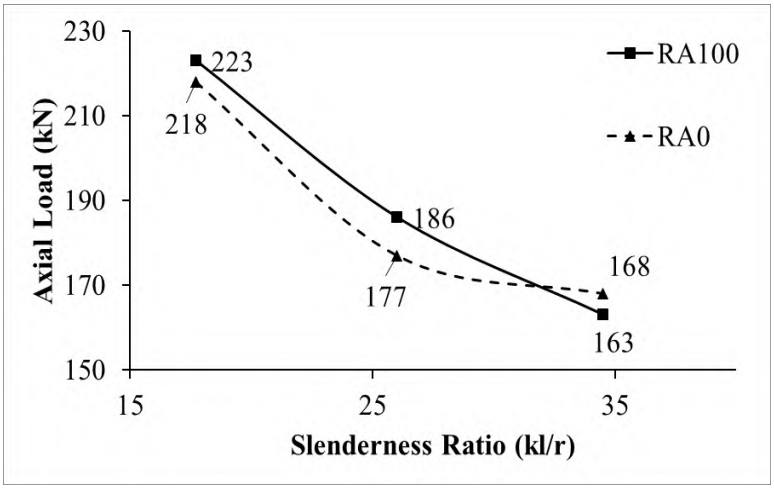

Figure 4.22: Effect of slenderness ratio on column capacity (e/h=0.5) (Vf=1%)

4.4.2.1.3 Effect of Steel Fiber Content (Vf) on Column Capacity

The addition of 1% steel fiber increased the strength of columns loaded at eccentricity (e/h=0.5) by 1.2% to 17.4%, see Table 4.15. For example, S-RA100Vf1E0.5 showed a 17.4% increase compared to S-RA100Vf0E0.5, both made of recycled aggregate. Conversely, L-RA100Vf1E0.5 exhibited a 1.2% increase compared to L-RA100Vf0E0.5, also made of recycled concrete aggregate.

Table 4.15 Effect of 1% steel fiber on column capacity (e/h=0.5)

Specimen ID	Failure Load (kN)	Specimen ID	Failure Load (kN)	Change in Strength
S-RA100Vf0E0.5	190	S-RA100Vf1E0.5	223	17.4%
S-RA0Vf0E0.5	210	S-RA0-Vf1E0.5	218	3.8%
T-RA100Vf0E0.5	176	T-RA100Vf1E0.5	186	5.7%
T-RA0Vf0E0.5	172	T-RA0Vf1E0.5	177	2.9%
L-RA100Vf0E0.5	161	L-RA100Vf1E0.5	163	1.2%
L-RA0Vf0E0.5	158	L-RA0Vf1E0.5	168	6.3%

Figures 4.23, 4.24, and 4.25 illustrate the impact of the steel fiber addition graphically across the slenderness ratios of 17.24, 26, and 34.5, respectively. The inclusion of the steel fiber enhanced the strength compared to samples without steel fiber.

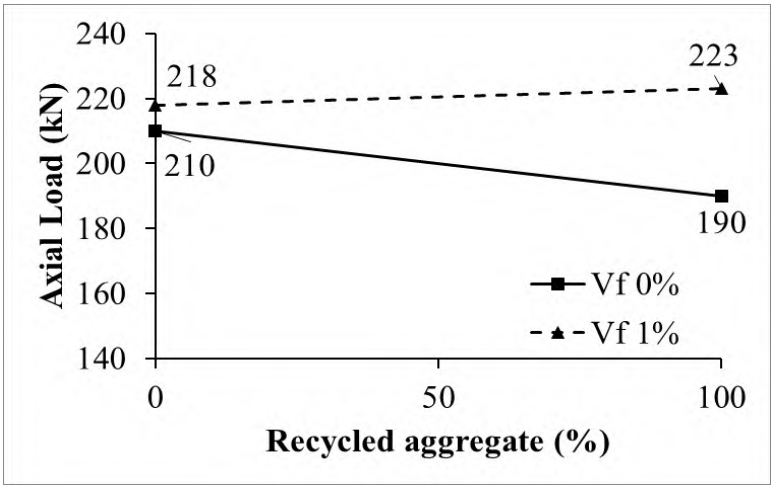

Figure 4.23: Effect of Vf on strength for different RA ratios (kl/r = 17.24, e/h = 0.5)

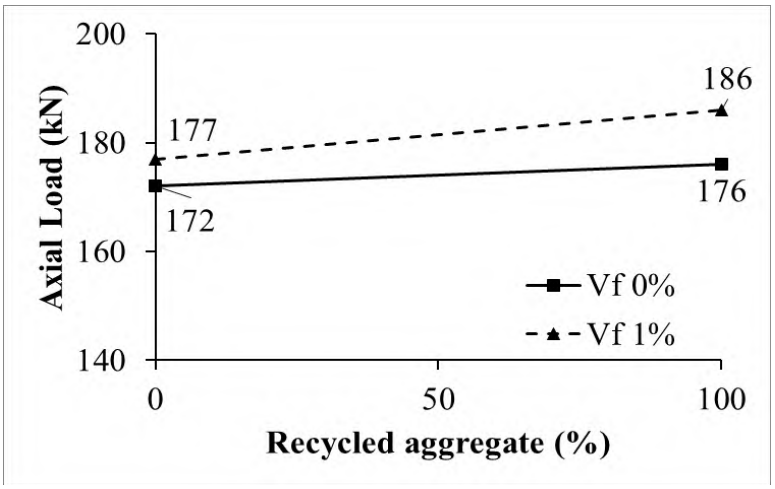

Figure 4.24: Effect of Vf on strength for different RA ratios (kl/r = 26, e/h = 0.5)

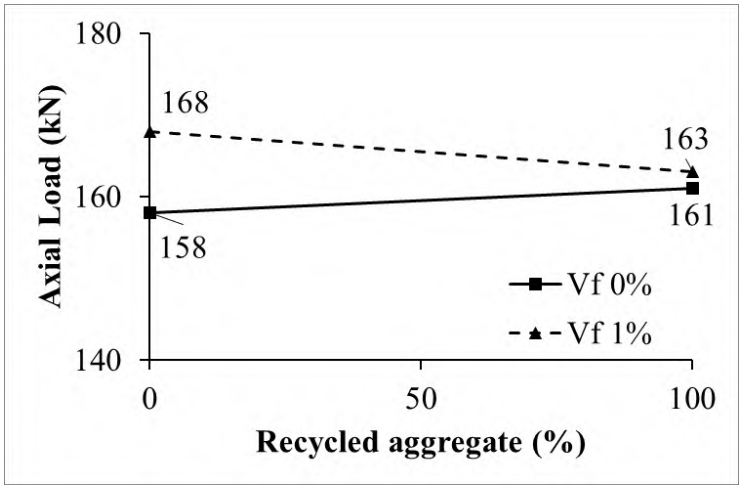

Figure 4.25: Effect of Vf on strength for different RA ratios (kl/r = 34.5, e/h = 0.5)

4.4.2.2 Analysis of Columns Subjected to Eccentric Loading (e/h = 1.0)

4.4.2.2.1 Effect of Recycled Aggregate (RA) on Column Capacity

Tables 4.16 and 4.17 display the impact of replacing natural aggregate with recycled aggregate on the column strength capacity, with and without the addition of steel fiber. In short columns (kl/r = 17.24), the strength of S-RA100Vf0E1.0 decreased by 4.76% compared to S-RA0Vf0E1.0. Similarly, in long columns with the slenderness ratio of 34.5, T-RA100Vf0E1.0 saw a decrease of 4.38% compared to T-RA0Vf0E1.0, while L-RA100Vf0E1.0

showed a 2.1% increase. The introduction of 1% steel fiber yielded comparable results, with S-RA100Vf1E1.0 experiencing a 4.46% decrease compared to S-RA0Vf1E1.0. T-RA100Vf1E1.0 showed a negligible decrease, while L-RA0Vf1E1.0 showed a 5.23% increase in the strength when the natural aggregate was replaced by the recycled aggregate.

Table 4.16 Effect of recycled aggregate on the strength (e/h-1.0) (Vf=0%)

Specimen ID	RA%	Kl/r	Failure Load (kN)	Change in strength
S-RA0Vf0E1.0	0	17.24	105	
S-RA100Vf0E1.0	100		100	-4.80%
T-RA0Vf0E1.0	0	26	80	
T-RA100Vf0E1.0	100		76.5	-4.38%
L-RA0Vf0E1.0	0	34.5	73	
L-RA100Vf0E1.0	100		74.5	+2.10%

Table 4.17 Effect of recycled aggregate on the strength (e/h-1.0) (Vf=1%)

Specimen ID	RA%	Kl/r	Failure Load (kN)	Change in strength
S-RA0Vf1E1.0	0	17.24	112	
S-RA100Vf1E1.0	100		107	-4.46%
T-RA0Vf1E1.0	0	26	87	
T-RA100Vf1E1.0	100		86.5	-0.57%
L-RA0Vf1E1.0	0	34.5	76.5	
L-RA100Vf1E1.0	100		80.5	+5.23%

Figure 4.26 illustrates the impact of replacing the natural aggregate with recycled aggregate. In samples with slenderness ratios of 17.24 and 26, the strength decreased, whereas it increased in samples with a slenderness ratio of 34.5. Similarly, Figure 4.27 demonstrates this trend for the columns with

the addition of steel fiber, with smaller slenderness ratios (17 and 26) showing a decreased strength while the larger slenderness ratio (34.5) exhibiting an increased strength when the natural aggregate was replaced by recycled aggregate.

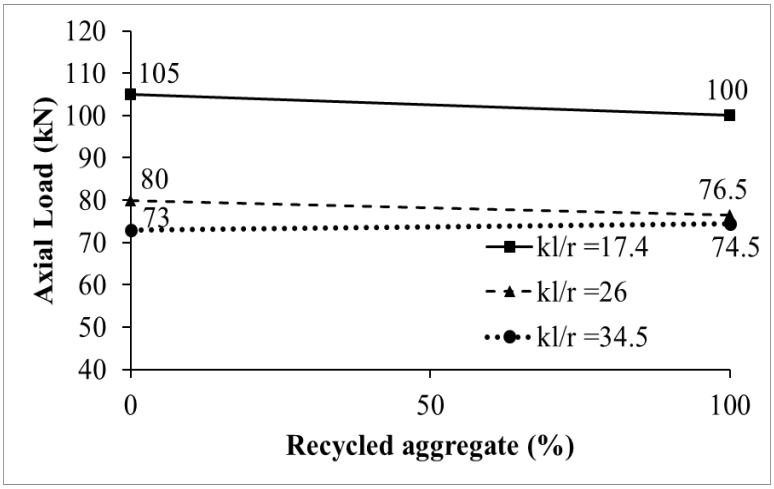

Figure 4.26: Effect of recycled aggregate on strength (e/h=1.0) (Vf=0)

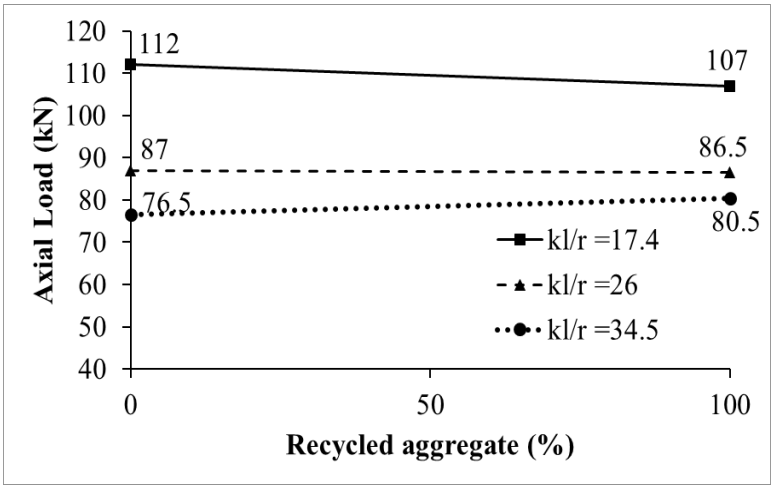

Figure 4.27: Effect of recycled aggregate on strength (e/h=1.0) (Vf=1.0)

4.4.2.2.2 The Effect of Slenderness Ratio (kl/r) on Column Capacity

In the columns loaded with the largest eccentricity (e/h = 1.0) and made with 100% recycled aggregate, the samples T-RA100Vf0E1.0 and L-RA100Vf0E1.0 experienced strength decreases of 23.5% and 25.5%, respectively, compared to S-RA100Vf0E1.0. Similar trends were observed in

columns with 100% natural aggregate: the slender column T-RA0Vf0E1.0 lost 23.8% of its strength compared to the short column S-RA0Vf0E1.0, and the slender column L-RA0Vf0E1.0 exhibited a 30.5% reduction in the strength compared to S-RA0Vf0E1.0. Table 4.18 provides the comparison, and Figure 4.28 displays it graphically.

In columns with 1% steel fiber and 100% recycled aggregate, the sample T-RA100Vf1E1.0 experienced a 19.2% reduction in the strength compared to S-RA100Vf1E1.0, while L-RA100Vf1E1.0 lost 24.8% of the strength compared to S-RA100Vf1E1.0.

While the addition of steel fibers generally improves the tensile strength and ductility of concrete, their effectiveness can be influenced by the aggregates used. In T-RA100Vf1E1.0, the fibers may better integrate with the recycled aggregate matrix, resulting in a smaller strength reduction compared to L-RA100Vf1E1.0. The way fibers are dispersed within the mix and their interaction with recycled aggregates can significantly impact the composite's overall performance. Ramesh et al. (2019)

Table 4.18 Effect of slenderness ratio on column capacity (e/h=1.0) (Vf=0%)

Specimen ID	RA%	Kl/r	Failure Load (kN)	Decrease (%)
S-RA100Vf0E1.0	100%	17.24	100	
T-RA100Vf0E1.0		26	76.5	23.5%
L-RA100Vf0E1.0		34.5	74.5	25.5%
S-RA0Vf0E1.0	0%	17.24	105	
T-RA0Vf0E1.0		26	80	23.8%
L-RA0Vf0E1.0		34.5	73	30.5%

Table 4.19 Effect of slenderness ratio on column capacity (e/h=1.0) (Vf=1%)

Specimen ID	RA%	Kl/r	Failure Load (kN)	Decrease (%)
S-RA100Vf1E1.0	100%	17.24	107	
T-RA100Vf1E1.0		26	86.5	19.2%
L-RA100Vf1E1.0		34.5	80.5	24.8%
S-RA0Vf1E1.0	0%	17.7	112	
T-RA0Vf1E1.0		26	87	22.3%
L-RA0Vf1E1.0		34.5	76.5	31.7%

In columns with 100% natural aggregate and 1% steel fiber, the maximum strength of the slender column T-RA0Vf1E1.0 decreased by 22.3% compared to the short column S-RA0Vf1E1.0, and the maximum strength of the slender column L-RA0Vf1E1.0 decreased by 31.7% compared to the short column S-RA0Vf1E1.0. Table 4.19 and Figure 4.29 provide comparisons. It appears that the column load capacity decreases as the slenderness ratio increases, regardless of the type of aggregate (recycled or natural) or the presence of steel fiber, increases in slenderness ratio lead to significant reductions in load-bearing capacity due to lateral deflections and buckling. Abdulla (2020).

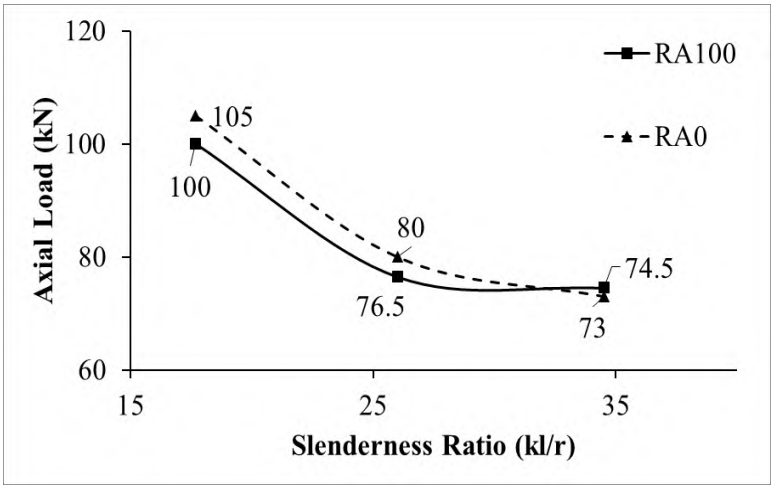

Figure 4.28: Effect of slenderness ratio on column capacity (e/h=1) (Vf=0%)

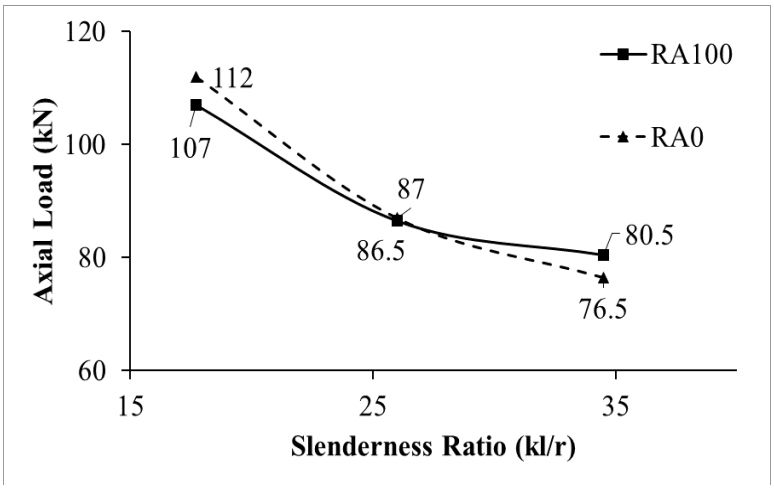

Figure 4.29: Effect of slenderness ratio on column capacity (e/h=1) (Vf=1%)

4.4.2.2.3 Effect of Steel Fiber Content (Vf) on Column Capacity

In columns loaded with the largest eccentricity (e/h = 1.0), the addition of the steel fiber increased the strength of the column, regardless of whether the columns were made of natural or recycled aggregate. Table 4.20 illustrates this effect of the steel fiber. For example, S-RA100Vf1E1.0 showed a 7% increase in the strength compared to C11-RA100-Vf0, while S-RA0Vf1E1.0 exhibited a 6.67% increase compared to S-RA0Vf0E1.0. Similarly, T-RA100Vf1E1.0 and T-RA0Vf1E1.0 experienced increases of 13.1% and 8.7%, respectively, compared to their counterparts without steel fiber. The long columns L-RA100Vf1E1.0 and L-RA0Vf1E1.0 demonstrated increases of 8.1% and 4.8%, respectively, compared to L-RA100Vf0E1.0 and L-RA0Vf0E1.0. Figures 4.30, 4.31, and 4.32 provide a graphical representation of this comparison, with separate graphs for the slenderness ratios of 17.24, 26, and 34.5. As a conclusion, the columns with steel fiber exhibit higher load values compared to those without it.

Table 4.20 Effect of 1% steel fiber on column capacity (e/h=1.0)

Specimen ID	Failure Load (kN)	Specimen ID	Failure Load (kN)	Change in Strength
S-RA100Vf0E1.0	100	S-RA100Vf1E1.0	107	7.0%
S-RA0Vf0E1.0	105	S-RA0Vf1E1.0	112	6.7%
T-RA100Vf0E1.0	76.5	T-RA100Vf1E1.0	86.5	13.1%
T-RA0Vf0E1.0	80	T-RA0Vf1E1.0	87	8.7%
L-RA100Vf0E1.0	74.5	L-RA100Vf1E1.0	80.5	8.1%
L-RA0Vf0E1.0	73	L-RA0Vf1E1.0	76.5	4.8%

4.4.3 Effect of Eccentricity on Column Capacity

In general, the ultimate strength of the columns decreased with the increase of the eccentricity. This decrease in the load-carrying capacity is attributed to the increase in the moment arm and subsequent increase in the moment. The impact of the eccentricity was more significant in columns with higher slenderness ratio, as the curvature increased. This observation was for all tested samples, irrespective of the aggregate type or the addition of steel fiber.

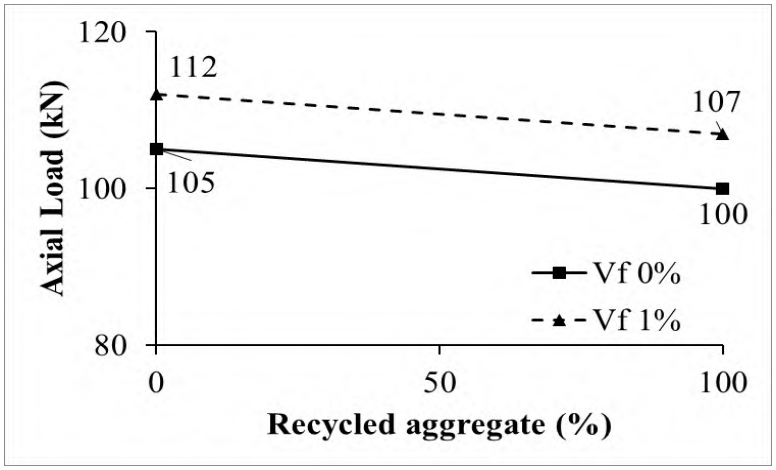

Figure 4.30: Effect of Vf on strength for different RA ratios (kl/r =17.24) (e/h = 1.0)

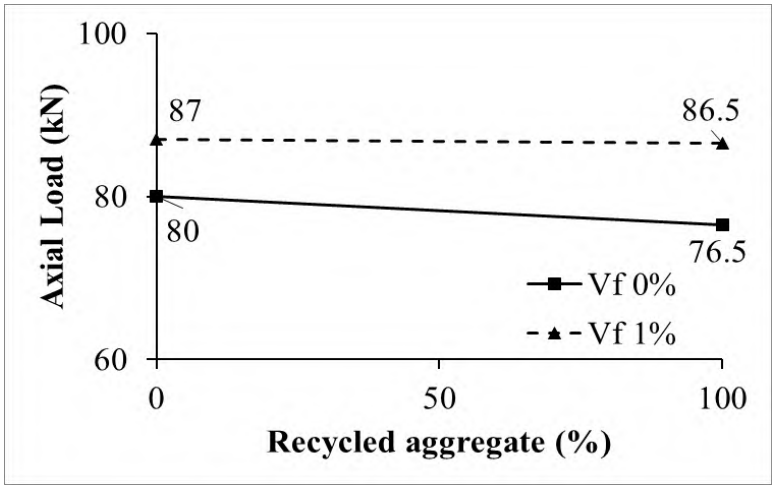

Figure 4.31: Effect of Vf on strength for different RA ratios (kl/r = 26, e/h = 1.0)

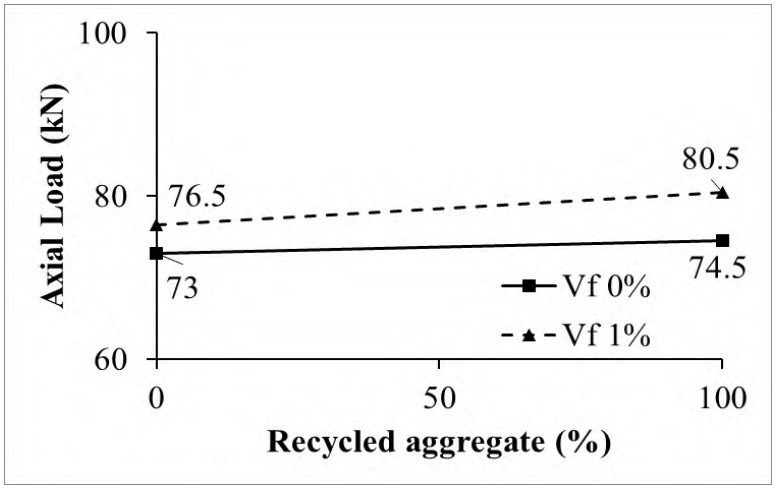

Figure 4.32: Effect of Vf on strength for different RA ratios (kl/r = 34.5, e/h = 1.0)

4.4.3.1 Effect of Eccentricity on Short Column Capacity (kl/r = 17.24).

Table 4.21 displays the results for samples made of 100% natural aggregate, indicating a loss of strength due to eccentric loading. For instance, the sample S-RA0Vf0E0.5 with e/h=0.5 lost 69.1% of its strength compared to S-RA0Vf0E0 with zero eccentricity, while S-RA0Vf0E1.0 with e/h=1 lost 84.6%. Similarly, samples made of 100% recycled aggregate also experienced strength loss with increased eccentricity. For example, S-RA100Vf0E0.5 lost 74.1% of its strength compared to S-RA100Vf0E0, and S-RA100Vf0E1.0 lost 86.4%. Figure 4.33 illustrates this comparison graphically, showing a significant drop in the curve's slope as eccentricity increases from e/h=0 to e/h=0.5.

Table 4.22 presents the results for the samples made of 100% natural aggregate, indicating a loss of strength due to eccentric loading. For instance, sample S-RA0-Vf1E0.5 with e/h=0.5 lost 69.5% of its strength compared to S-RA0Vf1E0 with zero eccentricity, while S-RA0Vf1E1.0 with e/h=1 lost 84.3% of its strength. Similarly, the samples made of 100% recycled aggregate also experienced strength loss with the increase in the eccentricity in loading. Figure 4.34 illustrates this comparison graphically, with a significant drop in the curve's slope observed from e/h=0 to e/h=0.5. To justify the results: eccentric loading introduces bending moments in addition to axial loads. When the load is not applied directly through the centroid of the cross-section, it creates a moment that leads to additional stresses in the material. As the ratio of eccentricity to height (e/h) increases, the moment increases, which leads to greater tensile and compressive stresses in the material. This is particularly critical for both natural and recycled aggregates, where the material properties may differ. Liu et al. (2023).

Table 4.21 Effect of eccentricity on column capacity (kl/r=17.24) (Vf=0%)

Specimen ID	RA (%)	Kl/r	e/h	Failure Load (kN)	Decrease in strength (%)
S-RA0Vf0E0	0	17.24	0	680	
S-RA0Vf0E0.5	0	17.24	0.5	210	69.1%
S-RA0Vf0E1.0	0	17.24	1	105	84.6%
S-RA100Vf0E0	100	17.24	0	735	
S-RA100Vf0E0.5	100	17.24	0.5	190	74.1%
S-RA100Vf0E1.0	100	17.24	1	100	86.4%

Table 4.22 Effect of eccentricity on column capacity (kl/r=17.24) (Vf=1%)

Specimen ID	RA (%)	Kl/r	e/h	Failure Load (kN)	Decrease in strength (%)
S-RA0Vf1E0	0	17.24	0	714	
S-RA0-Vf1E0.5	0	17.24	0.5	218	69.5%
S-RA0Vf1E1.0	0	17.24	1	112	84.3%
S-RA100Vf1E0	100	17.24	0	700	
S-RA100Vf1E0.5	100	17.24	0.5	223	68.1%
S-RA100Vf1E1.0	100	17.24	1	107	84.7%

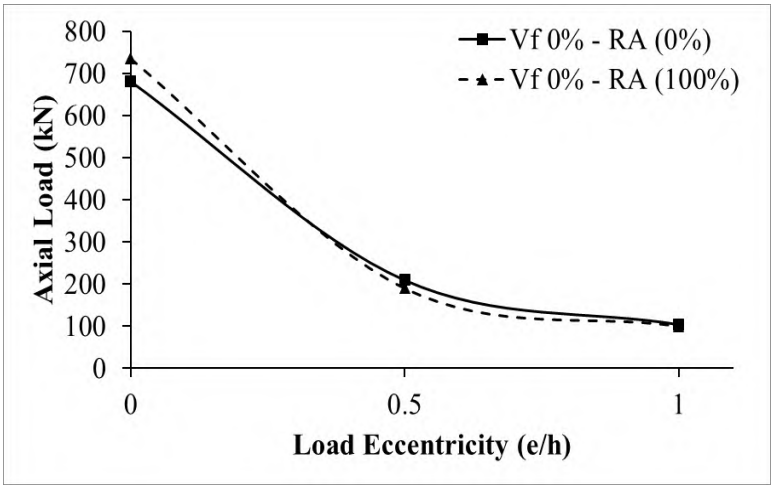

Figure 4.33: Effect of eccentricity on column capacity (kl/r =17.24) (Vf=0%)

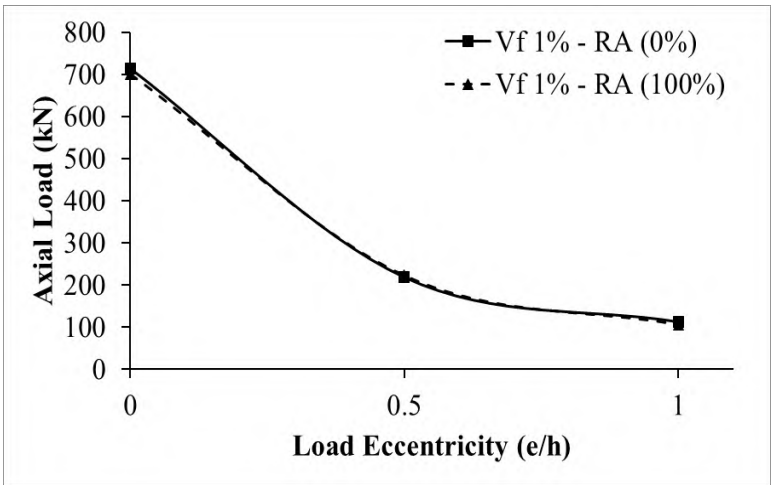

Figure 4.34: Effect of eccentricity on column Capacity (kl/r =17.24) (Vf=1%)

4.4.3.2 Effect of Eccentricity on Slender Column Capacity (kl/r = 26).

In columns with the slenderness ratio of 26 with no addition of steel fiber, the change in the e/h of the loading from zero to 0.5 and then to 1.0 significantly affected the strength. For instance, T-RA0Vf0E0.5 (e/h=0.5) lost 73.3% of its strength compared to T-RA0Vf0E0 (e/h=0), and T-RA0Vf0E1.0 (e/h=1.0) lost 87.6% of its strength compared to T-RA0Vf0E0, both samples made of 100% natural aggregate. Similarly, the samples made of 100% recycled aggregate exhibited the strength loss due to the eccentricity: T-RA100Vf0E0.5 (e/h=0.5) lost 74.9% compared to T-RA100Vf0E0 (e/h=0), and T-RA100Vf0E1.0 (e/h=1.0) lost 89.1% of its strength compared to T-RA100Vf0E0. Table 4.23 presents these results for samples without steel fiber, while Table 4.24 compares the samples with the addition of 1% steel fiber. Figure 4.35 illustrates the reduction in sample strength due to the eccentric loading, with a more significant loss observed when moving from e/h=0 to e/h=0.5 compared to e/h=0.5 to e/h=1.0.

Table 4.23 Effect of eccentricity on column capacity (kl/r=26) (Vf=0%)

Specimen ID	RA (%)	Kl/r	e/h	Failure Load (kN)	Decrease in strength (%)
T-RA0Vf0E0	0	26	0	645	
T-RA0Vf0E0.5	0	26	0.5	172	73.3%
T-RA0Vf0E1.0	0	26	1	80	87.6%
T-RA100Vf0E0	100	26	0	700	
T-RA100Vf0E0.5	100	26	0.5	176	74.9%
T-RA100Vf0E1.0	100	26	1	76.5	89.1%

Table 4.24 Effect of eccentricity on column capacity (kl/r=26) (Vf=1%)

Specimen ID	RA (%)	Kl/r	e/h	Failure Load (kN)	Decrease in strength (%)
T-RA0Vf1E0	0	26	0	678	
T-RA0Vf1E0.5	0	26	0.5	177	73.8%
T-RA0Vf1E1.0	0	26	1	87	87.1%
T-RA100Vf1E0	100	26	0	723	
T-RA100Vf1E0.5	100	26	0.5	186	74.3%
T-RA100Vf1E1.0	100	26	1	86.5	88.0%

Figure 4.36 presents a similar comparison with the addition of steel fiber, where there is no significant differences in the behavior of the column with the recycled aggregate with those with the natural aggregate. The relationship between loading eccentricity and strength loss is often nonlinear. Early stages of eccentric loading exert greater relative stress increases compared to later stages, leading to a more significant loss of load-carrying capacity when moving from e/h=0 to e/h=0.5. Mamlouk and Zaniewski (2014)

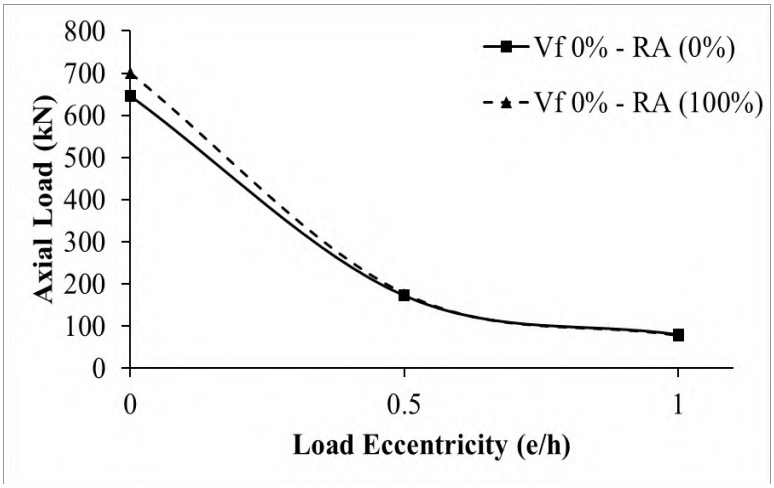

Figure 4.35: Effect of eccentricity on column capacity (kl/r =26) (Vf=0%)

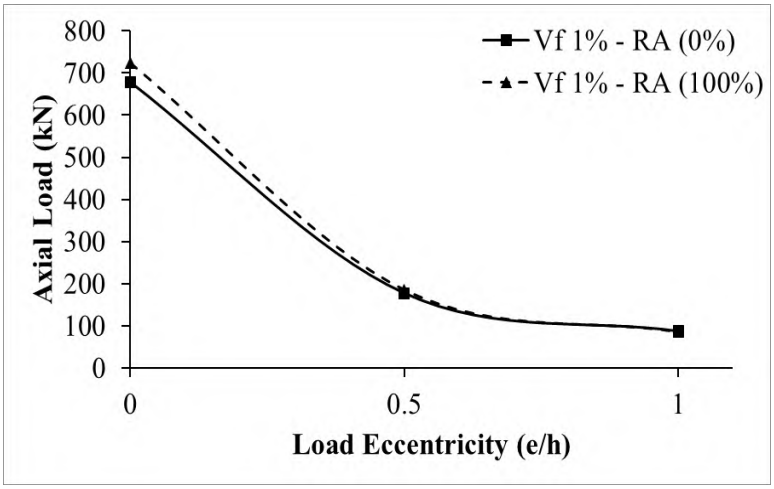

Figure 4.36: Effect of eccentricity on column capacity (kl/r =26) (Vf=1%)

4.4.3.3 Effect of Eccentricity on Slender Column Capacity (kl/r = 34.5).

Table 4.25 illustrates the impact of the slenderness ratio on the maximum strength, particularly at the largest eccentricity. For the columns without steel fiber and comprising 100% natural aggregate, L-RA0Vf0E0.5 (e/h=0.5) experienced a 75% strength reduction compared to L-RA0Vf0E0 (e/h=0), while L-RA0Vf0E1.0 lost 89% of its strength relative to L-RA0Vf0E0. Similarly, in samples without steel fiber and composed entirely of recycled aggregate, L-RA100Vf0E0.5 (e/h=0.5) suffered a 77% strength loss compared

to L-RA100Vf0E0 (e/h=0), and L-RA100Vf0E1.0 (e/h=1.0) experienced an 89% strength reduction compared to L-RA100Vf0E0. Figure 4.37 provides a graphical representation of this comparison, demonstrating the reduction in the strength as the loading eccentricity increases.

Table 4.25 Effect of eccentricity on column capacity (kl/r=34.5) (Vf=0%)

Specimen ID	RA (%)	Kl/r	e/h	Failure Load (kN)	Decrease in strength (%)
L-RA0Vf0E0	0	34.5	0	642	
L-RA0Vf0E0.5	0	34.5	0.5	158	75%
L-RA0Vf0E1.0	0	34.5	1	73	89%
L-RA100Vf0E0	100	34.5	0	690	
L-RA100Vf0E0.5	100	34.5	0.5	161	77%
L-RA100Vf0E1.0	100	34.5	1	74.5	89%

Table 4.26 illustrates the strength reduction in the columns with 1% of fiber content as the eccentricity increases from 0% to 100%. For columns containing steel fiber and composed of 100% natural aggregate, L-RA0Vf1E0.5 lost 75% of its strength compared to L-RA0Vf1E0, while L-RA0Vf1E1.0 experienced an 88% strength reduction compared to L-RA0Vf1E0. Similarly, in samples made entirely of recycled aggregate, L-RA100Vf1E0.5 lost 77% of its strength compared to L-RA100Vf1E0, and L-RA100Vf1E1.0 underwent an 89% strength reduction compared to L-RA100Vf1E0. Figure 4.38 visually represents this decline in column strength as the eccentricity increases.

Table 4.26 Effect of eccentricity on column capacity (kl/r=34.5) (Vf=1%)

Specimen ID	RA (%)	Kl/r	e/h	Failure Load (kN)	Decrease in strength (%)
L-RA0Vf1E0	0	34.5	0	665	
L-RA0Vf1E0.5	0	34.5	0.5	168	75%
L-RA0Vf1E1.0	0	34.5	1	76.5	88%
L-RA100Vf1E0	100	34.5	0	701	
L-RA100Vf1E0.5	100	34.5	0.5	163	77%
L-RA100Vf1E1.0	100	34.5	1	80.5	89%

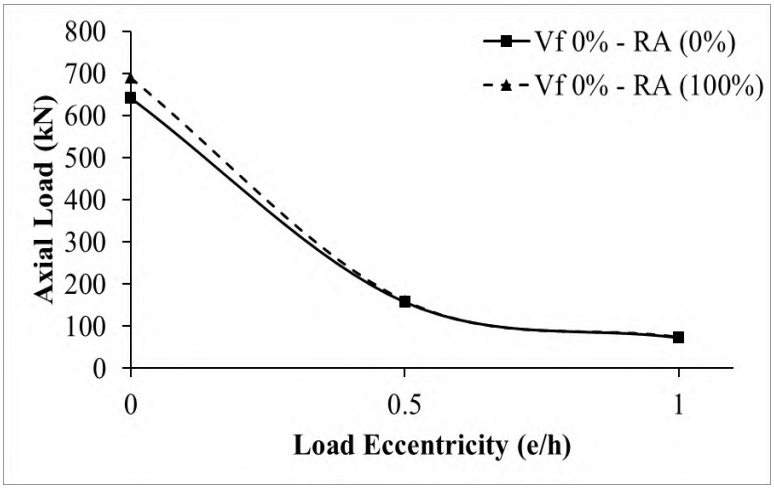

Figure 4.37: Effect of eccentricity on column capacity (kl/r =34.5) (Vf=0%)

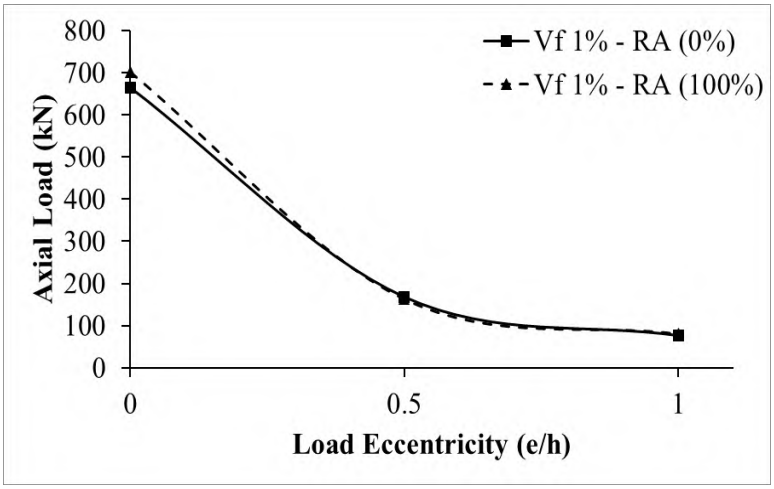

Figure 4.38: Effect of eccentricity on column capacity (kl/r =34.5) (Vf=1%)

4.5 CONCRETE STRAIN ANALYSIS

4.5.1 Concentrically Loaded Columns

4.5.1.1 Effect of Recycled Aggregate on Concrete Strain

Experimental test results in Table 4.27 show that the strain behavior of columns S-RA50Vf0E0, S-RA50Vf1E0, T-RA50Vf0E0, T-RA50Vf1E0, L-RA50Vf0E0, and L-RA50Vf1E0, made with 50% recycled aggregate, is quite similar to that of columns made with 100% recycled aggregate, as the strain test values are closely aligned. This behavior also matches that of samples S-RA0Vf0E0, S-RA0Vf1E0, T-RA0Vf0E0, T-RA0Vf1E0, L-RA0Vf0E0, and L-RA0Vf1E0 made of 100% natural aggregate. In the elastic stage of all concentrically loaded columns, compressive strain was linear, characterized by the sample resisting load with the entire cross-section in compression and no cracks. The slopes of the curves during this stage were similar across samples. Strains increased linearly to 80% or more of the maximum failure load before transitioning to a non-linear shape at the final stage. Table 4.28 indicates that differences in strain values are not due to the use of recycled aggregate, as they align with the 3000 micro-strains (με) specified by ACI318-19 for compression. Table 4.28 also shows the experimentally measured concrete strains on the tension face, which are comparable to the 3000 micro-strains (με) specified for compression. In concentrically loaded columns, the entire section is subjected to compression; however, differences in strain values between the compression and tension faces result from unintentional eccentricities during loading.

Table 4.27 Experimental test results

Specimen ID	Failure Load (kN)	Exp. Δ_{lat} (mm)	M_{1st} (kN.m)	M_{2nd} (kN.m)	$M_{1s}+M_{2nd}$	M2nd/M1st
S-RA0Vf0E0	680	1.03	0.00	0.70	0.70	----
S-RA50Vf0E0	710	1.10	0.00	0.78	0.78	----
S-RA100Vf0E0	735	0.93	0.00	0.68	0.68	----
T-RA0Vf0E0	645	2.55	0.00	1.64	1.64	----
T-RA50Vf0E0	685	2.62	0.00	1.79	1.79	----
T-RA100Vf0E0	700	2.40	0.00	1.68	1.68	----
L-RA0Vf0E0	642	3.50	0.00	2.25	2.25	----
L-RA50Vf0E0	678	4.50	0.00	3.05	3.05	----
L-RA100Vf0E0	690	4.20	0.00	2.90	2.90	----
S-RA0Vf1E0	714	1.11	0.00	0.79	0.79	----
S-RA50Vf1E0	730	1.25	0.00	0.91	0.91	----
S-RA100Vf1E0	748	1.08	0.00	0.81	0.81	----
T-RA0Vf1E0	678	2.65	0.00	1.72	1.72	----
T-RA50Vf1E0	700	2.80	0.00	1.96	1.96	----
T-RA100Vf1E0	723	2.30	0.00	1.66	1.66	----
L-RA0Vf1E0	665	3.73	0.00	2.48	2.48	----
L-RA50Vf1E0	692	5.40	0.00	3.74	3.74	----
L-RA100Vf1E0	701	4.39	0.00	3.08	3.08	----
S-RA100Vf0E0.5	190	2.79	11.88	0.53	12.40	4.46%
S-RA0Vf0E0.5	210	3.03	13.13	0.64	13.76	4.85%
T-RA100Vf0E0.5	176	6.00	11.00	1.06	12.06	9.60%
T-RA0Vf0E0.5	172	5.80	10.75	1.00	11.75	9.28%
L-RA100Vf0E0.5	161	10.34	10.06	1.66	11.73	16.55%
L-RA0Vf0E0.5	158	10.32	9.88	1.63	11.51	16.51%
S-RA100Vf1E0.5	223	3.59	13.94	0.80	14.74	5.75%
S-RA0-Vf1E0.5	218	3.45	13.63	0.75	14.38	5.51%
T-RA100Vf1E0.5	186	6.65	11.63	1.24	12.86	10.64%
T-RA0Vf1E0.5	177	6.70	11.06	1.19	12.25	10.72%
L-RA100Vf1E0.5	163	11.06	10.19	1.80	11.99	17.70%
L-RA0Vf1E0.5	168	11.58	10.50	1.95	12.45	18.53%
S-RA100Vf0E1.0	100	3.87	12.50	0.39	12.89	3.09%
S-RA0Vf0E1.0	105	3.52	13.13	0.37	13.49	2.82%
T-RA100Vf0E1.0	76.5	7.70	9.56	0.59	10.15	6.16%
T-RA0Vf0E1.0	80	7.90	10.00	0.63	10.63	6.32%
L-RA100Vf0E1.0	74.5	13.13	9.31	0.98	10.29	10.50%
L-RA0Vf0E1.0	73	13.03	9.13	0.95	10.08	10.42%
S-RA100Vf1E1.0	107	4.79	13.38	0.51	13.89	3.83%
S-RA0Vf1E1.0	112	4.13	14.00	0.46	14.46	3.30%
T-RA100Vf1E1.0	86.5	8.25	10.81	0.71	11.53	6.60%
T-RA0Vf1E1.0	87	8.50	10.88	0.74	11.61	6.80%
L-RA100Vf1E1.0	80.5	14.10	10.06	1.14	11.20	11.28%
L-RA0Vf1E1.0	76.5	13.49	9.56	1.03	10.59	10.79%

This stage was characterized by the sample resisting the load, with the entire cross-section in compression and no cracks forming yet. The slope of the curves during this stage was also similar across the samples. The strains increased linearly to 80% or more of the maximum failure load before transitioning to a non-linear shape at the final stage. As shown in Table 4.28, the differences in the strain values are not attributed to the use of the recycled aggregate; the values are comparable to the 3000 micro-strains (με) specified by ACI318-19 in compression.

Table 4.28 also shows the experimentally measured concrete strains on the tension face, which are comparable to the 3000 micro-strains (με) specified by ACI318-19 for compression. In the concentrically loaded columns, the entire section is subjected to compression. However, the differences in strain values between the compression face and the tension face are due to unintentional eccentricities that occurred during the loading process.

4.5.1.2 Effect of Steel Fiber on Concrete Strain

The addition of steel fiber increased the strain in the concrete. With the use of the steel fiber, the samples reached higher loads at lower strain. In columns without the use of the steel fiber, concrete failed in compression at strains of around 3350 με. With the use of the steel fiber, the failure strain increased to approximately 3800 με. This difference is attributed to the enhanced resistance strength provided by the steel fiber. Additionally, the incorporation of the steel fiber improved the deformability of both natural and recycled aggregate concrete columns.

Table 4.28 Maximum concrete strain in compression (e/h=0)

Specimen ID	Failure Load (kN)	c_{ACI}	The strain on the compression face		The strain on the tension face	
			ACI strain (με)	Exp. ε_{cc} (με)	ACI strain (με)	Exp. ε_{ct} (με)
S-RA0Vf0E0	680	∞	-3000	-2909	-3000	-2909
S-RA50Vf0E0	710	∞	-3000	-2995	-3000	-2995
S-RA100Vf0E0	735	∞	-3000	-3024	-3000	-3024
T-RA0Vf0E0	645	∞	-3000	-2988	-3000	-2988
T-RA50Vf0E0	685	∞	-3000	-3080	-3000	-3080
T-RA100Vf0E0	700	∞	-3000	-3106	-3000	-3106
L-RA0Vf0E0	642	∞	-3000	-3046	-3000	-3046
L-RA50Vf0E0	678	∞	-3000	-3158	-3000	-3158
L-RA100Vf0E0	690	∞	-3000	-3256	-3000	-3256
S-RA0Vf1E0	714	∞	-3000	-3150	-3000	-3150
S-RA50Vf1E0	730	∞	-3000	-3311	-3000	-3311
S-RA100Vf1E0	748	∞	-3000	-3392	-3000	-3392
T-RA0Vf1E0	678	∞	-3000	-3192	-3000	-3192
T-RA50Vf1E0	700	∞	-3000	-3324	-3000	-3324
T-RA100Vf1E0	723	∞	-3000	-3382	-3000	-3382
L-RA0Vf1E0	665	∞	-3000	-3486	-3000	-3486
L-RA50Vf1E0	692	∞	-3000	-3750	-3000	-3750
L-RA100Vf1E0	701	∞	-3000	-3852	-3000	-3852

4.5.1.3 Effect of Slenderness Ratio on Concrete Strain

The increase in the slenderness ratio resulted in an increased strain at the same load level, concrete reaches higher strains, or its crushing strain, at lower loads when the slenderness ratio is higher. The concrete achieves its crushing or failure strain independent of the load value; however, as the slenderness ratio increases, the sample becomes weaker than the shorter columns, leading to higher strains sooner and at lower loads. Overall, the effect of column

slenderness on the concrete strains at failure was insignificant and not observed, but the impact at the same load level was more evident. The effect of the slenderness ratio in columns with steel fiber was similar to those without steel fiber, although in a higher range, due to the minimal effect of steel fiber in compression.

4.5.2 Eccentrically Loaded Columns (e=0.5h)

4.5.2.1 Effect of Recycled Aggregate on Concrete Strain

Comparing the strain of the samples made with the natural aggregate to the samples made with the recycled aggregate, the differences are negligible. It is observed the behavior is similar to a large extent. The only difference that can be seen is the effect of the maximum failure load. This is correct for the samples made with and without steel fiber. Table 4.29 presents both the measured experimental strain values at the maximum failure load and the calculated strain values in tension and compression. The equation (4-2) was used to determine the strain values based on the compressive depth (C) value, which is taken from the P-M Diagram analysis at the loaded eccentricity.

$$\varepsilon_{ct} = \frac{h-c}{c} \times 0.003 \text{ ---------- (4-2)}$$

The experimental strain values are slightly higher than the theoretically calculated strain values in compression, which can be attributed to simplified assumptions in the calculations, such as the homogeneity of the section and the linear distribution of strain. Conversely, the calculated values for the tension face are higher than the experimentally measured concrete strains in

tension. This discrepancy is due to that the calculated values being purely mathematical, while the concrete in tension is weak normally. Additionally, the tension strains in the concrete are much higher in columns containing steel fibers and the cause has been explained earlier in this section.

4.5.2.2 Effect of Steel Fiber on Concrete Strain

The addition of the steel fiber enhances the deformability of samples made from both natural and recycled aggregates. The steel fiber reduces the strain at the same load level in both types of samples. This is because the steel fiber increases the stiffness, as the modulus of elasticity of steel fiber is significantly higher than that of concrete. In columns without steel fiber, the concrete failed in compression at strains of around 3240 με. With the inclusion of the steel fiber, the failure strain increased to approximately 3860 με. Consequently, the samples with steel fiber exhibited less strain compared to those without steel fiber at the same load level. Additionally, the samples with steel fiber achieved higher strain levels.

4.5.2.3 Effect of Slenderness Ratio on Concrete Strain

It has been shown in both cases, NA and RA, that the samples with a higher slenderness ratio reached their maximum load strains sooner than the shorter column samples. The early linear part of the curves was very close one to another. The behavior of concrete itself can explain this. In other words, the concrete had a maximum strain to reach at the time of failure in compression as the slenderness increased. Furthermore, the column fails in slightly lower load when the slenderness of the column increases

Table 4.29 Maximum concrete strain in compression (e/h=0.5)

Specimen ID	Failure Load (kN)	c_{ACI}	The strain on the compression face		The strain on the tension face	
			ACI strain (με)	Exp. εcc (με)	ACI strain (με)	Exp. εct (με)
S-RA100Vf0E0.5	190	61.60	-3000	-3287	3088	917
S-RA0Vf0E0.5	210	61.25	-3000	-3174	3122	284
T-RA100Vf0E0.5	176	57.02	-3000	-3374	3577	266
T-RA0Vf0E0.5	172	57.16	-3000	-3055	3561	929
L-RA100Vf0E0.5	161	55.78	-3000	-3327	3723	978
L-RA0Vf0E0.5	158	55.84	-3000	-3215	3716	177
S-RA100Vf1E0.5	223	63.20	-3000	-4191	2934	1755
S-RA0-Vf1E0.5	218	63.30	-3000	-3786	2924	57
T-RA100Vf1E0.5	186	57.44	-3000	-3850	3529	367
T-RA0Vf1E0.5	177	57.55	-3000	-3733	3516	1041
L-RA100Vf1E0.5	163	56.07	-3000	-3762	3688	1405
L-RA0Vf1E0.5	168	55.88	-3000	-3822	3711	1505

4.5.3 Eccentrically Loaded Columns (e=1.0h)

4.5.3.1 Effect of Recycled Aggregate on Concrete Strain

The effect of replacing the natural aggregate with recycled aggregate on the strain is small, as both types of columns exhibited similar behavior. Under eccentric loading of e/h=1.0, the strain in the concrete was lower than that in the samples loaded with the eccentricity of e/h=0.5 or concentrically loaded samples. The steel reinforcement yielded, reaching high strains and classifying these samples as tension-controlled, while the concrete in compression also reached high strains. A ductile behavior was observed in these samples. Samples T-RA100Vf0E1.0, T-RA0Vf0E1.0, L-RA0Vf0E1.0, L-RA100Vf1E1.0, and L-RA0Vf1E1.0 maintained strains below 3000 με at

the maximum failure load. Simultaneously, the steel in tension experienced higher tensile strain, as shown in the steel strain section. Table 4.30 presents the concrete compression strains at the maximum loads for columns loaded with (e/h = 1.0) eccentricity. The columns S-RA100Vf0E1.0 and S-RA0Vf0E1.0, with the slenderness ratio of 17.24, displayed similar behavior regarding the shape of the curves and the value of the loads versus the strains, this can be seen in the figures in appendix F. The column T-RA100Vf0E1.0, made of recycled aggregate, strained more than T-RA0Vf0E1.0, made of natural aggregate, at the same load level. Conversely, longer Column L-RA0Vf0E1.0, made of natural aggregate, strained more than L-RA100Vf0E1.0, made of recycled aggregate, at the same load level. Overall, the strain values were very close, indicating that the differences were not significant. Table 4.30 presents both the measured experimental strain values and the calculated strain values in tension and compression. The equation below was used to determine the strain values based on the compressive depth (C) value, which is taken from the P-M diagram analysis at the loaded eccentricity.

$$\varepsilon_{ct} = \frac{h-c}{c} \times 0.003$$ ---------- (4-2) repeated.

The experimental strain values were slightly higher than the theoretically calculated strain values in compression. This discrepancy can be attributed to simplified assumptions in the calculations, such as the homogeneity of the section and the linear distribution of strain. Conversely, the calculated values for the tension face were higher than the experimentally measured concrete strains in tension.

4.5.3.2 Effect of Steel Fiber on Concrete Strain

Table 4.30 present the concrete strain in compression on the compression face and tension face at failure loads. The concrete in columns lacking steel fiber experienced failure in compression at strains of approximately 3200 με, whereas with the addition of the steel fiber, the failure strain increased to around 3540 με on average. The inclusion of steel fiber enhances the deformability of samples, whether composed of natural or recycled aggregate, consistent with those loaded at eccentricity e/h=0.5. The steel fiber reduced the strain levels under matching loads compared to samples without the steel fiber, a trend observed across both aggregate types. In compression, the behavior remained consistent across all three sample heights. The steel fiber incorporation consistently decreased the strain levels under matching loads. However, samples containing steel fiber exhibit higher strains at failure loads for all three slenderness ratios of 17.24, 26, and 34.5. In tension, the experimental strain values indicated that the samples with steel fiber demonstrated higher strains than those without, as previously explained. However, both values were notably lower than the strain values calculated mathematically using the strain compatibility method, as explained in detail in Chapter 5.

4.5.3.3 Effect of Slenderness Ratio on Concrete Strain

The strain of the samples with the higher slenderness ratio of 34.5 was lower at the failure load compared with the columns with lower slenderness ratios of 26 and 17.24. This is likely attributed to the large eccentricity of e/h=1.0. In almost all the samples loaded with this large eccentricity, the reinforcement

on the compression face did not yield, consequently, the concrete did not strain to higher values. Conversely, the reinforcement in the tension face yielded and reached high values of strain, as it will be shown in section 4.8. The load was primarily resisted by the tension reinforcement rather than the compression reinforcement and concrete, classifying this behavior as ductile

4.5.4 Effect of Eccentricity on Compressive Strain of Concrete.

The failure in all the columns occurred by concrete crushing both in concentrically loaded columns and eccentrically loaded columns. Figures F1 to F15 in appendix F present the experimental axial load vs. longitudinal concrete compressive strain diagrams (at extreme compression fiber) for all the column specimens.

The concentrically loaded columns have a typical concrete strain curve. While the columns with e/h = 0.5 eccentricity have a short horizontal ending before the failure. However, the columns with e/h = 1.0 eccentricity have a longer horizontal ending before the failure of the columns.

Table 4.30 Maximum concrete strain in compression (e/h=1.0)

Specimen ID	Failure Load (kN)	C_{ACI}	The strain on the compression face		The strain on the tension face	
			ACI strain (με)	Exp. εcc (με)	ACI strain (με)	Exp. εct (με)
S-RA100Vf0E1.0	100	42.19	-3000	-3707	5888	700
S-RA0Vf0E1.0	105	42.78	-3000	-3761	5766	292
T-RA100Vf0E1.0	76.5	41.86	-3000	-2929	5958	955
T-RA0Vf0E1.0	80	40.93	-3000	-2991	6162	141
L-RA100Vf0E1.0	74.5	40.27	-3000	-2920	6312	181
L-RA0Vf0E1.0	73	41.15	-3000	-2954	6113	222
S-RA100Vf1E1.0	107	45.37	-3000	-3844	5265	1250
S-RA0Vf1E1.0	112	45.89	-3000	-3894	5172	1226
T-RA100Vf1E1.0	86.5	44.91	-3000	-3520	5350	1221
T-RA0Vf1E1.0	87	43.69	-3000	-3472	5583	1194
L-RA100Vf1E1.0	80.5	43.75	-3000	-3379	5571	1321
L-RA0Vf1E1.0	76.5	44.16	-3000	-3136	5492	1241

4.6 STEEL REINFORCEMENT STRAIN ANALYSIS

4.6.1 Concentrically Loaded Columns (e/h= 0)

4.6.1.1 Effect of Recycled Aggregate on Reinforcement Strain

All the concentrically loaded columns failed in compression, with all the longitudinal steel bars yielding in compression. Table 4.31 shows the percentage of the failure load at which the steel yielded, both in the compression and tension faces of the columns loaded concentrically. The columns yielded at a range between 73% and 95% of the failure load on the

compression face, and between 82% and 99% on the tension face, including columns with and without steel fiber. Table 4.31 also shows the compressive depth of concrete as theoretically infinite, since the entire section is under compression. However, "infinity" is a theoretical concept and, in practical terms, it can be understood as a very large number. The curves for columns with both types of aggregate appear similar to a great extent. Figures F16 to F36 in appendix F show that all the curves have a clear linear part as the load increases until the steel yields in compression. After yielding, the curve transitions to a non-linear portion, continues yielding, and then fails. Table 4.31 also compares the measured experimental strain and the strain calculated based on the strain compatibility method of ACI-318.

4.6.1.2 Effect of Steel Fiber on Reinforcement Strain

Tables 4.31 show the maximum strain values at the failure load of all the columns. The differences between the maximum strain values of columns with steel fiber and those without steel fiber are not significant. The steel fiber does not greatly affect the yield percentage, likely because all the columns were in compression. The average strain in columns without steel fiber is lower compared to the columns with steel fiber. However, at the same load level, the strains were lower in samples with steel fiber compared to those without. This difference is attributed to the increased stiffness due to the addition of steel fiber. Overall, the effect of the steel fiber on strain in compression is minor Caballero-Morrison et al. (2012).

4.6.1.3 Effect of Slenderness Ratio on Reinforcement Strain

In comparing columns with three different slenderness ratios, the strain curves are similar in both the linear part before yielding and the non-linear part after yielding, as shown in Figures F16 to F36 in appendix F. The different slenderness ratios do not result in noticeable differences in strain values at or before failure.

Table 4.31 Reinforcement strain for concentrically loaded columns

Specimen ID	Failure Load (kN)	c_{ACI}	The strain on the compression face			The strain on the tension face		
			ACI strain (με)	Exp. ε_{sc} (με)	Yield %	ACI strain (με)	Exp. ε_{st} (με)	Yield %
S-RA0Vf0E0	680	∞	-3000	-2932	75	-3000	-2932	92
S-RA50Vf0E0	710	∞	-3000	-2954	99	-3000	-2954	97
S-RA100Vf0E0	735	∞	-3000	-3055	97	-3000	-3055	89
T-RA0Vf0E0	645	∞	-3000	-2889	95	-3000	-2889	96
T-RA50Vf0E0	685	∞	-3000	-3064	99	-3000	-3064	99
T-RA100Vf0E0	700	∞	-3000	-3125	97	-3000	-3125	98
L-RA0Vf0E0	642	∞	-3000	-3194	98	-3000	-3194	85
L-RA50Vf1E0	678	∞	-3000	-3070	99	-3000	-3070	82
L-RA100Vf0E0	690	∞	-3000	-3261	93	-3000	-3261	89
S-RA0Vf1E0	714	∞	-3000	-3233	73	-3000	-3233	96
S-RA50Vf1E0	730	∞	-3000	-3244	98	-3000	-3244	88
S-RA100Vf1E0	748	∞	-3000	-3265	90	-3000	-3265	82
T-RA0Vf1E0	678	∞	-3000	-3200	97	-3000	-3200	96
T-RA50Vf1E0	700	∞	-3000	-3373	98	-3000	-3373	91
T-RA100Vf1E0	723	∞	-3000	-3488	99	-3000	-3488	93
L-RA0Vf1E0	665	∞	-3000	-3517	92	-3000	-3517	83
L-RA50Vf1E0	692	∞	-3000	-3701	95	-3000	-3701	82
L-RA100Vf1E0	701	∞	-3000	-3922	96	-3000	-3922	78

All the steel bars yielded in compression, and the strain values increased until the samples failed. However, the linear portions of the curves for columns with different slenderness ratios are similar, although longer columns failed at lower loads. The overall shape of the curves is consistent across different load values.

4.6.2 Eccentrically Loaded Columns (e= 0.5h)

4.6.2.1 Effect of Recycled Aggregate on Reinforcement Strain (e= 0.5h)

All the eccentrically loaded columns of e/h=0.5 failed in compression on the compression face and in tension on the tension face, with all longitudinal steel bars yielding in compression. However, the tension reinforcement did not yield in the short columns, whereas it did yield in the slender columns. Table 4.32 shows the percentage of the failure load at which the steel yielded, both in the compression and tension faces of the eccentrically loaded columns. The reinforcement yielded just before failure, around 99% of its load, and this is true for the reinforcement in both the tension and compression faces, including columns with and without steel fiber. Furthermore, the steel reinforcement reached its maximum values at much lower loads compared to the concentrically loaded columns. Table 4.32 also shows the compressive depth of concrete, which decreases as the slenderness ratio increases. This trend is observed in columns with steel fiber, albeit at larger compressive depth values. The value of C is smaller than in columns loaded concentrically but higher than in columns loaded with greater eccentricity, as it will be discussed in the next section.

The curves for columns with both types of aggregate appear to exhibit similar behavior and shape. Figures F16 to F36 in appendix F show that all the curves of the eccentrically columns have a shorter linear portion compared to those of concentrically loaded columns, as the load increases until the steel yields in compression and tension. After yielding, the curve transitions to a non-linear portion, continues to yield, and then fails. Table 4.32 compares the measured experimental strain with the strain calculated based on the strain compatibility method of ACI-318, which is taken from P-M interaction diagram analysis at certain eccentricities.

4.6.2.2 Effect of Steel Fiber on Reinforcement Strain (e = 0.5h)

Tables 4.32 show the maximum strain values at the failure load of all the eccentrically loaded columns. The differences between the maximum strain values of samples with steel fiber and those without are not significant. The steel fiber does not substantially affect the yield percentage in compression, though it has a more obvious effect in tension. At the same load level, strains are lower in samples with the steel fiber compared to those without. This difference is attributed to the increased stiffness due to the addition of steel fiber. Overall, the effect of the steel fiber on strain in compression is minor, but it is more pronounced in tension.

4.6.2.3 Effect of Slenderness Ratio on Reinforcement Strain (e = 0.5h)

For both groups of samples, with and without steel fiber, made with natural aggregate and recycled aggregate. The short column samples with a slenderness ratio (kl/r) of 17.24 had steeper slope curves than the other two

types of slender columns (kl/r = 26 and kl/r = 34.5). Samples with higher slenderness ratios had curves with smaller slopes than the shorter columns. The strain is inversely proportional to the slenderness ratio. Table 4.32 displays the strain values for eccentrically loaded columns at e/h = 0.5. Figures F16 to F36 in appendix F graphically show the effect of the parameters on the reinforcement strains for columns made without steel fiber compared to the columns made with the steel fiber.

Table 4.32 Reinforcement strain for eccentrically loaded columns (e/h = 0.5)

Specimen ID	Failure Load (kN)	c_{ACI}	The strain on the compression face			The strain on the tensinon face		
			ACI strain (με)	Exp. ε_{sc} (με)	Yield %	ACI strain (με)	Exp. ε_{st} (με)	Yield %
S-RA100Vf0E0.5	190	61.6	-1782	-2665	99%	-1870	-2273	-
S-RA0Vf0E0.5	210	61.3	-1775	-2687	98%	-1897	-2343	-
T-RA100Vf0E0.5	176	57.0	-1684	-2658	99%	-2261	-2787	96
T-RA0Vf0E0.5	172	57.2	-1688	-2776	98%	-2247	-2866	95
L-RA100Vf0E0.5	161	55.8	-1655	-2678	99%	-2377	-2827	99
L-RA0Vf0E0.5	158	55.8	-1657	-2812	98%	-2372	-2926	98
S-RA100Vf1E0.5	223	63.2	-1813	-2731	99%	-1746	-2452	-
S-RA0-Vf1E0.5	218	63.3	-1815	-2887	96%	-1739	-2395	-
T-RA100Vf1E0.5	186	57.4	-1694	-2688	100%	-2222	-2721	99
T-RA0Vf1E0.5	177	57.6	-1696	-2844	97%	-2212	-2919	99
L-RA100Vf1E0.5	163	56.1	-1662	-2659	100%	-2350	-2821	98
L-RA0Vf1E0.5	168	55.9	-1658	-2544	95%	-2367	-3069	98

4.6.3 Eccentrically Loaded Columns (e =1.0h)

4.6.3.1 Effect of Recycled Aggregate on Reinforcement Strain (e =1.0h)

Table 4.33 illustrates the impact of replacing natural aggregate with recycled aggregate. It reveals that the steel yielded in tension, with strains ranging between 4500 and 5000 με. The yielding occurred at a lower percentage of the failure load compared to columns loaded with lower eccentricity, as demonstrated in the preceding section. Conversely, the reinforcement steel in tension did not yield in any columns loaded eccentrically at e/h=1.0.

Moreover, Table 4.33 provides insight into the compressive depth of concrete, which decreases as the slenderness ratio increases. This trend holds for columns with steel fiber but at larger values of compressive depth. Additionally, it is observed that slender columns require less load to fail, yet the steel experiences high strains regardless of the applied load.

4.6.3.2 Effect of Steel Fiber on Reinforcement Strain (e =1.0h)

Tables 4.33 present the maximum strain values at the failure load of the all columns of e/h=1.0. The differences between the maximum strain values of samples with and without steel fiber are small. While the steel fiber has a minor impact on the yield percentage in compression, its effect is more evident in tension. The strains at the same load level are lower in samples with steel fiber compared to those without, which can be attributed to the increased stiffness resulting from the addition of steel fiber. In summary, while the effect of the steel fiber on strain in compression is minor, its influence is more pronounced in tension.

4.6.3.3 Effect of Slenderness Ratio on Reinforcement Strain (e =1.0h)

For both sets of samples, whether with or without steel fiber and composed of either natural or recycled aggregate, the slenderness ratio exhibited a consistent impact. Columns with a slenderness ratio (kl/r) of 17.24 displayed steeper slope curves compared to the other two types of slender columns (kl/r = 26 and kl/r = 34.5). Conversely, columns with higher slenderness ratios exhibited curves with smaller slopes than their shorter counterparts. The slopes observed are considerably smaller compared to those of columns loaded at lower eccentricity levels. Notably, the strain showed an inverse relationship with the slenderness ratio. This trend is represented in Table 4.32, which presents the strain values for eccentrically loaded columns at e/h = 1.0. Furthermore, Figures F16 to F36 in appendix F provide a graphical depiction of this effect.

4.6.4 Effect of Eccentricity on Reinforcement Strain

Figures F31 to F36 in appendix F display graphs of the axial load versus steel strain in tension and compression for eccentrically loaded columns. The response of axial strain in steel under compression and tension initially follows a linear path, then the slope decreases and flattens as the load approaches the failure load. The eccentrically loaded columns cracked earlier, causing the curve slope to change and flatten sooner compared to the concentrically loaded columns, as shown in Figures F16 to F30 in appendix F. The columns with steel fiber exhibited slightly a lower strain than those without steel fiber before yielding. However, this difference became more pronounced after the steel yielded.

Table 4.33 Reinforcement strain for eccentrically loaded columns (e/h = 1.0)

Specimen ID	Failure Load (kN)	c_{ACI}	The strain on the compression face			The strain on the tense face		
			ACI strain (με)	Exp. ε_{sc} (με)	Yield %	ACI strain (με)	Exp. ε_{st} (με)	Yield %
S-RA100Vf0E1.0	100	42.2	-1222	-1647	-	-4111	-4580	88
S-RA0Vf0E1.0	105	42.8	-1246	-2052	-	-4012	-4705	82
T-RA100Vf0E1.0	76.5	41.9	-1208	-1559	-	-4165	-4691	78
T-RA0Vf0E1.0	80	40.9	-1167	-1927	-	-4329	-4719	73
L-RA100Vf0E1.0	74.5	40.3	-1137	-1479	-	-4449	-4891	89
L-RA0Vf0E1.0	73	41.2	-1177	-1443	-	-4288	-4800	83
S-RA100Vf1E1.0	107	45.4	-1347	-1750	-	-3612	-4629	73
S-RA0Vf1E1.0	112	45.9	-1365	-1808	-	-3537	-4795	89
T-RA100Vf1E1.0	86.5	44.9	-1330	-1632	-	-3679	-4741	76
T-RA0Vf1E1.0	87	43.7	-1284	-1695	-	-3865	-4850	70
L-RA100Vf1E1.0	80.5	43.8	-1286	-1455	-	-3855	-5014	82
L-RA0Vf1E1.0	76.5	44.2	-1302	-1345	-	-3792	-4891	86

4.7 LATERAL DISPLACEMENT

4.7.1 Concentrically Loaded Columns (e/h = 0)

The load-displacement curves in Figures 4.39-4.52 can be divided into two distinct stages: the elastic stage and the elastic-plastic region. In the elastic stage, displacement increases linearly with load. However, as displacement continues into the elastic-plastic region, the load exhibits non-linear behavior until it peaks. Initially, displacements increase slowly, forming a linear branch up to about 70-80% of the failure load, followed by a flattened, semi-linear branch where displacement increases with little or no corresponding load increase. Finally, the maximum load is reached, leading to failure.

4.7.1.1 Effect of Recycled Aggregate on Lateral Displacement

Table 4.34 illustrates the influence of the recycled aggregate on the lateral displacement within concentrically loaded columns without the steel fiber reinforcement. The columns characterized by a kl/r ratio of 17.24, featuring S-RA100Vf0E0 incorporating 100% recycled aggregate, show a 10% decrease in the displacement in S-RA0Vf0E0 constituted solely of natural aggregate. Correspondingly, S-RA50Vf0E0, integrating a 50% substitution of the natural aggregate with recycled counterpart, demonstrates a 7% increase in the displacement. For columns with kl/r = 26, T-RA100Vf0E0, made entirely of recycled aggregate, shows a 6% reduction in the lateral displacement at the mid-height relative to T-RA0Vf0E0, which uses 100% natural aggregate. Conversely, T-RA50Vf0E0, featuring a 50% replacement of recycled aggregate, indicates a 3% increase in the displacement compared to T-RA0Vf0E0. In the columns characterized by kl/r = 34.5, a 20% increase in displacement is observed in L-RA100Vf0E0, entirely composed of recycled aggregate, in contrast to L-RA0Vf0E0 uses 100% natural aggregate. Conversely, L-RA50Vf1E0, incorporating a 50% substitution of recycled aggregate, shows only a 29% increase in the displacement relative to L-RA0Vf0E0. Table 4.34 outlines the influence of the recycled aggregate on the lateral displacement in the concentrically loaded columns enhanced with steel fiber. Contrary to the previous findings, the effect of recycled aggregate varies in columns with steel fiber reinforcement. The column S-RA100Vf1E0, incorporating 100% recycled aggregate, exhibits a 3% reduction in displacement compared to S-RA0Vf1E0, while S-RA50Vf1E0, with a 50% replacement, experiences 13% increase. Columns S-RA0Vf1E0, S-RA50Vf1E0, and S-RA100Vf1E0 share a slenderness ratio of 17.24. Within

the T-series columns, T-RA100Vf1E0 demonstrates a 6% decrease in displacement relative to T-RA0Vf1E0 and a 6% increase compared to T-RA50Vf1E0. The columns L-RA0Vf1E0, L-RA50Vf1E0, and L-RA100Vf1E0 possess a slenderness ratio of 34.5. L-RA100Vf1E0 exceeds L-RA0Vf1E0 by 18% in displacement and exceeds it by 45% compared to L-RA0Vf1E0. To justify the results, the increase and decrease in the value of displacement is a reflection of compressive strength and modulus of elasticity more than the type of aggregate.

Table 4.34: Effect of recycled aggregate on lateral displacement (e/h= 0)

Specimen ID	Vf %	Failure Load (kN)	ΔLat. (mm)	Effect of RA
S-RA0Vf0E0	0	680	1.03	
S-RA50Vf0E0	0	710	1.1	7%
S-RA100Vf0E0	0	735	0.93	-10%
T-RA0Vf0E0	0	645	2.55	
T-RA50Vf0E0	0	685	2.62	3%
T-RA100Vf0E0	0	700	2.4	-6%
L-RA0Vf0E0	0	642	3.5	
L-RA50Vf1E0	0	678	4.5	29%
L-RA100Vf0E0	0	690	4.2	20%
S-RA0Vf1E0	1	714	1.11	
S-RA50Vf1E0	1	730	1.25	13%
S-RA100Vf1E0	1	748	1.08	-3%
T-RA0Vf1E0	1	678	2.65	
T-RA50Vf1E0	1	700	2.8	6%
T-RA100Vf1E0	1	723	2.5	-6%
L-RA0Vf1E0	1	665	3.73	
L-RA50Vf1E0	1	692	5.4	45%
L-RA100Vf1E0	1	701	4.39	18%

4.7.1.2 Effect of Steel Fiber on Lateral Displacement

The introduction of the steel fiber increased the displacement capacity of the columns. However, when comparing S-RA100Vf1E0 to S-RA100Vf0E0, the former exhibited an 8% lower displacement, possibly attributable to a slightly lower failure load rather than the presence of steel fiber itself. Table 4.35 illustrates the percentage change in displacement resulting from the steel fiber addition.

In columns with a slenderness ratio of 17.24, both S-RA50Vf1E0 and S-RA0Vf1E0 demonstrated higher displacements than their counterparts S-RA50Vf0E0 and S-RA0Vf0E0, with increases of 14% and 8%, respectively. Similarly, columns T-RA0Vf1E0, T-RA50Vf1E0, and T-RA100Vf1E0 with a slenderness ratio of 26 exceeded the displacement of T-RA0Vf0E0, T-RA50Vf0E0, and T-RA100Vf0E0 by 4%, 7%, and 4%, respectively.

In columns with the slenderness ratio of 34.5, L-RA0Vf1E0, L-RA50Vf1E0, and L-RA100Vf1E0 displayed higher displacements than their counterparts L-RA0Vf0E0, L-RA50Vf1E0, and L-RA100Vf0E0, with increases of 5%, 20%, and 7%, respectively.

The addition of the steel fiber resulted in a reduced displacement at closely matching loads and generally showed a greater displacement under higher loads. This phenomenon can be attributed to the enhanced tensile resistance of concrete due to the presence of the steel fiber.

Table 4.35: Effect of steel fiber on lateral displacement (e/h = 0)

Specimen ID	Failure Load (kN)	ΔLat. (mm)	Specimen ID	Failure Load (kN)	ΔLat. (mm)	Effect of Vf
S-RA0Vf0E0	680	1.03	S-RA0Vf1E0	714	1.11	8%
S-RA50Vf0E0	710	1.1	S-RA50Vf1E0	730	1.25	14%
S-RA100Vf0E0	735	0.93	S-RA100Vf1E0	748	1.08	16%
T-RA0Vf0E0	645	2.55	T-RA0Vf1E0	678	2.65	4%
T-RA50Vf0E0	685	2.62	T-RA50Vf1E0	700	2.8	7%
T-RA100Vf0E0	700	2.4	T-RA100Vf1E0	723	2.5	4%
L-RA0Vf0E0	642	3.5	L-RA0Vf1E0	665	3.73	7%
L-RA50Vf0E0	678	4.5	L-RA50Vf1E0	692	5.4	20%
L-RA100Vf0E0	690	4.2	L-RA100Vf1E0	701	4.39	5%

4.7.1.3 Effect of slenderness ratio on Lateral Displacement

The columns with the slenderness ratio of 26, namely T-RA0Vf0E0, T-RA50Vf0E0, and T-RA100Vf0E0, exhibited significantly higher displacement compared to those with the ratio of 17.24 (S-RA0Vf0E0, S-RA50Vf0E0, and S-RA100Vf0E0) by 148%, 138%, and 158%, respectively. This data is presented in Tables 4.36 and 4.37, which detail the percentage increase in the lateral displacement for the slenderness ratios of 17.24, 26, and 34.5. Similarly, the columns with the slenderness ratio of 34.5, such as L-RA0Vf0E0, L-RA50Vf1E0, and L-RA100Vf0E0, exhibited notably a higher displacement compared to those with the ratio of 17.24 by 240%, 309%, and 352%, respectively. Upon introducing the steel fiber, a comparable trend is observed, as depicted in Table 4.37. The columns with the slenderness ratio of 26, including T-RA0Vf1E0, T-RA50Vf1E0, and T-RA100Vf1E0, displayed a higher displacement than those with the ratio of 17.24 (S-RA0Vf1E0, S-RA50Vf1E0, and S-RA100Vf1E0) by 139%, 124%, and

131%, respectively. Likewise, for the columns with the slenderness ratio of 34.5, such as L-RA0Vf1E0, L-RA50Vf1E0, and L-RA100Vf1E0, the displacement exceeded that of the 17.24 ratio columns. These results align with the column behavior mechanism: as the column length increases, the curvature rises, resulting in a greater displacement.

Table 4.36: Effect of slenderness on lateral displacement (e/h = 0, Vf = 0%)

Specimen ID	Kl/r	Failure Load (kN)	ΔLat. (mm)	Effect of kl/r
S-RA0Vf0E0	17.24	680	1.03	
T-RA0Vf0E0	26	645	2.55	147%
L-RA0Vf0E0	34.5	642	3.5	239%
S-RA50Vf0E0	17.24	710	1.1	
T-RA50Vf0E0	26	685	2.62	138%
L-RA50Vf1E0	34.5	678	4.5	309%
S-RA100Vf0E0	17.24	735	0.93	
T-RA100Vf0E0	26	700	2.4	158%
L-RA100Vf0E0	34.5	690	4.2	352%

Table 4.37: Effect of slenderness on lateral displacement (e/h = 0, Vf = 1%)

Specimen ID	Kl/r	Failure Load (kN)	ΔLat. (mm)	Effect of kl/r
S-RA0Vf1E0	17.24	714	1.11	
T-RA0Vf1E0	26	678	2.65	139%
L-RA0Vf1E0	34.5	665	3.73	236%
S-RA50Vf1E0	17.24	730	1.25	
T-RA50Vf1E0	26	700	2.8	124%
L-RA50Vf1E0	34.5	692	5.4	332%
S-RA100Vf1E0	17.24	748	1.08	
T-RA100Vf1E0	26	723	2.5	131%
L-RA100Vf1E0	34.5	701	4.39	306%

4.7.2 Eccentrically loaded columns, e=0.5h

4.7.2.1 Effect of Recycled Aggregate on Lateral Displacement

In the columns with a kl/r ratio of 17.24, those composed of 100% natural aggregate (S-RA0Vf0E0.5) exhibited a 9% higher horizontal displacement compared to counterpart with 100% recycled aggregate (S-RA100Vf0E0.5). Similarly, in the kl/r=26 columns, the displacement in the columns with 100% natural aggregate (T-RA0Vf0E0.5) was 3% lower than those with 100% recycled aggregate (T-RA100Vf0E0.5).

Adding the steel fiber to the columns with an eccentric loading of (e=0.5h) resulted in different maximum displacement compared to those without steel fiber. In the kl/r=17.24 columns, the displacement in the specimens with 100% natural aggregate (S-RA0Vf1E0.5) was 4% lower than those with 100% recycled aggregate (S-RA100Vf1E0.5). In the kl/r=26 columns, the displacement in the specimens with 100% natural aggregate (T-RA0Vf1E0.5) was 1% higher than those with 100% recycled aggregate (T-RA100Vf1E0.5). In the kl/r=34.5 columns, the displacement in the specimens with 100% natural aggregate (L-RA0Vf1E0.5) was only 2% lower than those with 100% recycled aggregate (L-RA100Vf1E0.5).

Table 4.38 demonstrates the effect of replacing 100% natural aggregate with recycled aggregate in the column samples. It's noted that not all specimens with the recycled aggregate exhibit greater displacement; some with natural aggregate displace further. Table 4.39 presents effect of RA on the lateral displacement for the columns made with steel fiber and loaded at eccentricity of e/h = 0.5.

Table 4.38: Effect of recycled aggregate on lateral displacement (e/h=0.5, Vf=0)

Specimen ID	RA%	Kl/r	Failure Load (kN)	ΔLat. (mm)	Effect of RA
S-RA100Vf0E0.5	100	17	190	2.79	
S-RA0Vf0E0.5	0	17	210	3.03	9%
T-RA100Vf0E0.5	100	26	176	6	
T-RA0Vf0E0.5	0	26	172	5.8	-3%
L-RA100Vf0E0.5	100	34.5	161	10.34	
L-RA0Vf0E0.5	0	34.5	158	10.32	-0.2%

Table 4.39: Effect of recycled aggregate on lateral displacement (e/h=0.5, Vf=1)

Specimen ID	RA%	Kl/r	Failure Load (kN)	ΔLat. (mm)	Effect of RA
S-RA100Vf1E0.5	100	17	223	3.59	
S-RA0-Vf1E0.5	0	17	218	3.45	-4%
T-RA100Vf1E0.5	100	26	186	6.65	
T-RA0Vf1E0.5	0	26	177	6.7	1%
L-RA100Vf1E0.5	100	34.5	163	11.06	
L-RA0Vf1E0.5	0	34.5	168	11.58	5%

4.7.2.2 Effect of Steel Fiber on Lateral Displacement

The comparison of the columns with 50% eccentricity, both with and without steel fiber, revealed significant differences. In the columns with a kl/r ratio of 17.24, S-RA100Vf1E0.5 exhibited a 29% higher displacement than S-RA100Vf0E0.5, while S-RA0-Vf1E0.5 showed a 14% increase compared to S-RA0Vf0E0.5. Moving to the columns with the kl/r ratio of 26, both T-RA100Vf1E0.5 and T-RA0Vf1E0.5 demonstrated 11% and 16% higher displacement, respectively, compared to their counterparts without steel fiber reinforcement, T-RA100Vf0E0.5, and T-RA0Vf0E0.5. Similarly, in the columns with the kl/r ratio of 34.5, both L-RA100Vf1E0.5 and L-

RA0Vf1E0.5 exhibited a higher displacement than L-RA100Vf0E0.5 and L-RA0Vf0E0.5, with increases of 7% and 12%, respectively. Table 4.40 provides a detailed analysis of the percentage increases for each sample with and without steel fibers.

Table 4.40: Effect of steel fiber on lateral displacement (e/h = 0.5)

Specimen ID	Failure Load (kN)	ΔLat. (mm)	Sample Name	Failure Load (kN)	ΔLat. (mm)	Effect of Vf
S-RA100Vf0E0.5	190	2.79	S-RA100Vf1E0.5	223	3.59	29%
S-RA0Vf0E0.5	210	3.03	S-RA0-Vf1E0.5	218	3.45	14%
T-RA100Vf0E0.5	176	6.00	T-RA100Vf1E0.5	186	6.65	11%
T-RA0Vf0E0.5	172	5.80	T-RA0Vf1E0.5	177	6.70	16%
L-RA100Vf0E0.5	161	10.34	L-RA100Vf1E0.5	163	11.06	7%
L-RA0Vf0E0.5	158	10.32	L-RA0Vf1E0.5	168	11.58	12%

4.7.2.3 Effect of Slenderness Ratio on Lateral Displacement

The columns T-RA100Vf0E0.5 and T-RA0Vf0E0.5, Figures 4.39-4.52, with the slenderness ratio of 26, exhibit higher displacements than S-RA100Vf0E0.5 and S-RA0Vf0E0.5 (kl/r=17.24) by 115% and 91%, respectively. Similarly, comparing the columns L-RA100Vf0E0.5 and L-RA0Vf0E0.5, with the slenderness ratio of 34.5, to the columns S-RA100Vf0E0.5 and S-RA0Vf0E0.5 (kl/r=17.24), revealed displacements 271% and 241% higher in the slender columns, respectively. In the case of the columns T-RA100Vf1E0.5 and T-RA0Vf1E0.5, with the slenderness ratio of 26, their displacements surpass those of S-RA100Vf1E0.5 and S-RA0-Vf1E0.5 (kl/r=17.24) by 85% and 94%, respectively. Likewise, comparing the columns L-RA100Vf1E0.5 and L-RA0Vf1E0.5, with a slenderness ratio of

34.5, to the columns S-RA100Vf1E0.5 and S-RA0-Vf1E0.5 (kl/r=17.24), indicated having higher displacements 208% and 236% in the slender columns. Table 4.41 provides a comparison between columns without steel fiber, while Table 4.42 compares the columns with steel fiber.

Table 4.41: Effect of slenderness on lateral displacement (e/h = 0.5, Vf = 0%)

Specimen ID	RA%	Kl/r	Failure Load (kN)	ΔLat. (mm)	Effect of kl/r
S-RA100Vf0E0.5	100	17.24	190	2.79	-
T-RA100Vf0E0.5	100	26	176	6	115%
L-RA100Vf0E0.5	100	34.5	161	10.34	271%
S-RA0Vf0E0.5	0	17.24	210	3.03	-
T-RA0Vf0E0.5	0	26	172	5.8	91%
L-RA0Vf0E0.5	0	34.5	158	10.32	241%

Table 4.42: Effect of slenderness on lateral displacement (e/h = 0.5, Vf = 1%)

Specimen ID	RA%	Kl/r	Failure Load (kN)	ΔLat. (mm)	Effect of kl/r
S-RA100Vf1E0.5	100	17.24	223	3.59	-
T-RA100Vf1E0.5	100	26	186	6.65	85%
L-RA100Vf1E0.5	100	34.5	163	11.06	208%
S-RA0-Vf1E0.5	0	17.24	218	3.45	-
T-RA0Vf1E0.5	0	26	177	6.7	94%
L-RA0Vf1E0.5	0	34.5	168	11.58	236%

4.7.3 Eccentrically loaded columns, e=1.0h

4.7.3.1 Effect of Recycled Aggregate on Lateral Displacement

For columns without steel fiber, the columns with a slenderness ratio of 17.24, Figures 4.39-4.52, the displacement of S-RA0Vf0E1.0 (NA) is 9% lower than that of S-RA100Vf0E1.0 (RA). Similarly, in the columns with a slenderness ratio of 26, the displacement of T-RA0Vf0E1.0 (NA) is 3% higher than that

of T-RA100Vf0E1.0 (RA). For the columns with kl/r=34.5, the displacement of L-RA0Vf0E1.0 (NA) is 1% lower than that of L-RA100Vf0E1.0 (RA). For the samples with steel fiber, the columns with the slenderness ratio of 17.24, the displacement of S-RA0Vf1E1.0 (NA) is 14% lower than that of S-RA100Vf1E1.0 (RA). Similarly, in the columns with a slenderness ratio of 26, the displacement of T-RA0Vf1E1.0 (NA) is 3% higher than that of T-RA100Vf1E1.0 (RA). For the columns with kl/r=34.5, the displacement of L-RA0Vf1E1.0 (NA) is 4% lower than that of L-RA100Vf1E1.0 (RA). Table 4.43 illustrates the effect of the use of the recycled aggregate on the lateral displacement by presenting the percentage of increase and decrease in the displacement compared to using natural aggregate. Similarly, Table 4.44 provides a comparison of the samples with steel fiber.

Table 4.43: Effect of recycled aggregate on lateral displacement (e/h=1.0, Vf=0)

Specimen ID	RA%	Kl/r	Failure Load (kN)	ΔLat. (mm)	Effect of RA
S-RA100Vf0E1.0	100	17.24	100	3.87	-
S-RA0Vf0E1.0	0	17.24	105	3.52	-9%
T-RA100Vf0E1.0	100	26	76.5	7.7	-
T-RA0Vf0E1.0	0	26	80	7.9	3%
L-RA100Vf0E1.0	100	34.5	74.5	13.13	-
L-RA0Vf0E1.0	0	34.5	73	13.03	-1%

Table 4.44: Effect of recycled aggregate on lateral displacement (e/h=1.0, Vf=1)

Sample Name	RA%	Kl/r	Failure Load (kN)	ΔLat. (mm)	Effect of RA
S-RA100Vf1E1.0	100	17.24	107	4.79	-
S-RA0Vf1E1.0	0	17.24	112	4.13	-14%
T-RA100Vf1E1.0	100	26	86.5	8.25	-
T-RA0Vf1E1.0	0	26	87	8.5	3%
L-RA100Vf1E1.0	100	34.5	80.5	14.1	-
L-RA0Vf1E1.0	0	34.5	76.5	13.49	-4%

4.7.3.2 Effect of Steel Fiber on Lateral Displacement

Comparing the columns with steel fiber with those without steel fiber, it became clear that there are notable differences in displacement. In the columns with a slenderness ratio of 17.24, the displacement of S-RA100Vf1E1.0 with steel fiber was 24% higher than that of S-RA100Vf0E1.0 without steel fiber. Similarly, S-RA0Vf1E1.0 exhibited a 17% increase in the displacement compared to S-RA0Vf0E1.0.Moving to the columns with a slenderness ratio of 26, both T-RA100Vf1E1.0 and T-RA0Vf1E1.0 show 7% and 8% higher displacement, respectively, compared to their counterparts without steel fiber, T-RA100Vf0E1.0, and T-RA0Vf0E1.0.

For the columns with the slenderness ratio of 34.5, the columns L-RA100Vf1E1.0 and L-RA0Vf1E1.0 exhibited higher displacements than L-RA100Vf0E1.0 and L-RA0Vf0E1.0 by 7% and 4%, respectively. Table 4.45 illustrates the effect of steel fiber on the displacement, displaying the percentage of the increase in displacement due to the addition of steel fiber in columns loaded with the largest eccentricity (e/h=1.0).

Table 4.45: Effect of steel fiber on lateral displacement (e/h = 1.0)

Specimen ID	Failure Load (kN)	ΔLat. mm)	Specimen ID	Failure Load (kN)	ΔLat. (mm)	Effect of Vf
S-RA100Vf0E1.0	100	3.87	S-RA100Vf1E1.0	107	4.79	24%
S-RA0Vf0E1.0	105	3.52	S-RA0Vf1E1.0	112	4.13	17%
T-RA100Vf0E1.0	76.5	7.70	T-RA100Vf1E1.0	86.5	8.25	7%
T-RA0Vf0E1.0	80	7.90	T-RA0Vf1E1.0	87	8.50	8%
L-RA100Vf0E1.0	74.5	13.13	L-RA100Vf1E1.0	80.5	14.10	7%
L-RA0Vf0E1.0	73	13.03	L-RA0Vf1E1.0	76.5	13.49	4%

4.7.3.3 Effect of Slenderness Ratio on Lateral Displacement

The columns T-RA100Vf0E1.0 and T-RA0Vf0E1.0, with a slenderness ratio of 26, exhibit higher displacements than S-RA100Vf0E1.0 and S-RA0Vf0E1.0, with a slenderness ratio of 17.24, by 99% and 124%, respectively. Similarly, comparing columns L-RA100Vf0E1.0 and L-RA0Vf0E1.0, with a slenderness ratio of 34.5, to columns S-RA100Vf0E1.0 and S-RA0Vf0E1.0, with a slenderness ratio of 17.24, reveals that the slender columns have displacements 239% and 270% higher, respectively. The columns T-RA100Vf1E1.0 and T-RA0Vf1E1.0, with a slenderness ratio of 26, show higher displacements than S-RA100Vf1E1.0 and S-RA0Vf1E1.0 (kl/r=17) by 72% and 106%, respectively. Similarly, the comparison of the columns L-RA100Vf1E1.0 and L-RA0Vf1E1.0, with a slenderness ratio of 34.5, to columns S-RA100Vf1E1.0 and S-RA0Vf1E1.0 (kl/r=17.24) indicates that the slender columns have higher displacements by 194% and 227%, respectively.

Table 4.46 and Table 4.47 demonstrate the effect of the slenderness on the lateral displacement. The former compares the samples without steel fiber, while the latter compares the samples with steel fiber. In both cases, the longer columns exhibit greater displacement compared to the shorter ones.

Table 4.46 and Table 4.47 demonstrate the effect of the slenderness on the lateral displacement. The former compares the samples without steel fiber, while the latter compares the samples with steel fiber. In both cases, the longer columns exhibit greater displacement compared to the shorter ones.

Table 4.46: Effect of slenderness on lateral displacement (e/h = 1.0, Vf = 0%)

Specimen ID	RA%	Kl/r	Failure Load (kN)	ΔLat. (mm)	Effect of kl/r
S-RA100Vf0E1.0	100	17.24	100	3.87	-
T-RA100Vf0E1.0	100	26	76.5	7.7	99%
L-RA100Vf0E1.0	100	34.5	74.5	13.13	239%
S-RA0Vf0E1.0	0	17.24	105	3.52	-
T-RA0Vf0E1.0	0	26	80	7.9	124%
L-RA0Vf0E1.0	0	34.5	73	13.03	270%

Table 4.47: Effect of slenderness on lateral displacement (e/h = 1.0, Vf = 1%)

Specimen ID	RA%	Kl/r	Failure Load (kN)	ΔLat. (mm)	Effect of kl/r
S-RA100Vf1E1.0	100	17.24	107	4.79	-
T-RA100Vf1E1.0	100	26	86.5	8.25	72%
L-RA100Vf1E1.0	100	34.5	80.5	14.1	194%
S-RA0Vf1E1.0	0	17.24	112	4.13	-
T-RA0Vf1E1.0	0	26	87	8.5	106%
L-RA0Vf1E1.0	0	34.5	76.5	13.49	227%

4.7.4 Load versus Lateral Displacement Relationship

The lateral displacement of the tested columns at the mid-height is an indication of the column stiffness. The cross-sectional stiffness, which consists of area of concrete and the area of steel reinforcement is constant in this research, therefore they all have the same stiffness, except the height which is different and its effect has been discussed. Figures 4.39 to 4.52 are the displacement curves and they show the effect of steel fiber, Recycled aggregate, the slenderness of the columns as well as the eccentricity.

Comparing the recycled concrete aggregate columns with those made using the natural aggregate, the displacement curves start with the same increasing

slope and are almost identical but the RA columns show higher displacement values at the failure compared with the NA columns.

The slope of lateral displacement curves for the samples L-RA100Vf0E1.0 and L-RA0Vf0E1.0, they have almost identical slopes except that L-RA100Vf0E1.0 has a larger displacement. Similar comparisons can be observed between L-RA100Vf1E1.0 and L-RA0Vf1E1.0, both of which include steel fiber. This consistent behavior is evident across all comparisons among the columns, regardless of their eccentricity and length, with a few minor exceptions.

In concentric columns, the lateral displacement varies significantly compared to columns with eccentric loading. While the shapes of the displacement curves are similar between the two eccentricities, the actual displacement values differ due to varying load conditions.

The effect of the steel fiber on the lateral displacement is notable in all the columns with all the variables. It can be seen that the samples with steel fiber are mostly have lower displacement values compared with the samples with no steel fiber, but sometimes they are very close. Not in all the samples higher displacement for the samples with steel fiber can be seen in any sample. In addition to this similarity, also it can be noted that the samples with steel fiber have a higher displacement at the maximum failure loads. It must be mentioned here that the samples with steel fiber have flatter slopes near the failure.

The impact of steel fiber on lateral displacement is significant across all column variables. Generally, samples with steel fiber exhibit lower displacement values compared to those without, although sometimes the differences are minimal. Higher displacement in samples with steel fiber is not consistently observed across all samples. Additionally, it is noted that

samples with steel fiber experience higher displacement at maximum failure loads. Furthermore, it is important to mention that samples with steel fiber have flatter slopes near failure.

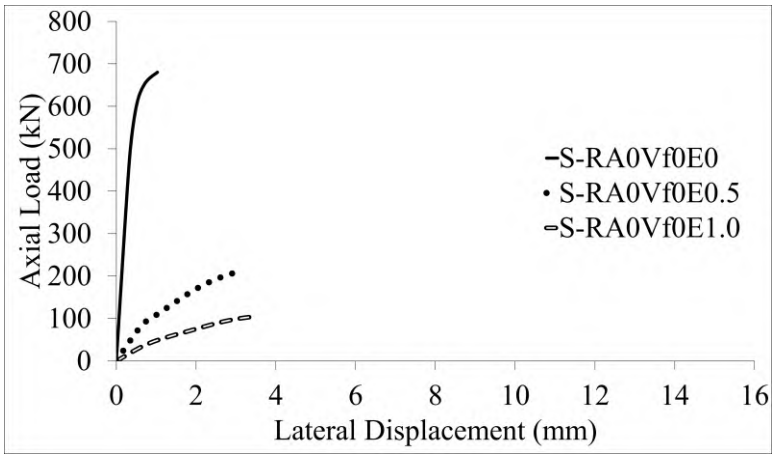

Figure 4.39: Mid-height lateral displacement for short columns (NA) (Vf = 0)

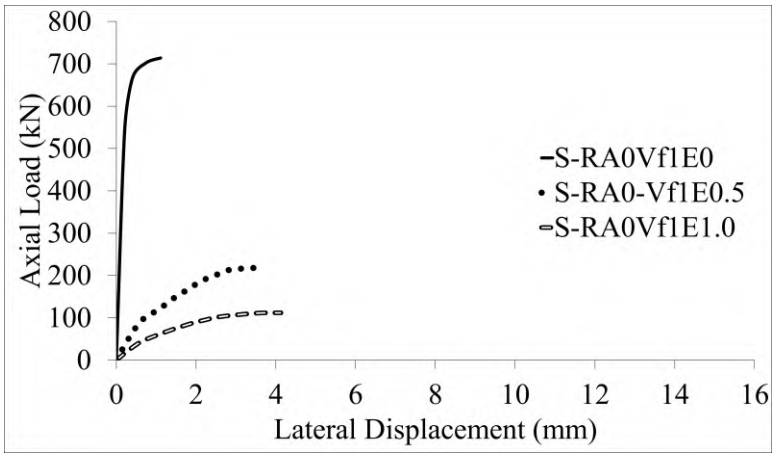

Figure 4.40: Mid-height lateral displacement for short columns (NA) (Vf = 1)

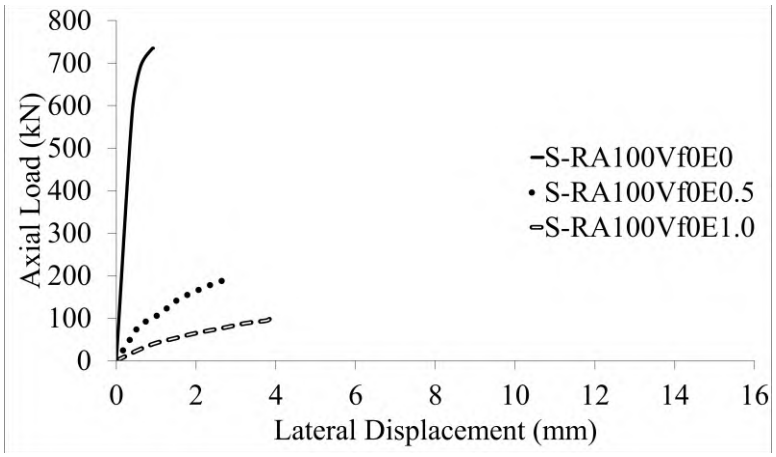

Figure 4.41: Mid-height lateral displacement for short columns (RA) (Vf = 0)

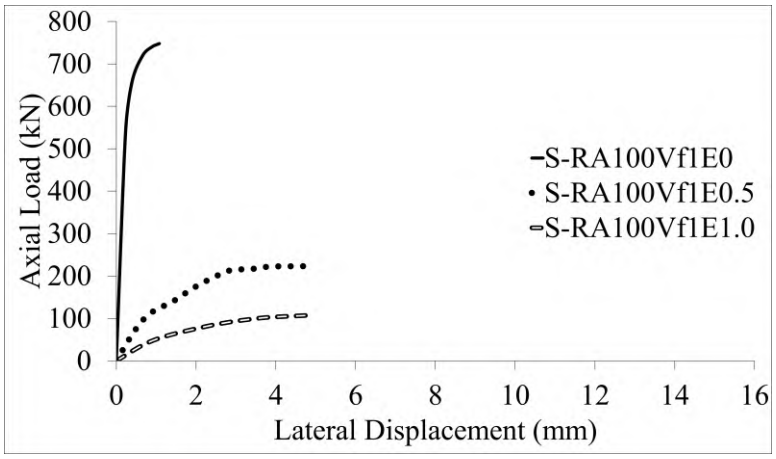

Figure 4.42: Mid-height lateral displacement for short columns (RA) (Vf = 1)

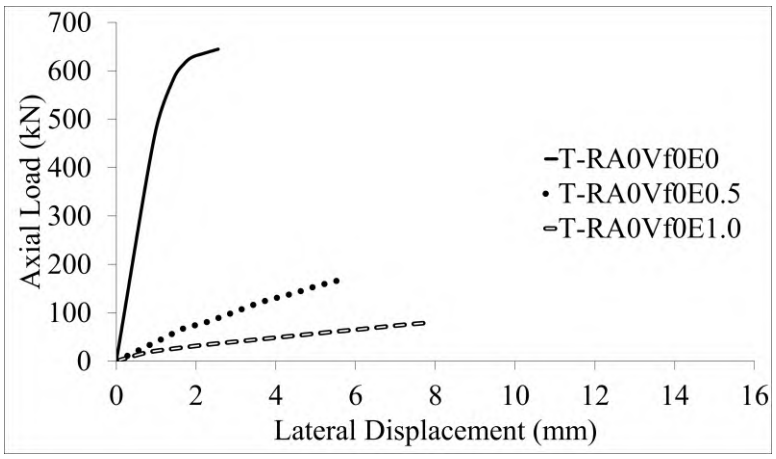

Figure 4.43: Mid-height lateral displacement for columns kl/r =26 (NA) (Vf = 0)

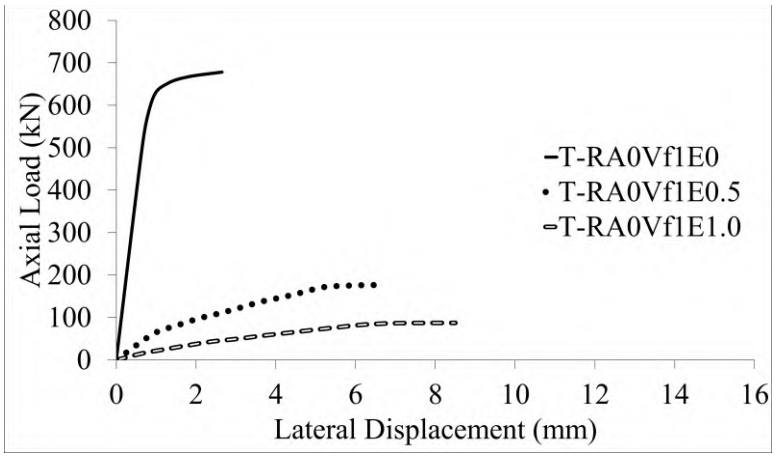

Figure 4.44: Mid-height lateral displacement for columns kl/r =26 (NA) (Vf = 1)

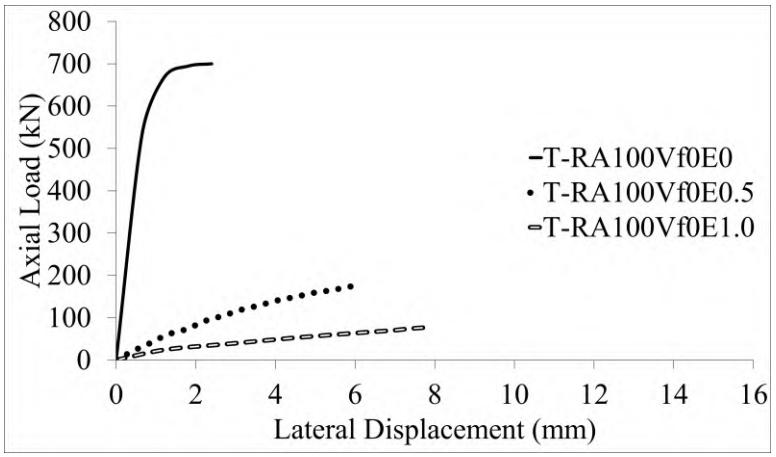

Figure 4.45: Mid-height lateral displacement for columns kl/r =26 (RA) (Vf = 0)

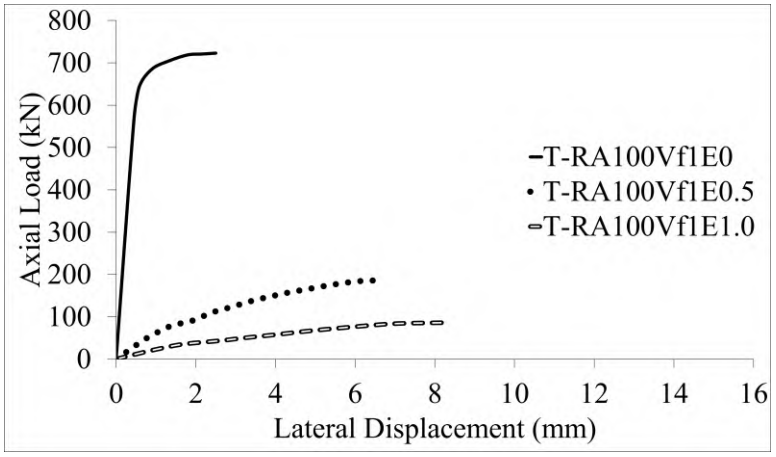

Figure 4.46: Mid-height lateral displacement for columns kl/r =26 (RA) (Vf = 1)

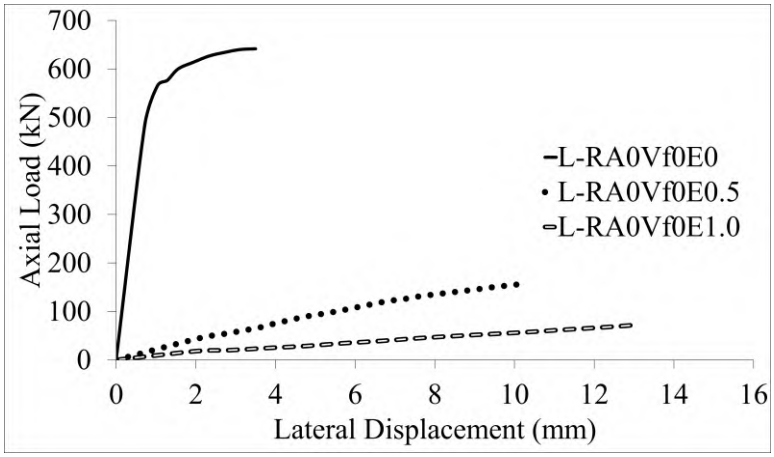

Figure 4.47: Mid-height lateral displacement for columns kl/r =34.5(NA) (Vf = 0)

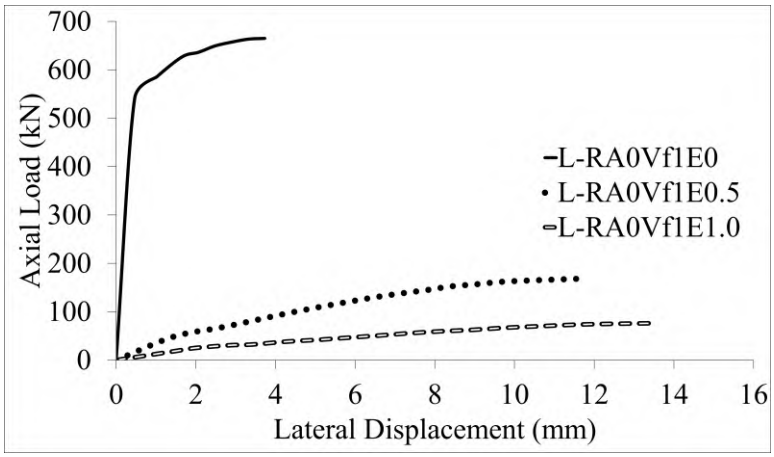

Figure 4.48: Mid-height lateral displacement for columns kl/r =34.5(NA) (Vf = 1)

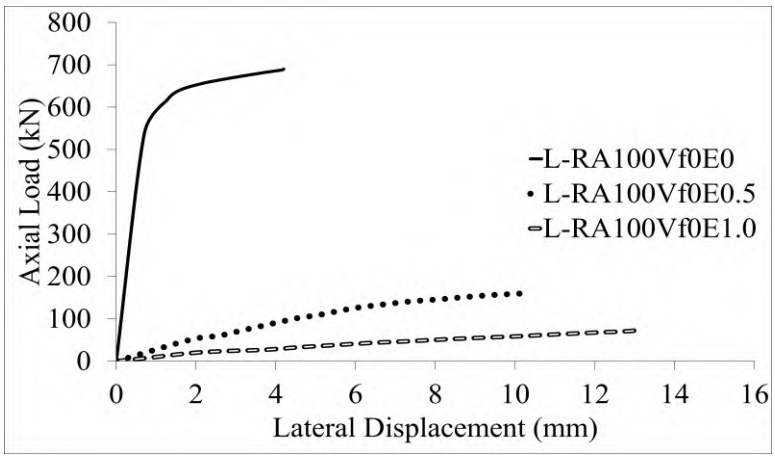

Figure 4.49: Mid-height lateral displacement for columns kl/r =34.5(RA) (Vf = 0)

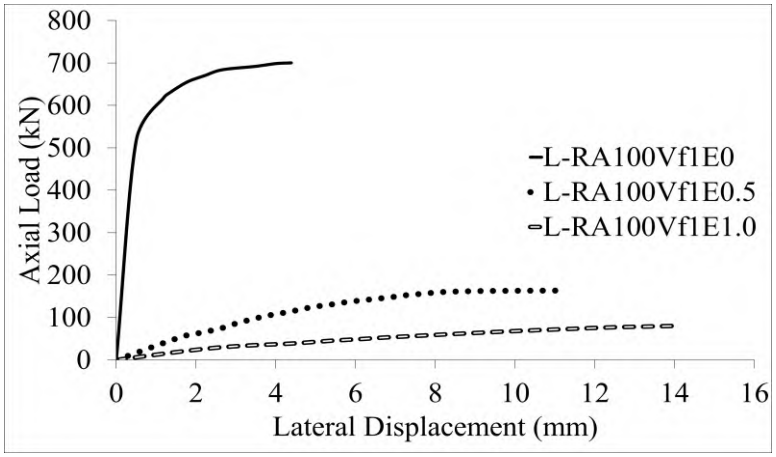

Figure 4.50: Mid-height lateral displacement for columns kl/r =34.5(RA) (Vf = 1)

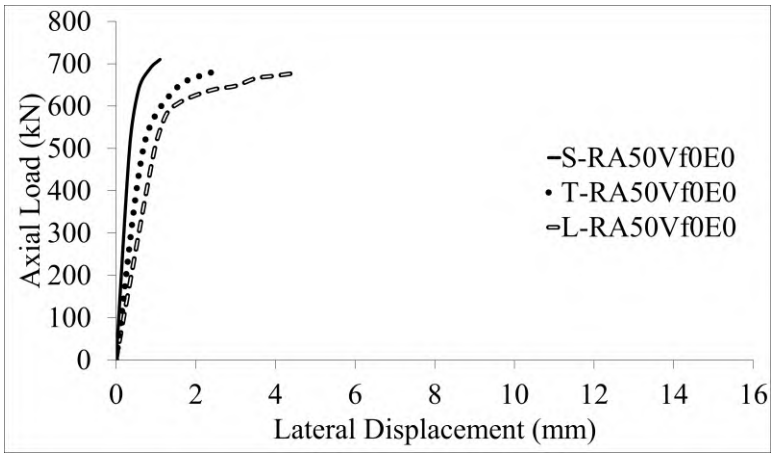

Figure 4.51: Mid-height lateral displacement (50% NA & 50%RA)
(e/h =0, Vf = 0)

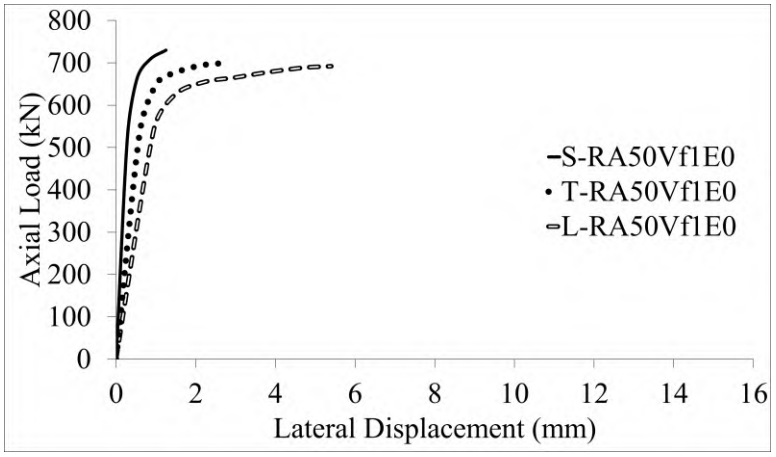

Figure 4.52: Mid-height lateral displacement (50% NA & 50%RA)
(e/h =0, Vf = 1)

4.8 VERTICAL DISPLACEMENT

4.8.1. Effect of Recycled Aggregate on Vertical Displacement

Table 4.48 presents the effect of the recycled aggregate on the vertical displacement of concentrically loaded columns. The vertical displacement of S-RA100Vf0E0, with 100% recycled aggregate, is 17% higher than that of S-RA0Vf0E0, with 100% natural aggregate. The column S-RA50Vf0E0, containing 50% recycled aggregate, exhibits 5% higher displacement than S-RA0Vf0E0.

Table 4.49 displays the vertical displacement of the columns loaded with the eccentricity of e/h=0.5. The column S-RA100Vf0E0.5, made with recycled aggregate, shows 6% less vertical displacement than S-RA0Vf0E0.5, made with 100% natural aggregate. The column T-RA100Vf0E0.5 has a 12% greater displacement than T-RA0Vf0E0.5, and L-RA100Vf0E0.5 has a 12% greater displacement than L-RA0Vf0E0.5 —generally, the samples with the recycled aggregate displaced more vertically than those with natural aggregate. However, L-RA100Vf1E0.5 and L-RA0Vf1E0.5, made with recycled and natural aggregates respectively, had identical displacements. This similarity in behavior could be attributed to the high compressive strengths and controlled sourcing of the parent concrete used in the production of the recycled aggregate.

Table 4.50 shows the vertical displacement of the columns loaded with an eccentricity of e/h=0.5. The results are mixed: some columns with the recycled aggregate displaced more, such as L-RA100Vf0E1.0 compared to L-RA0Vf0E1.0, while others displaced less, like T-RA100Vf0E1.0 compared to T-RA0Vf0E1.0. Additionally, S-RA100Vf1E1.0 and S-RA0Vf1E1.0 showed

no change in the displacement. These findings indicate that the replacement of the natural aggregate with recycled aggregate did not have a consistent effect on the vertical displacement, though the columns behaved similarly overall, this is because the recycled aggregate worked and behaved just like natural aggregate.

4.8.2 Effect of Steel Fiber on Vertical Displacement

The addition of 1% steel fiber did not consistently increase the vertical displacement in the concentrically loaded columns. Table 4.48 presents data for the samples containing 1% steel fiber. As shown in the table, samples S-RA0Vf1E0 and L-RA100Vf1E0 exhibited less displacements by 3% and 11%, respectively. However, the rest of the samples displayed higher displacements, and sample S-RA100Vf1E0 showed no change in the displacement due to the addition of the steel fiber. Table 4.49 compares the vertical displacements for the columns loaded eccentrically at e/h=0.5. It illustrates the increase in displacement in samples with 1% steel fiber compared to those without steel fiber. The increase in the displacement varied from 3% to 27%. Generally, the samples with the steel fiber displaced less than those without steel fiber at the same load level. Overall, the results indicate that the differences in displacement are not significant, which is expected since the failure loads are very close.

Table 4.50 shows the effect of using the steel fiber on the vertical displacement in columns loaded at e/h=1.0. The table displays an increase in the displacement ranging from 2% to 17% due to the addition of the steel fiber. These increases in the vertical displacement are observed at the maximum failure load. However, at the same load level, columns with steel fiber

displaced less displacement than those without steel fiber, regardless of changes made in the slenderness ratio or the replacement of coarse aggregate.

4.8.3 Effect of Slenderness Ratio on Vertical Displacement

Table 4.48 presents the effect of the slenderness ratio on the vertical displacement of the concentrically loaded columns. Columns T-RA0Vf0E0, T-RA50Vf0E0, and T-RA100Vf0E0, with a slenderness ratio of 26, deformed 40.3%, 34.3%, and 31.2% more than columns S-RA0Vf0E0, S-RA50Vf0E0, and S-RA100Vf0E0, which have a slenderness ratio of 17.24, respectively. The columns L-RA0Vf0E0, L-RA50Vf1E0, and L-RA100Vf0E0, with a slenderness ratio of 34.5, exhibited higher vertical displacements than columns S-RA0Vf0E0, S-RA50Vf0E0, and S-RA100Vf0E0 by 101%, 99%, and 100%, respectively. These results are expected, as displacement is inversely proportional to height and directly proportional to load.

Table 4.49 shows the effect of the slenderness ratio on the columns loaded eccentrically at e/h=0.5. The column T-RA100Vf0E0.5, with a slenderness ratio of 26, had a vertical displacement 27% higher than column S-RA100Vf0E0.5, which has a slenderness ratio of 17.24. The columns L-RA100Vf0E0.5 and L-RA0Vf0E0.5, with a slenderness ratio of 34.5, displaced 32% and 10% more than columns S-RA100Vf0E0.5 and S-RA0Vf0E0.5, which have a slenderness ratio of 17.24, respectively. Table 4.50 displays the increase in vertical displacement due to the increase in slenderness ratio for columns loaded eccentrically at e/h=1.0. An increase in displacement was observed as the slenderness ratio increased.

Table 4.48: Effect of kl/r, RA, and Vf on vertical displacement (e/h= 0)

Specimen ID	Kl/r	RA%	Failure Load	Δv (mm)	Effect of		
					kl/r	RA	Vf
S-RA0Vf0E0	17.24	0	680	1.40			
S-RA50Vf0E0	17.24	50	710	1.47		5%	
S-RA100Vf0E0	17.24	100	735	1.64		17%	
T-RA0Vf0E0	26	0	645	1.96	40%		
T-RA50Vf0E0	26	50	685	1.98	34%	1%	
T-RA100Vf0E0	26	100	700	2.15	31%	10%	
L-RA0Vf0E0	34.5	0	642	2.81	101%		
L-RA50Vf1E0	34.5	50	678	2.93	99%	4%	
L-RA100Vf0E0	34.5	100	690	3.29	100%	17%	
S-RA0Vf1E0	17.24	0	714	1.36			-3%
S-RA50Vf1E0	17.24	50	730	1.51		11%	2%
S-RA100Vf1E0	17	100	748	1.65		21%	0%
T-RA0Vf1E0	26	0	678	2.07	52%		5%
T-RA50Vf1E0	26	50	700	2.17	44%	5%	9%
T-RA100Vf1E0	26	100	723	2.19	33%	6%	2%
L-RA0Vf1E0	34.5	0	665	2.96	118%		5%
L-RA50Vf1E0	34.5	50	692	3.12	107%	5%	7%
L-RA100Vf1E0	34.5	100	701	2.92	78%	-1%	-11%

4.8.4 Load versus Vertical Displacement Relationship

Figures 4.53 to 4.66 shows the load versus vertical displacement relationship. Once the axial compressive load increases the vertical displacement curve increases linearly. This continues beyond the yield strain of the longitudinal reinforcement. This statement is correct for all the columns regardless of the level of the eccentricity, the length of each part of the curve is different. The higher eccentricity has a shorter linear part of the curve.

Table 4.49: Effect of kl/r, RA, and Vf on vertical displacement (e/h= 0.5)

Specimen ID	Kl/r	RA%	Vf%	Failure Load	Δv (mm)	Effect of		
						kl/r	RA	Vf
S-RA0Vf0E0.5	17.24	0	0	210	2.47			
S-RA100Vf0E0.5	17.24	100	0	190	2.31		-6%	
T-RA0Vf0E0.5	26	0	0	172	2.62	6%		
T-RA100Vf0E0.5	26	100	0	176	2.93	27%	12%	
L-RA0Vf0E0.5	34.5	0	0	158	2.71	10%		
L-RA100Vf0E0.5	34.5	100	0	161	3.05	32%	12%	
S-RA0-Vf1E0.5	17.24	0	1	218	2.59			5%
S-RA100Vf1E0.5	17.24	100	1	223	2.93		13%	27%
T-RA0Vf1E0.5	26	0	1	177	2.70	4%		3%
T-RA100Vf1E0.5	26	100	1	186	3.18	8%	18%	9%
L-RA0Vf1E0.5	34.5	0	1	168	3.12	20%		15%
L-RA100Vf1E0.5	34.5	100	1	163	3.13	7%	0%	3%

Table 4.50: Effect of kl/r, RA, and Vf on vertical displacement (e/h= 1.0)

Specimen ID	Kl/r	RA%	Vf%	Failure Load	Δv (mm)	Effect of		
						kl/r	RA	Vf
S-RA0Vf0E1.0	17.24	0	0	105	3.30			
S-RA100Vf0E1.0	17.24	100	0	100	3.23		-2%	
T-RA0Vf0E1.0	26	0	0	80	3.73	13%		
T-RA100Vf0E1.0	26	100	0	76.5	3.50	8%	-6%	
L-RA0Vf0E1.0	34.5	0	0	73	3.44	4%		
L-RA100Vf0E1.0	34.5	100	0	74.5	3.69	14%	7%	
S-RA0Vf1E1.0	17.24	0	1	112	3.36			2%
S-RA100Vf1E1.0	17.24	100	1	107	3.37		0%	4%
T-RA0Vf1E1.0	26	0	1	87	3.92	17%		5%
T-RA100Vf1E1.0	26	100	1	86.5	3.84	14%	-2%	10%
L-RA0Vf1E1.0	34.5	0	1	76.5	4.02	20%		17%
L-RA100Vf1E1.0	34.5	100	1	80.5	4.24	26%	5%	15%

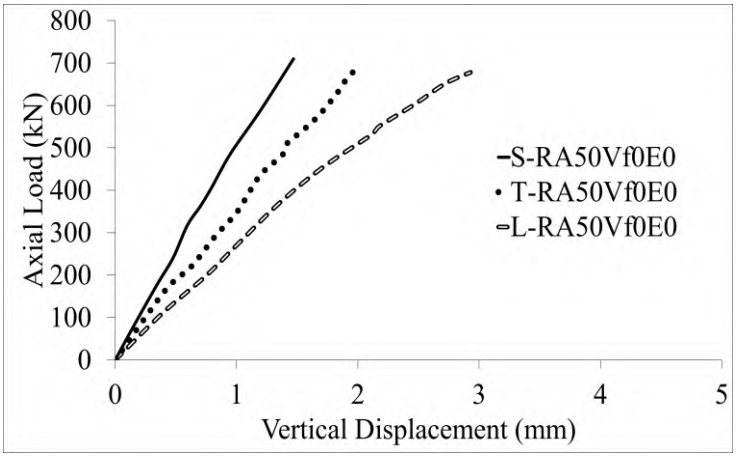

Figure 4.53: Vertical displacement for columns (50% of NA & 50% RA) (e/h = 0, Vf =0)

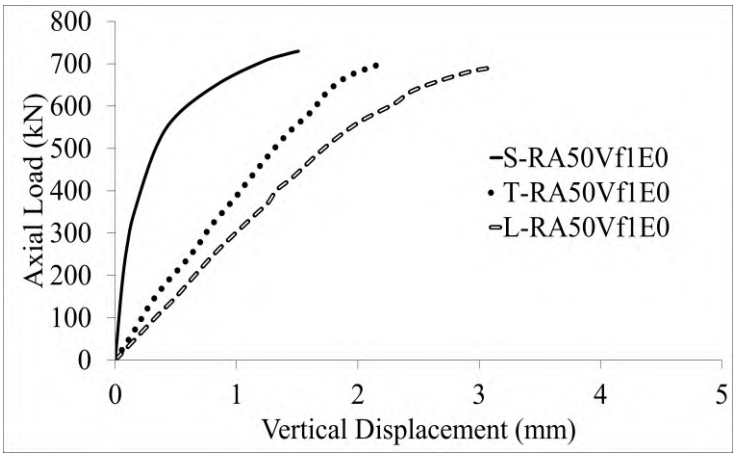

Figure 4.54: Vertical displacement for columns (50% of NA & 50% RA) (e/h =0, Vf = 1)

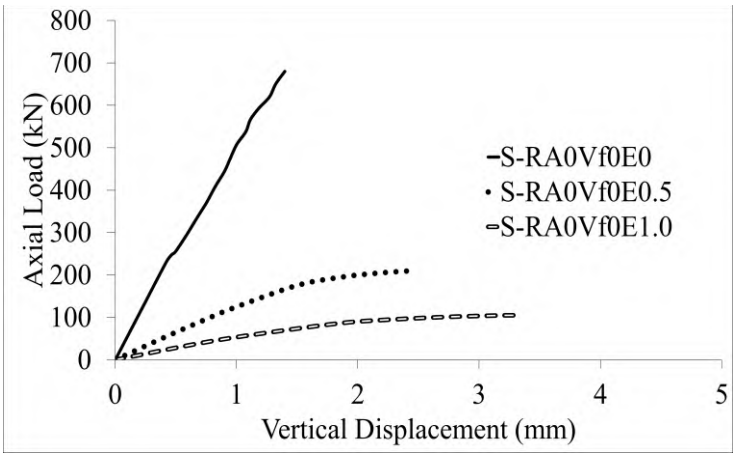

Figure 4.55: Vertical displacement for short columns (NA) (Vf = 0)

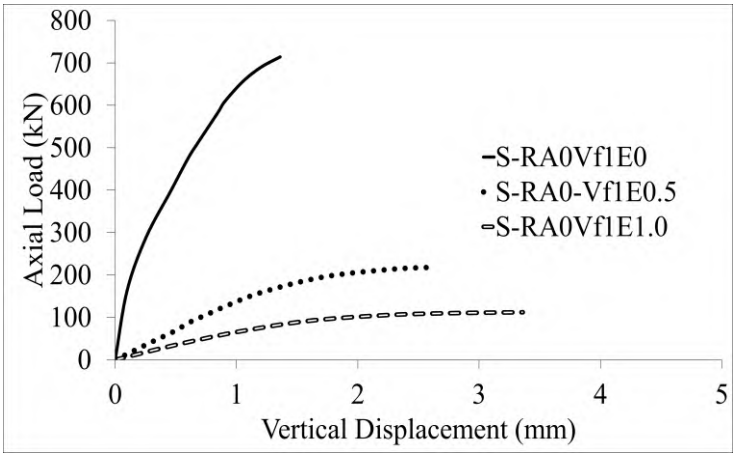

Figure 4.56: Vertical displacement for short columns (NA) (Vf = 1)

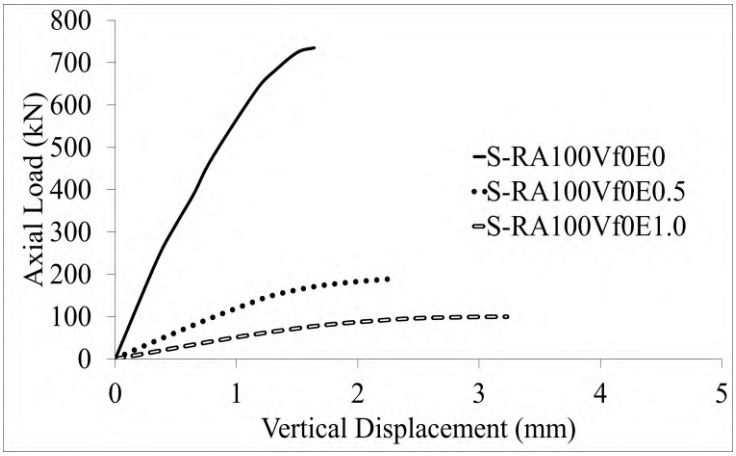

Figure 4.57: Vertical displacement for short columns (RA) (Vf = 0)

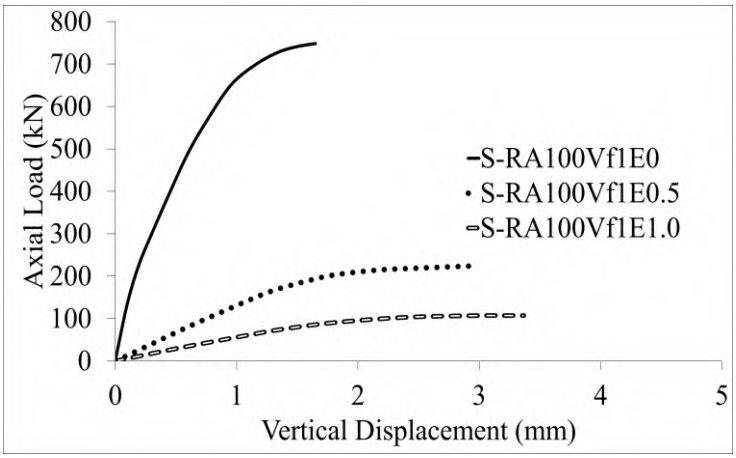

Figure 4.58: Vertical displacement for short columns (RA) (Vf = 1)

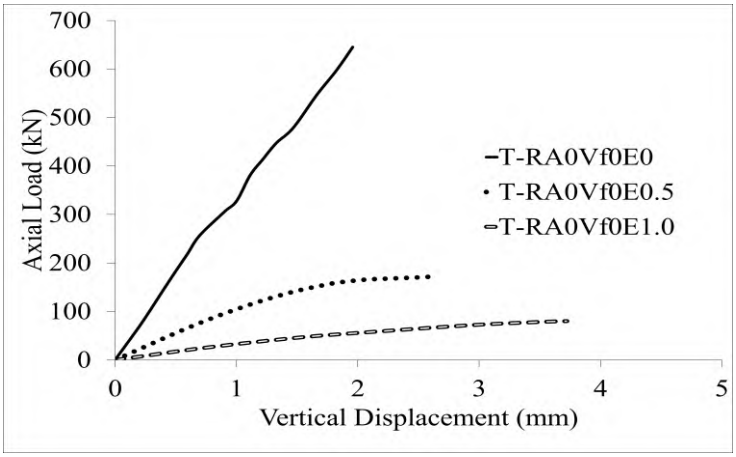

Figure 4.59: Vertical displacement for slender columns (kl/r = 26) (NA) (Vf = 0)

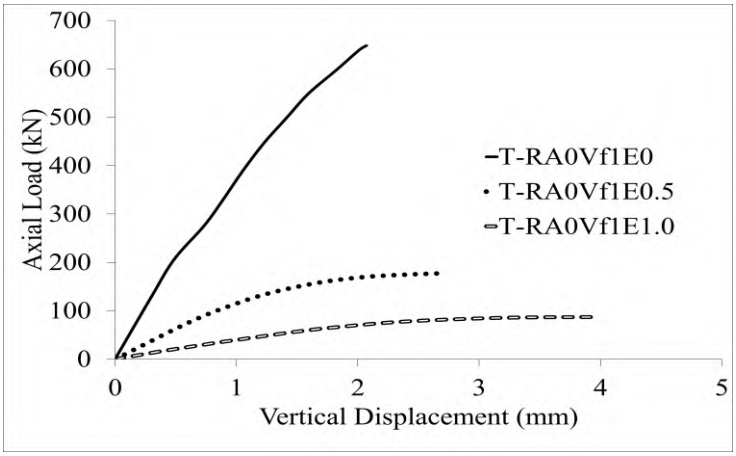

Figure 4.60: Vertical displacement for slender columns (kl/r = 26) (NA) (Vf = 1)

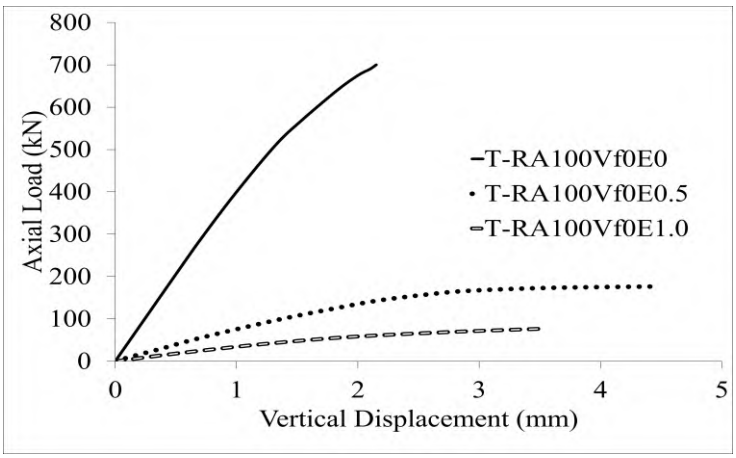

Figure 4.61: Vertical displacement for slender columns (kl/r = 26) (RA) (Vf = 0)

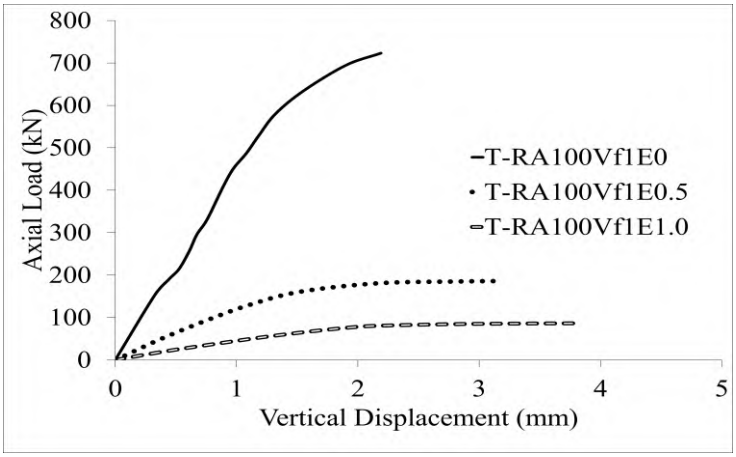

Figure 4.62: Vertical displacement for slender columns (kl/r = 26) (RA) (Vf = 1)

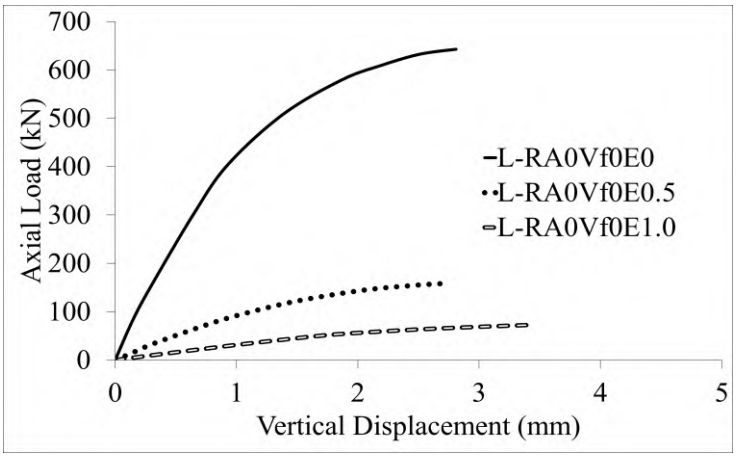

Figure 4.63: Vertical displacement for slender columns (kl/r = 34.5) (NA) (Vf = 0)

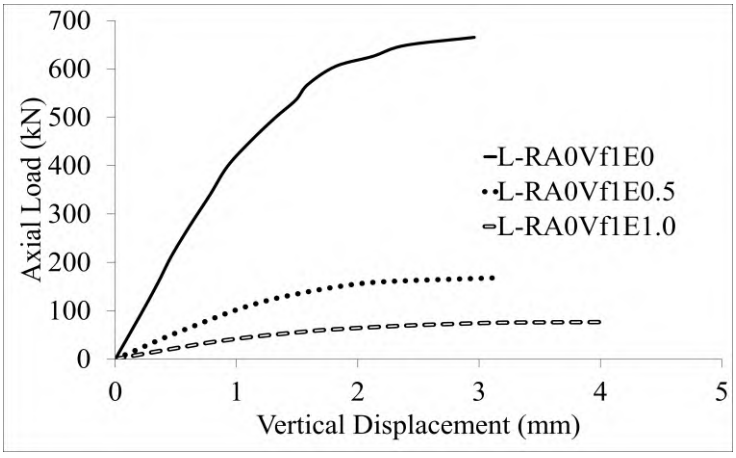

Figure 4.64: Vertical displacement for slender columns (kl/r = 34.5) (NA) (Vf = 1)

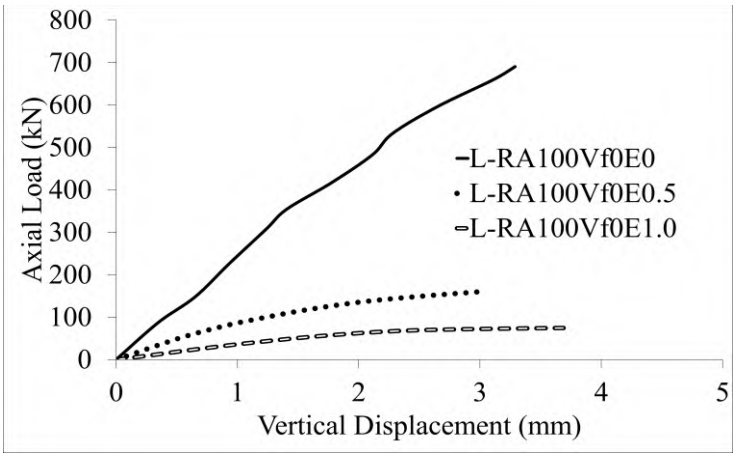

Figure 4.65: Vertical displacement for slender columns (kl/r = 34.5) (RA) (Vf = 0)

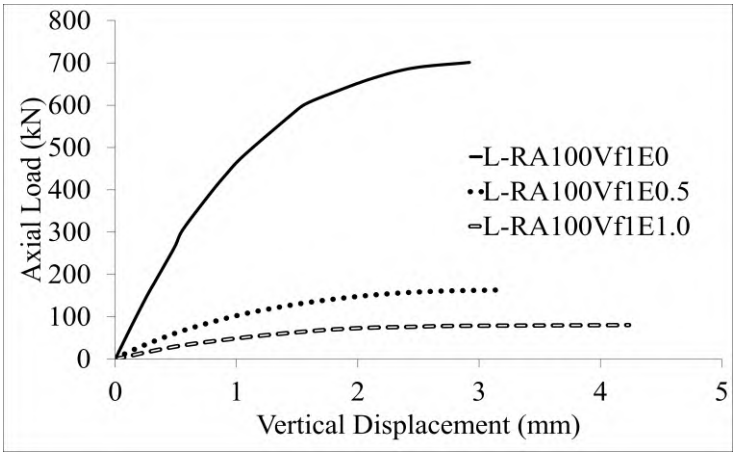

Figure 4.66: Vertical displacement for slender columns (kl/r = 34.5) (RA) (Vf = 1)

4.9 DUCTILITY

4.9.1 Calculation of Ductility

The ability of an element to deform elastically and absorb energy is measured by its ductility. There are various types of ductility, including displacement, rotation, and curvature ductility. The ductility index is defined as the ratio of the maximum mid-span displacement at peak load to the first yield displacement. (Azizinamini et al., 1999, Ahmad and Barker, 1991, Yang et al., 2010). This definition is used in this research. According to (Hadi and Elbasha, 2007, Shin et al., 1989), the ultimate deflection is defined as the deflection corresponding to 80% of the peak load along the descending branch of the load-deflection curve. A ductile system provides sufficient warning before any catastrophic failure. The ductility of a concrete structure serves as a measure of the resistance of the structural member or system to deformation during the transition from the elastic to the plastic zone until failure. It can also be interpreted as a measure of the energy absorption capacity of the structural member. The ductility, denoted as μ or $\Delta p/\Delta y$, is calculated using the deflection at the ultimate state and the maximum failure load state. In this research study, the peak load deflection Δp is measured at the maximum failure load, and Δy is the deflection of the member at the yielding load of the columns.

4.9.1.1 Effect of Recycled Aggregate

Table 4.51 compares the ductility of columns made with natural aggregate to those made with recycled aggregate, both without steel fiber, and provides a similar comparison for columns made with 1% steel fiber. Replacing natural aggregate with either 50% or 100% recycled aggregate does not significantly affect ductility. For example, column S-RA50Vf0E0 showed a 7% decrease in ductility compared to S-RA0Vf0E0 made of natural aggregate. Additionally, column L-RA50Vf1E0 had a 4% decrease compared to L-RA0Vf1E0, while L-RA100Vf1E0 exhibited no significant change in ductility compared to L-RA0Vf1E0. However, in most columns, ductility increased with the replacement of natural aggregate with recycled aggregate, regardless of the percentage, as supported by the reasoning in section 4.4.1.1 with references.

These observations for the concentrically loaded columns also apply to the columns loaded at eccentricities of e/h=0.5 and e/h=1.0, as shown in Tables 4.52 and 4.53, respectively. In both tables, there is no clear trend indicating whether the recycled aggregate or the natural aggregate leads to more ductile columns. In some cases, using recycled aggregate increased ductility, while in others, it decreased.

Table 4.51: Effect of RA, Vf, and kl/r on ductility of columns with (e/h = 0)

Spacemen ID	RA%	Vf%	Δp mm	Δy mm	Δp/Δy	Effect of RA	Effect of Vf	Effect of kl/r
S-RA0Vf0E0	0	0	1.03	0.64	1.61			
S-RA50Vf0E0	50	0	1.10	0.74	1.49	-7%		
S-RA100Vf0E0	100	0	0.93	0.57	1.64	2%		
T-RA0Vf0E0	0	0	2.55	1.49	1.72			7%
T-RA50Vf0E0	50	0	2.62	1.43	1.83	7%		23%
T-RA100Vf0E0	100	0	2.40	1.13	2.13	24%		30%
L-RA0Vf0E0	0	0	3.50	1.43	2.44			52%
L-RA50Vf0E0	50	0	4.50	1.83	2.45	1%		64%
L-RA100Vf0E0	100	0	4.20	1.64	2.57	5%		57%
S-RA0Vf1E0	0	1	1.11	0.60	1.84		14%	
S-RA50Vf1E0	50	1	1.25	0.66	1.91	4%	28%	
S-RA100Vf1E0	100	1	1.08	0.55	1.95	6%	19%	
T-RA0Vf1E0	0	1	2.65	1.20	2.21		29%	20%
T-RA50Vf1E0	50	1	2.80	1.22	2.29	4%	25%	20%
T-RA100Vf1E0	100	1	2.50	1.05	2.38	8%	12%	22%
L-RA0Vf1E0	0	1	3.73	1.42	2.64		8%	44%
L-RA50Vf1E0	50	1	5.40	2.13	2.54	-4%	3%	33%
L-RA100Vf1E0	100	1	4.39	1.67	2.64	0%	3%	35%

4.9.1.2 Effect of Steel Fiber

The addition of the steel fiber to the column samples increased their ductility. This is evident from the results presented in Table 4.51, which show that a 1% steel fiber content enhances the ductility regardless of changes in the slenderness ratio from 17.24 to 26 and then to 34.5. Furthermore, replacement of the natural aggregate with 50% and 100% recycled aggregate also resulted in a higher ductility when the steel fiber was added.

Table 4.52 illustrates the effect of the steel fiber on columns loaded with an eccentricity of e=0.5h. Regardless of the slenderness ratio or whether the sample was made with natural aggregate or recycled aggregate, the steel fiber increased ductility by 5% to 15%. Similarly, Table 4.53 shows the effect of adding steel fiber in the columns loaded with an eccentricity of e/h=1.0. In all cases, the addition of 1% steel fiber increased the ductility by 9% to 26%. This could return to higher interlocking and the ability of steel fiber in resisting tension.

Table 4.52: Effect of RA, Vf, and kl/r on ductility of columns with (e/h = 0.5)

Specimen ID	RA%	Vf%	Δp mm	Δy mm	Δp/Δy	Effect of RA	Effect of Vf	Effect of kl/r
S-RA100Vf0E0.5	100	0	2.79	1.13	2.48	-5.2%		
S-RA0Vf0E0.5	0	0	3.03	1.16	2.62			
T-RA100Vf0E0.5	100	0	6.00	2.02	2.97	4.5%		20%
T-RA0Vf0E0.5	0	0	5.80	2.04	2.84			9%
L-RA100Vf0E0.5	100	0	10.34	3.03	3.41	1.7%		38%
L-RA0Vf0E0.5	0	0	10.32	3.08	3.35			28%
S-RA100Vf1E0.5	100	1	3.59	1.27	2.84	1.4%	15%	
S-RA0-Vf1E0.5	0	1	3.45	1.23	2.80		7%	
T-RA100Vf1E0.5	100	1	6.65	2.02	3.30	1.8%	11%	16%
T-RA0Vf1E0.5	0	1	6.70	2.07	3.24		14%	16%
L-RA100Vf1E0.5	100	1	11.06	3.09	3.58	-4.9%	5%	26%
L-RA0Vf1E0.5	0	1	11.58	3.08	3.76		12%	34%

4.9.1.3 Effect of Slenderness Ratio

Table 4.51 summarizes the percentage of improvement in the ductility for various columns relative to their control specimens considering the effects of the slenderness ratio. The columns T-RA0Vf0E0, T-RA50Vf0E0, and T-

RA100Vf0E0 with a slenderness ratio (kl/r) of 26 showed improvements of 7%, 23%, and 30% respectively, compared to columns S-RA0Vf0E0, S-RA50Vf0E0, and S-RA100Vf0E0 with a slenderness ratio of 17.24. Columns L-RA0Vf0E0, L-RA50Vf1E0, and L-RA100Vf0E0 with a slenderness ratio of 34.5 enhanced displacement ductility by 52%, 64%, and 57% respectively, relative to the columns with the slenderness ratio of 17.24. The replacement of natural aggregate with recycled aggregate did not affect ductility as significantly as the change in slenderness ratio. A similar comparison was conducted for columns containing steel fiber. The columns with kl/r= 26 showed improvements of 20%, 20%, and 22% compared to the columns with a slenderness ratio of 17.24. The columns with a slenderness ratio of 34.5 improved by 44%, 33%, and 35% relative to columns with a slenderness ratio of 17.24. Table 4.52 displays the improvement in ductility with the increase of the slenderness ratio for samples loaded at an eccentricity of e/h = 0.5. Columns T-RA100Vf0E0.5 and T-RA0Vf0E0.5 with a slenderness ratio of 26 showed gains of 20% and 9% compared to columns S-RA100Vf0E0.5 and S-RA0Vf0E0.5 with a slenderness ratio of 17.24. Columns L-RA100Vf0E0.5 and L-RA0Vf0E0.5 with a slenderness ratio of 34.5 improved ductility by 38% and 28% compared to columns with a slenderness ratio of 17.24. Table 4.53 summarizes the improvement in the ductility for samples loaded at an eccentricity of e/h = 1.0. The ductility increased with the increase of the slenderness ratios. The columns T-RA100Vf0E1.0 and T-RA0Vf0E1.0 with a slenderness ratio of T-RA0Vf0E1.0 showed gains of 20% and 14% compared to columns S-RA100Vf0E1.0 and S-RA100Vf0E1.0 with a slenderness ratio of 17.24. Columns L-RA100Vf0E1.0 and L-RA0Vf0E1.0 with a slenderness ratio of 34.5 enhanced the ductility by 25% each compared to columns with a slenderness ratio of 17.24.

Table 4.53: Effect of RA, Vf, and kl/r on ductility of columns with (e/h = 1.0)

Specimen ID	RA%	Vf%	Δp mm	Δy mm	Δp/Δy	Effect of RA	Effect of Vf	Effect of kl/r
S-RA100Vf0E1.0	100	0	3.87	1.20	3.21	-1.4%		
S-RA0Vf0E1.0	0	0	3.52	1.08	3.26			
T-RA100Vf0E1.0	100	0	7.70	1.99	3.87	4.0%		20%
T-RA0Vf0E1.0	0	0	7.90	2.12	3.72			14%
L-RA100Vf0E1.0	100	0	13.13	3.27	4.01	-1.2%		25%
L-RA0Vf0E1.0	0	0	13.03	3.21	4.06			25%
S-RA100Vf1E1.0	100	1	4.79	1.18	4.06	14.5%	26%	
S-RA0Vf1E1.0	0	1	4.13	1.16	3.54		9%	
T-RA100Vf1E1.0	100	1	8.25	1.93	4.27	-1.0%	10%	5%
T-RA0Vf1E1.0	0	1	8.50	1.97	4.32		16%	22%
L-RA100Vf1E1.0	100	1	14.10	3.11	4.53	-1.7%	13%	12%
L-RA0Vf1E1.0	0	1	13.49	2.93	4.61		13%	30%

4.9.2 Effect of Eccentricity on Ductility

4.9.2.1 Effect of eccentricity on ductility (kl/r=17.24)

Table 4.54 displays the percentage the increase in ductility as the eccentricity (e/h) changes from zero to 0.5 and then to 1.0 in short columns made with both natural aggregate and recycled aggregate, with and without the addition of 1% steel fiber.

4.9.2.2 Effect of eccentricity on ductility (kl/r=26)

Table 4.55 displays the percentage of the increase in the ductility as the eccentricity (e/h) changes from zero to 0.5 and then to 1.0 in slender columns

(kl/r = 26) made with both natural aggregate and recycled aggregate, with and without the addition of 1% steel fiber.

Table 4.54: Effect of eccentricity on ductility of columns with (kl/r = 17.24)

Specimen ID	RA%	Vf%	e/h	Δp mm	Δy mm	Δp/Δy	Increase
S-RA0Vf0E0	0	0	0	1.03	0.64	1.61	
S-RA0Vf0E0.5	0	0	0.5	3.03	1.16	2.62	62%
S-RA0Vf0E1.0	0	0	1	3.52	1.08	3.26	102%
S-RA100Vf0E0	100	0	0	0.93	0.57	1.64	
S-RA100Vf0E0.5	100	0	0.5	2.79	1.13	2.48	52%
S-RA100Vf0E1.0	100	0	1	3.87	1.20	3.21	96%
S-RA0Vf1E0	0	1	0	1.11	0.60	1.84	
S-RA0-Vf1E0.5	0	1	0.5	3.45	1.23	2.80	53%
S-RA0Vf1E1.0	0	1	1	4.13	1.16	3.54	93%
S-RA100Vf1E0	100	1	0	1.08	0.55	1.95	
S-RA100Vf1E0.5	100	1	0.5	3.59	1.27	2.84	46%
S-RA100Vf1E1.0	100	1	1	4.79	1.18	4.06	108%

Table 4.55: Effect of eccentricity on ductility of columns with (kl/r = 26)

Specimen ID	RA%	Vf%	e/h	Δp mm	Δy mm	Δp/Δy	Increase
T-RA0Vf0E0	0	0	0	2.55	1.49	1.72	
T-RA0Vf0E0.5	0	0	0.5	5.80	2.04	2.84	66%
T-RA0Vf0E1.0	0	0	1	7.90	2.12	3.72	117%
T-RA100Vf0E0	100	0	0	2.40	1.13	2.13	
T-RA100Vf0E0.5	100	0	0.5	6.00	2.02	2.97	39%
T-RA100Vf0E1.0	100	0	1	7.70	1.99	3.87	82%
T-RA0Vf1E0	0	1	0	2.65	1.20	2.21	
T-RA0Vf1E0.5	0	1	0.5	6.70	2.07	3.24	47%
T-RA0Vf1E1.0	0	1	1	8.50	1.97	4.32	96%
T-RA100Vf1E0	100	1	0	2.50	1.05	2.38	
T-RA100Vf1E0.5	100	1	0.5	6.65	2.02	3.30	38%
T-RA100Vf1E1.0	100	1	1	8.25	1.93	4.27	79%

4.9.2.3 Effect of eccentricity on ductility (kl/r=34.5)

Table 4.56 displays the percentage increase in the ductility as the eccentricity (e/h) changes from zero to 0.5 and then to 1.0 in slender columns (kl/r = 34.5) made with both natural aggregate and recycled aggregate, with and without the addition of 1% steel fiber.

Table 4.56: Effect of eccentricity on ductility of columns with (kl/r = 34.5)

Specimen ID	RA%	Vf%	e/h	Δp mm	Δy mm	Δp/Δy	Increase
L-RA0Vf0E0	0	0	0	3.50	1.43	2.44	
L-RA0Vf0E0.5	0	0	0.5	10.32	3.08	3.35	37%
L-RA0Vf0E1.0	0	0	1	13.03	3.21	4.06	66%
L-RA100Vf0E0	100	0	0	4.20	1.64	2.57	
L-RA100Vf0E0.5	100	0	0.5	10.34	3.03	3.41	33%
L-RA100Vf0E1.0	100	0	1	13.13	3.27	4.01	56%
L-RA0Vf1E0	0	1	0	3.73	1.42	2.64	
L-RA0Vf1E0.5	0	1	0.5	11.58	3.08	3.76	43%
L-RA0Vf1E1.0	0	1	1	13.49	2.93	4.61	75%
L-RA100Vf1E0	100	1	0	4.39	1.67	2.64	
L-RA100Vf1E0.5	100	1	0.5	11.06	3.09	3.58	36%
L-RA100Vf1E1.0	100	1	1	14.10	3.11	4.53	72%

From the above data, it is observed that the ductility increases with the addition of the steel fiber, with the increase of slenderness ratio, and with increasing the eccentricity.

CHAPTER FIVE

THEORETICAL ANALYSIS

CHAPTER FIVE
ANALYTICAL SOLUTION

5.1 INTRODUCTION

This chapter covers the analysis methods to compute the theoretical load-moment capacity of the columns made with the natural aggregate as well as the columns made with the recycled aggregate, considering the effects of the slenderness, eccentricity, steel fiber and recycled aggregate. To verify and compare the experimental load capacities of the columns, three methods have been utilized:

- (ACI-318-19) is utilized to predict the load and the moments.
- A theoretical method based on the second-order effects on column is applied to calculate loads and moments.
- A proposed model to predict maximum failure loads and moments.

5.2 METHOD OF ACI 318-19

To determine the column axial load and moment capacity, an interaction diagram has been plotted to obtain the failure envelope of the designed sections. Provisions of ACI-318-19 have been followed to plot the load-moment interaction diagrams. The test results of the axial force and moment from the applied eccentricity, as well as the second-order effects, are plotted on a diagram for comparison. The calculated results such as load-carrying capacity, lateral displacement and strain values confirmed that the experimentally tested columns had a higher values. The results of ACI-318-19 are more conservative. One of the reasons, a common practice by design

codes is not to account for the tensile strength of concrete in the P-M curves. However, the experimental results show that there is an inclusion of the concrete's strength in tension.

The interaction diagram have been developed utilizing the conventional method of section analysis based on the principles of the equilibrium of internal forces and strain compatibility, with a considered maximum concrete strain value of 0.003 at the extreme compression fiber. The cross-section, strain diagram, stress diagram, and internal forces are shown in Figure 5.1. This method is applied to both short and slender columns, as well as to assess the effect of adding the steel fiber. The loads in the P-M diagrams, shown in Figures A1 to A12 (see Appendix A), include un-factored axial loads and moments. The experimental results are represented as points on the diagrams, indicating the axial load versus moment. The moments are calculated by multiplying the axial loads by the initial eccentricity plus the displacement due to second-order effects. The experimental load path was drawn for each column from the start of loading extending to the experimental point capacity; the load path was determined by multiplying the axial load by the lateral displacement from start to failure.

The principles for plotting the P-M diagrams for the slender columns are based on the method adopted by ACI-318-19, which was further developed and improved by MacGregor and Breen (1970), MacGregor (1993), Mockry and Darwin (1982), and Mirza (1990). In this method, for each point (P, M), the moment for the short column is divided by the moment magnification factor to draw the new M-P diagram for slender columns, demonstrating how the slenderness reduces the column strength. The P-delta effect is significant in

the compression zone but negligible in the tension zone. For each axial load, the moment value for slender columns is smaller for than for short columns. Table 4.27 presents the test values of moments (M1st) for the columns subjected to different eccentricities at the mid-height of the columns, as well as the secondary moment (M2nd), calculated by multiplying the failure load by the lateral displacement. The total moment is the sum of the two moments (M1st and M2nd). The addition of steel fiber greatly increased both the moment and load capacities, with the impact of steel fiber being most noticeable in the tension zone.

Knowing the cross-sectional properties that include dimensions, material properties, and reinforcement details. The following assumptions are adopted in the analysis of the section under investigation:

I. Plane sections remain plane after bending.
II. A complete bond is developed between the concrete and steel reinforcement.
III. At the tension side, the strength of the concrete is omitted.
IV. A rectangular stress block is assumed instead of the actual stress diagram.
V. The contribution of steel fibers to the strength at the tension side after cracking is considered.

The stress block, shown in Figure 5.1, has an intensity of 0.85 $f'c$ and a depth of a, which is given by the following equation:

$$a = \beta_1 \times c \quad \text{----------} \quad (5.1)$$

β_1 is a factor that depends on the concrete's strength in compression and c is the distance from the extreme compression fiber to the neutral axis. According to ACI 318-19, the axial capacity of reinforced concrete columns is given by:

$$P_{ACI} = 0.85\, f_c' A_c + f_y A_s \quad \text{----------} \quad (5.2)$$

Where $f'c$ is the concrete cylinder compressive strength, fy represents the yield stress of the longitudinal steel reinforcement, and Ac and As are the cross-sectional areas of the concrete and the longitudinal reinforcement, respectively. The contribution of transverse reinforcement is ignored, as allowed by the code. This equation considers the column's cross-section but does not account for the eccentricity and slenderness of the columns. This equation is used to determine the axial capacity of the short columns with kl/r=17.24.

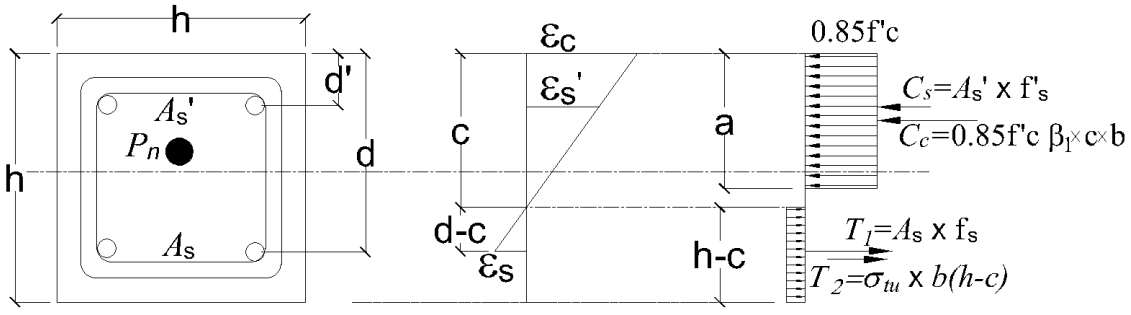

Figure 5.1: Column section analysis

Table 4.27 Experimental test results (Repeated)

Specimen ID	Failure Load (kN)	Exp. Δ_{lat} (mm)	M_{1st} (kN.m)	M_{2nd} (kN.m)	$M_{1s}+M_{2nd}$	M2nd/M1st
S-RA0Vf0E0	680	1.03	0.00	0.70	0.70	----
S-RA50Vf0E0	710	1.10	0.00	0.78	0.78	----
S-RA100Vf0E0	735	0.93	0.00	0.68	0.68	----
T-RA0Vf0E0	645	2.55	0.00	1.64	1.64	----
T-RA50Vf0E0	685	2.62	0.00	1.79	1.79	----
T-RA100Vf0E0	700	2.40	0.00	1.68	1.68	----
L-RA0Vf0E0	642	3.50	0.00	2.25	2.25	----
L-RA50Vf0E0	678	4.50	0.00	3.05	3.05	----
L-RA100Vf0E0	690	4.20	0.00	2.90	2.90	----
S-RA0Vf1E0	714	1.11	0.00	0.79	0.79	----
S-RA50Vf1E0	730	1.25	0.00	0.91	0.91	----
S-RA100Vf1E0	748	1.08	0.00	0.81	0.81	----
T-RA0Vf1E0	678	2.65	0.00	1.72	1.72	----
T-RA50Vf1E0	700	2.80	0.00	1.96	1.96	----
T-RA100Vf1E0	723	2.30	0.00	1.66	1.66	----
L-RA0Vf1E0	665	3.73	0.00	2.48	2.48	----
L-RA50Vf1E0	692	5.40	0.00	3.74	3.74	----
L-RA100Vf1E0	701	4.39	0.00	3.08	3.08	----
S-RA100Vf0E0.5	190	2.79	11.88	0.53	12.40	4.46%
S-RA0Vf0E0.5	210	3.03	13.13	0.64	13.76	4.85%
T-RA100Vf0E0.5	176	6.00	11.00	1.06	12.06	9.60%
T-RA0Vf0E0.5	172	5.80	10.75	1.00	11.75	9.28%
L-RA100Vf0E0.5	161	10.34	10.06	1.66	11.73	16.55%
L-RA0Vf0E0.5	158	10.32	9.88	1.63	11.51	16.51%
S-RA100Vf1E0.5	223	3.59	13.94	0.80	14.74	5.75%
S-RA0-Vf1E0.5	218	3.45	13.63	0.75	14.38	5.51%
T-RA100Vf1E0.5	186	6.65	11.63	1.24	12.86	10.64%
T-RA0Vf1E0.5	177	6.70	11.06	1.19	12.25	10.72%
L-RA100Vf1E0.5	163	11.06	10.19	1.80	11.99	17.70%
L-RA0Vf1E0.5	168	11.58	10.50	1.95	12.45	18.53%
S-RA100Vf0E1.0	100	3.87	12.50	0.39	12.89	3.09%
S-RA0Vf0E1.0	105	3.52	13.13	0.37	13.49	2.82%
T-RA100Vf0E1.0	76.5	7.70	9.56	0.59	10.15	6.16%
T-RA0Vf0E1.0	80	7.90	10.00	0.63	10.63	6.32%
L-RA100Vf0E1.0	74.5	13.13	9.31	0.98	10.29	10.50%
L-RA0Vf0E1.0	73	13.03	9.13	0.95	10.08	10.42%
S-RA100Vf1E1.0	107	4.79	13.38	0.51	13.89	3.83%
S-RA0Vf1E1.0	112	4.13	14.00	0.46	14.46	3.30%
T-RA100Vf1E1.0	86.5	8.25	10.81	0.71	11.53	6.60%
T-RA0Vf1E1.0	87	8.50	10.88	0.74	11.61	6.80%
L-RA100Vf1E1.0	80.5	14.10	10.06	1.14	11.20	11.28%
L-RA0Vf1E1.0	76.5	13.49	9.56	1.03	10.59	10.79%

5.2.1 Constructing Load- Moment Interaction Diagram

The interaction diagram (P-M diagram) are constructed using the above mentioned materials' constitutive relationships, compatibility, and equilibrium equations. The process is started as follows:

- The column axial strength is calculated using equation (5.2)
- The value of the neutral axis depth is assumed, starting with a depth more than the column depth (h).
- Internal forces C1, C2, T1 and T2 are calculated as below:

$$C_1 = 0.85\, f_c'\ \beta_1\ \times c\ \times b \quad \text{----------} \quad (5.3)$$

$$C_2 = A_s'(f_s' - 0.85 f_c') \quad \text{----------} \quad (5.4)$$

$$T_1 = f_s \times A_s \quad \text{----------} \quad (5.5)$$

$$T_2 = \sigma_{tu} \times b\ \times (h - c) \quad \text{----------} \quad (5.6)$$

$$f_s = \frac{d-c}{c}\ E_s\ \varepsilon_{cu}\ \leq f_y \quad \text{----------} \quad (5.7)$$

$$f_s' = \frac{c-d'}{c}\ E_s\ \varepsilon_{cu}\ \leq f_y \quad \text{----------} \quad (5.8)$$

- The moments about the centroid of the columns are then equated to the external moment (Pn . e) to find the eccentricity e.
- This process is repeated for the points in the tension, compression, and balanced points.
- At different c values the eccentricity e is determined.
- For each axial load Pn, a moment Mn calculated and that plotted as a single point on the interaction diagram and so forth.

In the analysis of the no sway slender columns, it is essential to account for the second-order effect, commonly referred to as P-delta. To assess this effect, the slenderness ratio (klu/r) is calculated, where 'k' represents the effective length factor, set at 1.0 in this study due to the pin-ended nature of all columns. Here, 'lu' denotes the effective length of the column, while 'r' stands for the radius of gyration of the section. As per ACI-318-19 standards, a slenderness ratio exceeding 22 indicates a slender column. However, it's noteworthy that the critical threshold typically lies around 34. ACI-318-19 mandates an amplification of the moment to accommodate the second-order effect, achieved by multiplying the moment by the factor δ.

$$M_c = \delta . M_2 \quad \text{----------} \quad (5.9)$$

The moment magnification factor (δ) is calculated using the equation below:

$$\delta = \frac{c_m}{1-\frac{P_u}{\phi_K P_c}} \geq 1.0 \quad \text{----------} \quad (5.10)$$

$$c_m = 0.6 - 0.4\frac{M_1}{M_2} \leq 1.0 \quad \text{----------} \quad (5.11)$$

$$P_c = \frac{\pi^2 EI}{(kl)^2} \quad \text{----------} \quad (5.12)$$

$$EI_{eff} = \frac{0.4E_c I_g}{1+\beta_d} \quad \text{----------} \quad (5.13)$$

$$EI_{eff} = \frac{0.2E_c I_g + E_s I_s}{1+\beta_d} \quad \text{----------} \quad (5.14)$$

$$EI_{eff} = \frac{E_c I}{1+\beta_d} \quad \text{----------} \quad (5.15)$$

Equation 5.13 has been used to determine the effective stiffness of the section, as it is recommended by ACI-318-19 for sections with low ratio of steel reinforcement. At this stage, the development of the interaction points between the axial load and moment. The initial three points outline specific conditions: the first represents pure compression, the second represents a balanced state, and the third signifies pure moment (with zero axial load). Subsequently, additional points can be plotted between these primary points to further clarify the interaction dynamics.

The addition of 1% steel fiber to the concrete mixes resulted in increased strength of the columns, with this enhancement being more pronounced in the eccentrically loaded columns compared to the concentrically loaded ones. This discrepancy can be attributed to the greater resistance of the fiber in tension as opposed to compression. The tensile strength of the steel fiber (σtu) serves a crucial role in the force equilibrium and strain compatibility diagram of the column cross-section, as defined by Bentur and Mindess (2006). The equation for calculating the steel fiber stress is provided below:

$$\sigma_{tu} = \eta_o \times \tau_u \times V_f \times \frac{L_f}{D_f} \quad \text{----------} \quad (5.16)$$

η_o = 0.333, 0.41 and 0.5 (Hannant, 1978), 0.5 used in this study.

τ_u = bond strength between steel fiber and the concrete.

$$\tau_u = k_s\sqrt{f_c'} \quad \text{(Ng et al., 2012)----------} \quad (5.17)$$

$$\tau_u = 0.6\, f_c'^{2/3} \quad \text{(Marti et al., 1999) ----------} \quad (5.18)$$

k_s = 0.4 for plain fibers

V_f , L_f and D_f : volume fraction, length, and diameter of steel fiber.

5.2.2 Effect of Slenderness on a Slender Column

MacGregor and Breen (1970) the effect of slenderness on a slender column is illustrated in Figure 5.2. The maximum moment in the column occurs at Section A-A, resulting from the combination of the initial eccentricity (e) and the deflection Δ at this point. Two types of failure can occur:

1. Material Failure: The column may remain stable at deflection Δ_1; however, the axial load P and the moment M at Section A-A may exceed the strength of the cross-section. This type of failure is depicted by Column 1 in Figure 5.2c.

2. Stability Failure: Conversely, if the column is very slender, it may reach a deflection Δ_2 due to the axial force P and the end moment Pe. In this case, the ratio $\delta M/\delta P$ may be zero or negative. This type of failure is illustrated by Column 2 in Figure 5.2c and can occur in slender columns under certain conditions.

   In stability can be investigated only via second order because it is a loss of equilibrium of the deformed structure that causes the instability.

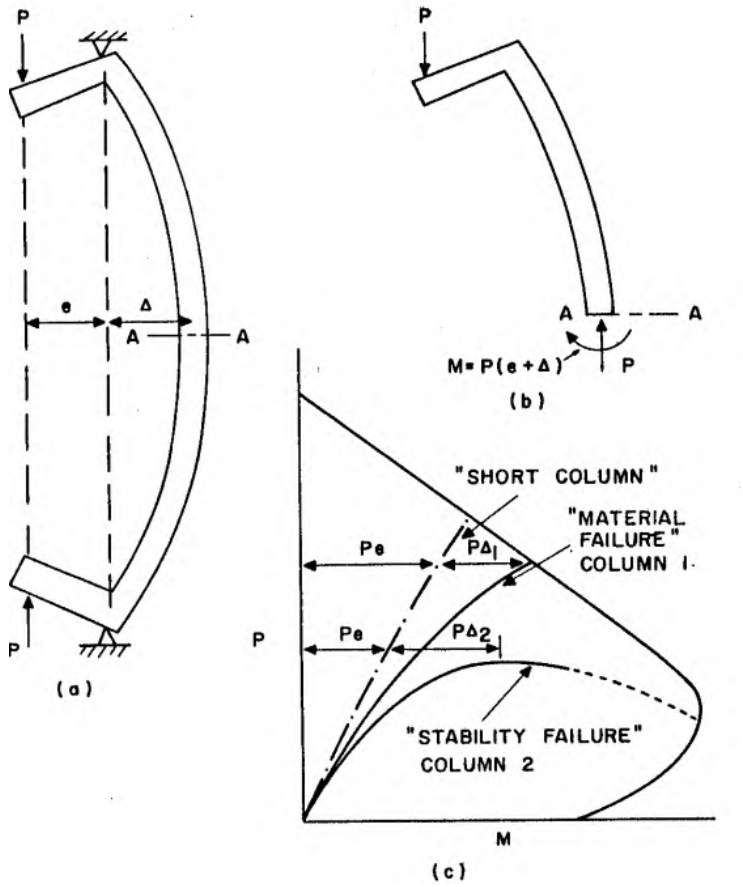

Figure 5.2 Load and moment in a slender column. MacGregor and Breen (1970).

5.3 METHOD OF SECOND-ORDER EFFECT (THEORETICAL)

The lateral displacement of a column under eccentric compression, as illustrated in Figure 5.3, prompts an increase in the moment along the normal section, represented as the secondary moment (M2), indicating second-order effects. These effects are in addition to the primary moments (M1) generated by the initial applied eccentricity. For a column with an equal axial force on the hinged ends, the greatest lateral displacement occurs at the mid-height section. Consequently, the moment resulting from increased lateral displacement must be considered. In general, the sum of the moments exerted on columns under maximum loads consists of primary moments (M1) and the

secondary moments resulting from second-order effects (M2), as represented by the equation

$$M_{total} = M_1 + M_2 \quad \text{---------- (5.19)}$$

$$M_1 = \mathrm{P.e}$$

$$M_2 = P.\Delta_{lat.}$$

Furthermore, the second-order effects, also known as P-Delta effects, represent a nonlinear phenomenon characterized by an additional moment generated through the interaction of maximum axial loads and associated lateral displacements. The magnitude of these second-order moments is mainly influenced by the initial eccentricity and the column's slenderness ratio. It is noteworthy that introducing an initial load eccentricity increases the mid-height displacement in the column, thereby enhancing the likelihood of the second-order effects. However, the initial eccentricity also reduces the column's load-bearing capacity, potentially diminishing the secondary moment.

The sum of moments (M_{total}) at the column's mid-height is:

$$M_{total} = \mathrm{P}(\mathrm{e} + \Delta_{lat.}) \quad \text{---------- (5.20)}$$

P: Axial Load (kN)

e: Eccentricity (mm)

$\Delta_{lat.}$: Horizontal displacement at columns mid-height.

The lateral displacement shape of a hinge ended column due to second-order effects can be approximately represented as a sinusoidal curve (half-sine curve) Bazant et al. (1991) Jiang (2013). With having the boundary conditions

as illustrated in Figure 5.3, the corresponding equation is derived from the differential equation of the displacement curve:

$$y = -\Delta_{lat.} \sin \frac{\pi x}{l_u} \quad \text{---------- (5.21)}$$

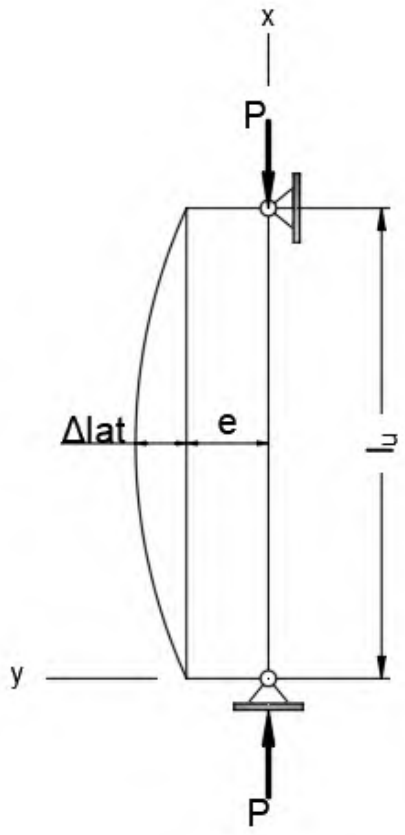

Figure 5.3 Single curvature of a pin-ended column.

y: This variable measures the lateral displacement at a given x value, x: This variable represents the height of the column up to the length, lu: the effective column length. Applying the axial load results in an increase in the value of y. When x equals lu/2, y reaches its maximum displacement value (Δ_{lat}).

Taking the second derivative of equation (5.21) will result in the equation of curvature as shown below:

$$\psi_c = \Delta_{lat.} \frac{\pi^2}{l_u^2} \sin \frac{\pi x}{l_u} \quad \text{---------- (5.22)}$$

ψ_c: is the curvature, substituting (lu/2) for x will result in the following equation:

$$\Delta_{lat} = \psi_c . \frac{l_u^2}{\pi^2} \quad \text{---------- (5.23)}$$

In the context of reinforced concrete design mechanics, the curvature can be calculated from the strain value at the failure load. The compressive strain is measured at the top fiber of the section under investigation, as illustrated below:

$$\psi_c = \frac{\varepsilon_c}{c} \quad \text{---------- (5.24)}$$

The flowchart of the analytical model procedure is presented in Figure 5.4. An Excel spreadsheet was developed to implement this procedure. The process begins by defining the column cross-section and material properties. An initial value for concrete strain at the outermost compression fiber is assumed. Subsequently, an increment value for the concrete compression block depth (c) is selected, and the compression block is divided into N segments, ensuring that the segment thickness (h) is sufficiently small to achieve precise results. The section is then analyzed iteratively, applying 0.85f'c of Whitney's block for the stress value. The force is calculated for each value of (c) in each fiber of the compression and tension zones, for concrete and steel reinforcement.

Next, the load capacity (Pn) and bending moment (Mn) are determined. Following this, the corresponding column curvature and lateral displacement are calculated. The iterative process continues until the computed percentage error, as defined by the following equation, is less than 0.5%:

$$Error = \frac{M_{total} - M_n}{M_{total}} \times 100 < 0.5\% \quad \text{---------- (5.25)}$$

Afterward, an additional increment was introduced for the concrete strain, and the procedure was reiterated until the entire loading path to failure was plotted. The failure was defined as reaching the ultimate concrete strain of 3,000 με.

The analytical method described above is utilized to plot the interaction diagram of the axial load versus the bending moment for both short and slender columns in this research study. Following the load path derived from the preceding procedure in the flowchart, the calculated values of Pn and Mn are used to plot a point on the diagram. Advancing to the next eccentricity (e) value in the flowchart yields the subsequent point, continuing this process from zero eccentricity to a high level of eccentricity, which is assumed to be 15h , (15h is an arbitrarily large number for compressive depth of the section) in the flowchart. This iterative process will result in the complete interaction diagram as shown in Figures B1 to B42 (see Appendix B).

In this study, a model for an iterative inelastic second-order analysis has been developed by integrating the material nonlinearity and member curvature. The model, based on the numerical integration technique initially proposed by (Newmark, 1943), has extensive application in analyzing steel-reinforced concrete (RC) columns, as supported by previous work (Pfrang and Siess, 1961) (Cranston, 1972, Bazant et al., 1991) . Notably, this study extends the application of the model to include recycled aggregate and steel fiber components. The first step in the implementing the numerical integration approach involves conducting a cross-sectional analysis of the concrete column. This method follows to the principle of compatibility between internal resultant forces, externally applied loads, and deformations. To

simplify the model development process, several assumptions were integrated:

1. The column's mid-height lateral deflection is deemed negligible compared to its overall length.
2. The stress-strain relationship initiates with a linear phase before transitioning to non-linearity.
3. A strong bond created between the steel reinforcement and the surrounding concrete, with strain in both materials assumed to be directly proportional to the distance from the neutral axis.
4. The maximum allowable strain at the extreme concrete compression fibers is capped at 3,000 με, following ACI 318-19 standards.
5. The tensile strength of concrete is disregarded, though steel fiber effects are considered
6. Based on experimental findings indicating limited impact, the effect of lateral confinement induced by the steel ties is disregarded in this study

The above assumptions are consistent with a prior research done by Martin et al. (1966) on steel RC columns.

As shown in Figures 5.5 to 5.8, the second-to-first-order moment ratio (M2nd/M1st) was higher in the columns under moderate eccentricity (e/h = 0.5) loadings than the columns tested under high eccentricity (e/h = 1.0) loadings. This observations align with the experimental results reported by Abdelazim et al. (2020) for circular slender columns and by Hamid and Yousif (2024). In general, it can be observed that M2nd/M1st for all columns was lower than 40%. This indicates that according to ACI 318-19 (ACI 2019), none of the tested columns experienced instability failure, and the predominant failure mode was due to material failure rather than instability failure.

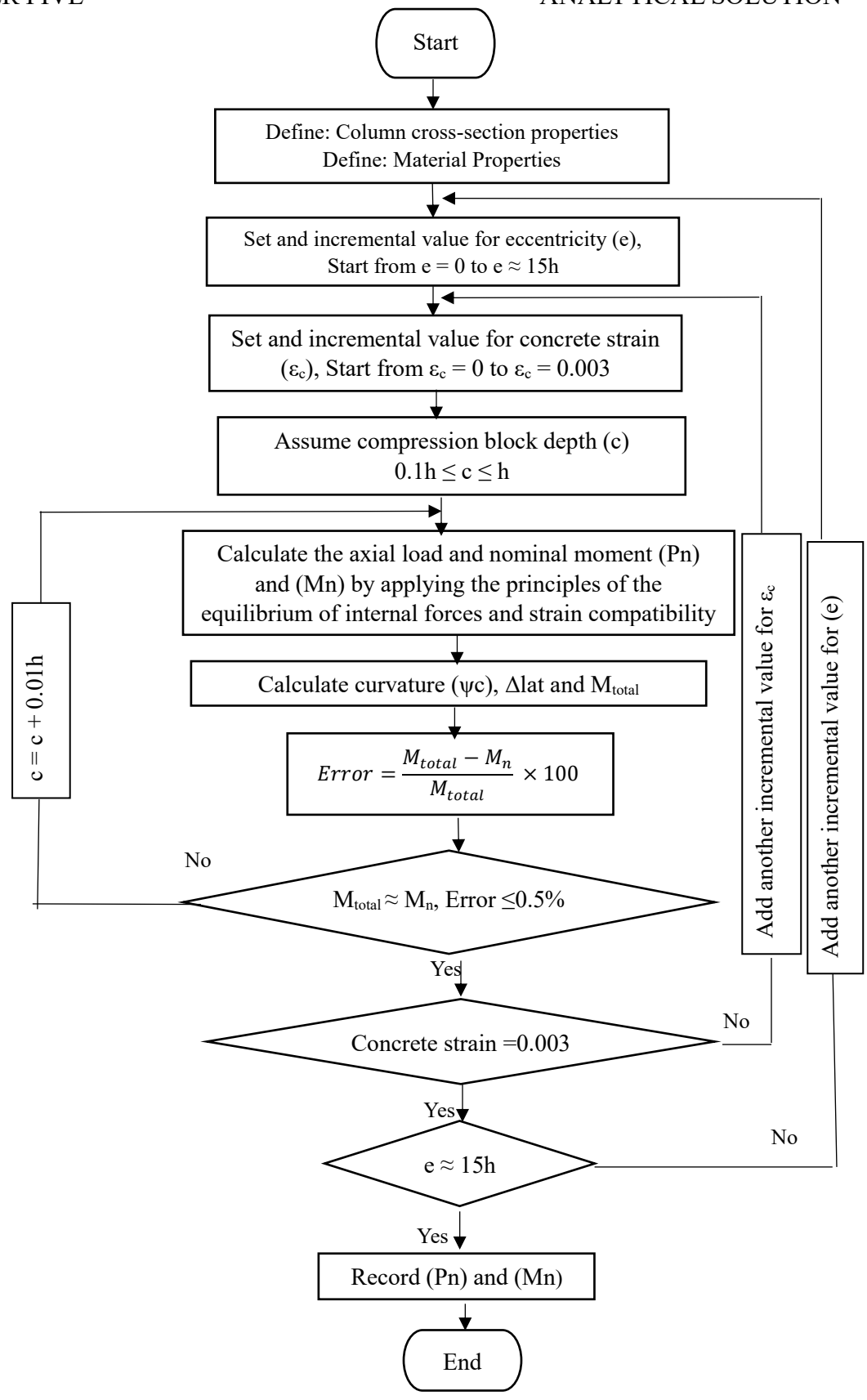

Figure 5.4: Flow chart to construct P-M diagram and Load path at any eccentricity

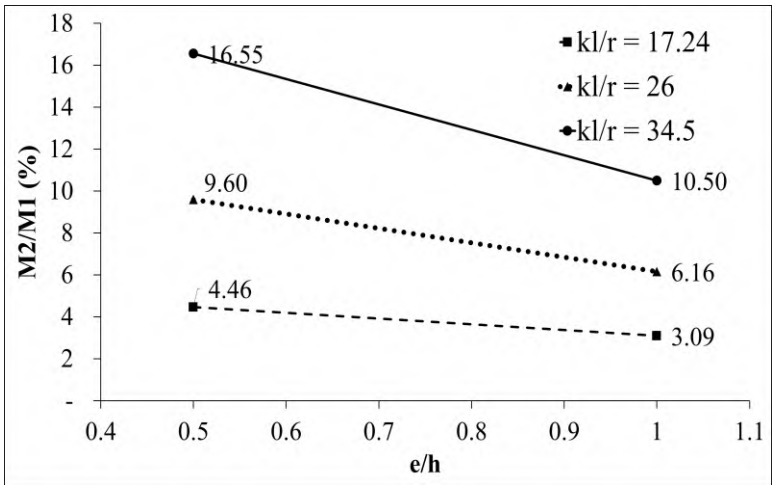

Figure 5.5: Effect of eccentricity on 2nd -to-1st order moment ratio (RA, Vf=0)

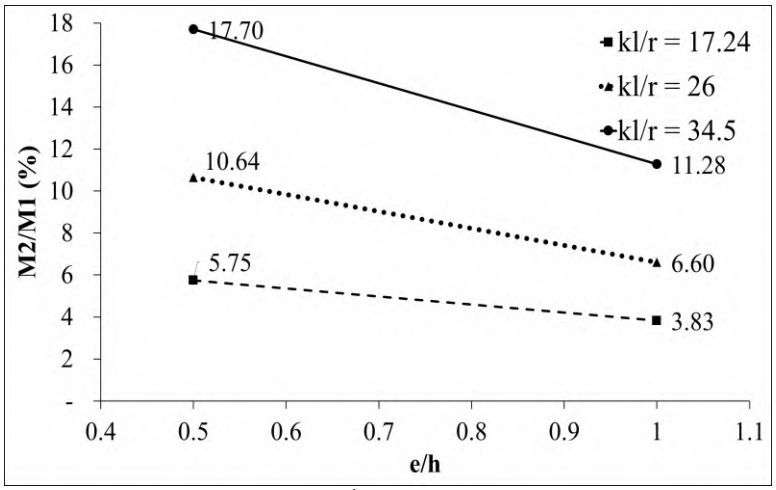

Figure 5.6: Effect of eccentricity on 2nd -to-1st order moment ratio (RA, Vf=1)

5.3.1 Analytical Model Verification

Method of second-order effect was used to develop load– moment diagrams for the columns tested in this experimental work. In Figure 5.4, the outer loop, where the eccentricity is larger than the depth of the section, plots the interaction diagram. The inner loop, where the strain reaches 0.003, plots a load path for one point. These specimens included columns with various slenderness ratios, ranging from short to

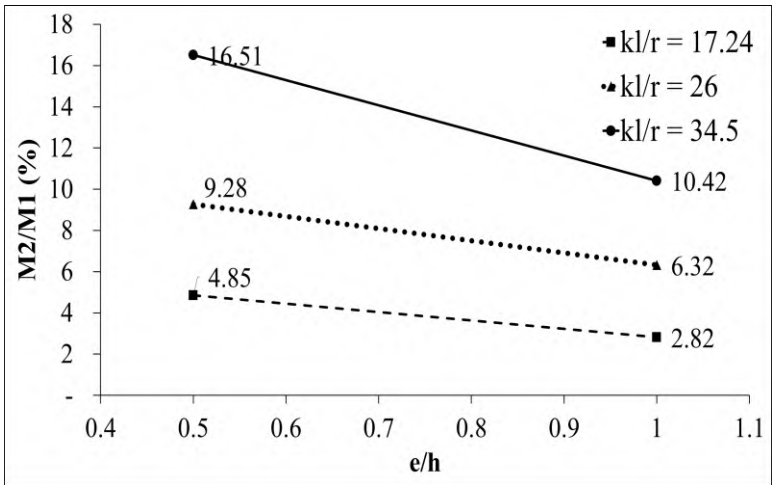

Figure 5.7: Effect of eccentricity on 2nd -to-1st order moment ratio (NA,Vf = 0)

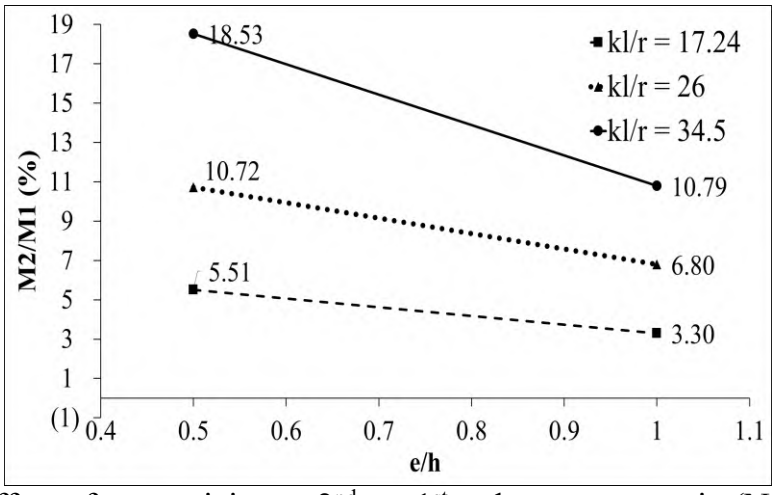

Figure 5.8: Effect of eccentricity on 2nd -to-1st order moment ratio (NA, Vf = 1)

The inner loop, where the strain reaches 0.003, plots a load path for one point. These specimens included columns with various slenderness ratios, ranging from short to very slender, different cross-sectional shapes and sizes, varying reinforcement ratios, and different concrete compressive strengths. In the theoretical/experimental study of Hamid and Yousif (2024), approximately 64% of the columns had experimental results that represented an upper bound, with theoretical predictions consistently falling within safe limits. This observation highlights the conservative nature of the theoretical model, as it

consistently provides predictions that prioritize safety and align closely with experimental data.

5.4 PROPOSED ANALYTICAL MODEL FOR COLUMN LOAD-CARRYING CAPACITY (ACI-Improved equation).

Following ACI 318-19, the axial capacity of reinforced concrete columns is given by the formula:

$$P_{ACI} = 0.85\, f_c' A_c + f_y A_s \quad \text{---------- (5.2) Repeated}$$

Here, fc' is the compressive strength of concrete cylinders, fy represents the yield stress of steel, and Ac and As stand for the cross-sectional areas of concrete and longitudinal reinforcement, respectively. It is worth noting that the contribution of the transverse reinforcement is disregarded, as permitted by ACI-318-19. This equation considers the section of the column but does not account for neither eccentricity nor slenderness.

This study proposes equations to determine both the load carrying capacity and the moment capacity of columns, the proposed equations are listed in Table 5.1. These proposed equations are utilized to create the Axial Load - Bending Moment interaction diagrams, which account for the impact of the slenderness and various levels of eccentric loading. Additionally, the proposed equations indicate the percentage of the ACI-318-19 column section capacity, considering the material properties and section characteristics.

Two equations proposed using experimental axial loads of 238 reinforced concrete columns based on the values of ($P_{Exp.}/P_{Proposed}$). The steel-reinforced concrete columns featured square, rectangular, and circular cross-sections.

The proposed equation (1) created based on 158 columns (Table A, Appendix D) included only the normal concrete column, while the proposed equation (2) used data of 193 columns (Table A, Appendix D) included both normal concrete and high-strength concrete. Equation (2) used in the analysis of this current study. The columns, drawn from both existing literature and those investigated in this study, included various concrete types (normal and high-strength), different reinforcement ratios, and features such as recycled aggregate and natural aggregate. They were also studied with and without steel fiber, varying slenderness ratios, and subjected to both eccentric and concentric loading. Figure 5.9 illustrates the ratio of $P_{Exp}/P_{Proposed}$ plotted against the ratio of P_{Exp}/P_{ACI} based on the proposed equation one, Figure 5.10 displays the ratio for equation two. The diagonal distribution of the data indicates an agreement between the experimental results and the proposed theoretical results versus the results using P_{ACI}. Moreover, statistical parameters for the two proposed models, including the coefficient of variation, mean, and standard deviation, have been calculated and are presented in Table 5.1. To study the effect of various parameters, the ratio of $P_{Exp}/P_{proposed}$ was plotted against slenderness (kL/r), eccentricity to depth ratio (e/h), and compressive strength of concrete (fc') in Figure 5.11 for proposed equation (1), and Figure 5.12 for proposed equation (2). These curves are plotted to evaluate the influence of these variables on the theoretical proposed model. The well-distributed data support the use of the proposed equation to determine the load capacity and subsequently the moments of the columns, which are used to plot the force-moment interaction diagrams for each column, Figures C1 to C42 (see Appendix C). A comparison was made among the experimental axial loads, the axial load capacity calculated using ACI-318-19 equations, the axial load capacity based on the theoretical second-

order effect, and the axial load capacity determined using the proposed equation. Table 5.2 demonstrates results using the ACI equations, the theoretical second-order effect equations, and the proposed equation all the results provided are conservative compared to the experimental results.

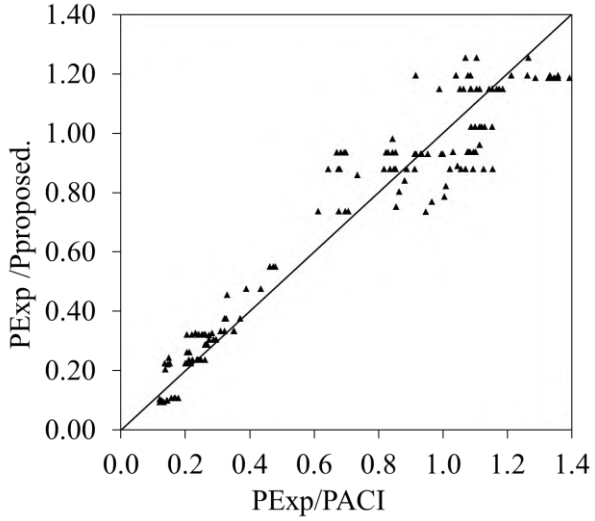

Figure 5.9: Comparison of experimental-to-theoretical axial load capacity ratios with experimental-to-aci axial load capacity ratios for proposed equation (1).

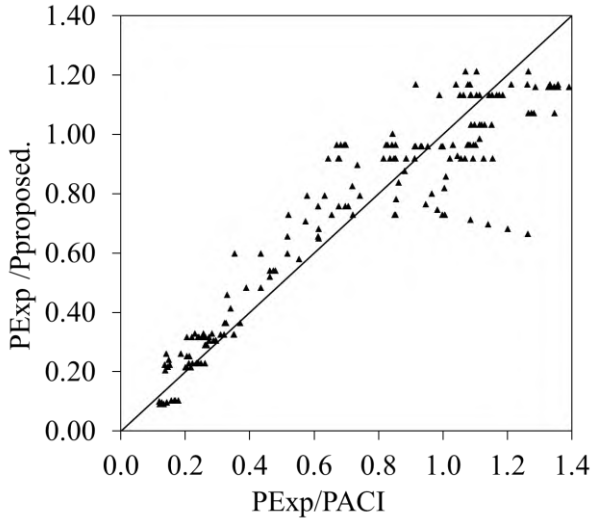

Figure 5.10: Comparison of experimental-to-theoretical axial load capacity ratios with experimental-to-aci axial load capacity ratios for proposed equation (2).

Table 5.1: Proposed models

$1.\ P_n = P_{ACI}\,(1.89\ e^{-2.2425\,(e/h)}\ (kl/r)^{-0.2158})$						
Type of data	N	r	r^2	Ravg	St. Dev.	Var.
NC	158	0.984	0.968	1.007	0.197	0.039
$2.\ P_n = P_{ACI}\,(1.6706\ e^{-2.306\,(e/h)}\ (kl/r)^{-0.1686})$						
	N	r	r^2	Ravg	St. Dev.	Var.
NC + HS Modified	193	0.980	0.959	1.015	0.232	0.054

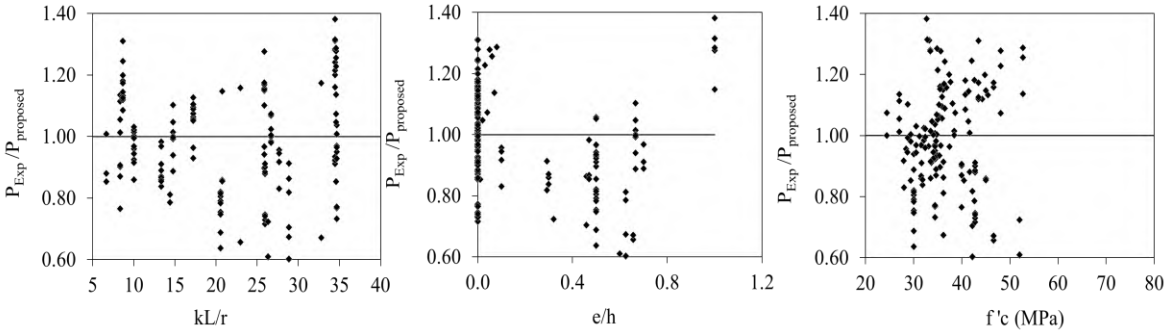

Figure 5.11: Effect of kL/r, e/h and $f'c$ on the ratio of experimental axial load to theoretical axial load for the proposed model (Equation 1)

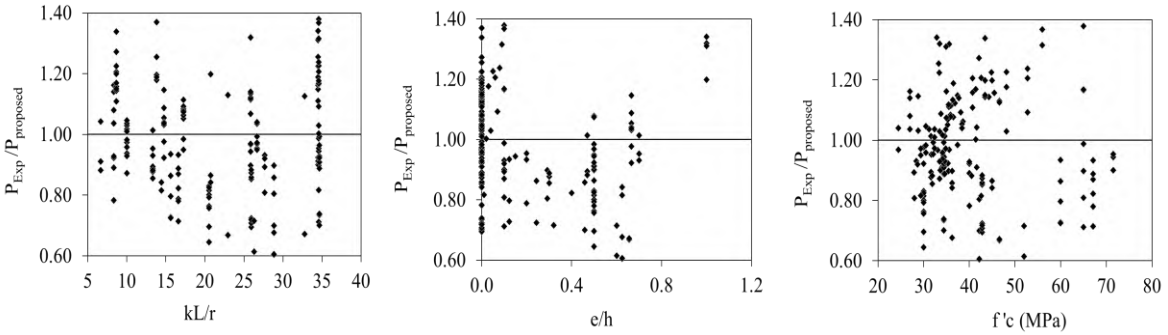

Figure 5.12: Effect of kL/r, e/h and $f'c$ on the ratio of experimental axial load to theoretical axial load for the proposed model (Equation 2)

To include the effect of the recycled aggregate and steel fiber content in addition to the effect of eccentricity and slenderness effects. The following additional equation is proposed to improve the ACI318-19 equation for the section strength.

$$P_n = (1.4623\, e^{-2.11\left(\frac{e}{h}\right)}.\left(\frac{kl}{r}\right)^{-0.1922}.e^{0.0012(\%RCA)}.e^{0.3215(F)})P_{ACI}$$

Where;

e: eccentricity of the load. (mm)

h: total depth of the column. (mm)

k: effective length coefficient

l: effective length of column (unsupported length). (mm)

r: radius of gyration (mm)

RCA%: Recycled aggregate percentage

F: Fiber factor $= \text{Vf\%}.\left(\frac{\text{L}}{\text{d}}\right)\text{f}.\,\text{d}_\text{f}$,

Vf%: volumetric percetage of steel fiber

$\left(\frac{\text{L}}{\text{d}}\right)$ f: length to diameter rtion of the steel fiber (aspect ratio)

df: bond factor depends on the type of steel fiber, it's value: 0.5 or 1.0

$$P_{ACI} = 0.85\, f_c' A_c + f_y A_s ---------(\text{ACI318} - 19)$$

The predicted results obtained from the above equation gives excellent correlation and very close to the experimental data of this study and the available columns which obtained from previous studies. The ratio between the experimental and predicted results $R = \frac{P_{n.experimneal}}{P_{n.theoretical}}$ ranging between the maximum value (1.537) and minimum value (0.434), and the average value ($\text{r}_{\text{avg}} = 1.03,$ standard deviation ($\sigma = 0.730$), variance ($\text{var} = 0.050$). The cofficient of correlation ($\text{r} = 0.977$)and ($\text{r}^2 = 0.955$).Generally the proposed equation gives very good results and very close to the experimental data and show excellent correlation.

Table 5.2: Comparison of experimental axial load with P_{ACI}, $P_{Proposed}$, and $P_{Theoretical}$

Specimen ID	$P_{Exp.}$ (kN)	P_{ACI} (kN)	Proposed (kN)	$P_{Theoretical}$ (kN	P_{Exp} / P_{ACI}	P_{Exp} / $P_{proposed}$	P_{Exp} / $P_{Theoretical}$
S-RA0Vf0E0	680	625.39	646.45	602.70	1.09	1.05	1.13
S-RA50Vf0E0	710	633.84	655.19	611.50	1.12	1.08	1.16
S-RA100Vf0E0	735	668.98	691.51	648.20	1.10	1.06	1.13
T-RA0Vf0E0	645	625.39	603.73	576.70	1.03	1.07	1.12
T-RA50Vf0E0	685	636.19	614.16	596.80	1.08	1.12	1.15
T-RA100Vf0E0	700	645.82	623.46	618.30	1.08	1.12	1.13
L-RA0Vf0E0	642	628.51	578.02	583.80	1.02	1.11	1.10
L-RA50Vf1E0	678	601.96	553.61	598.00	1.13	1.22	1.13
L-RA100Vf0E0	690	653.24	600.76	608.00	1.06	1.15	1.13
S-RA0Vf1E0	714	641.52	663.13	619.00	1.11	1.08	1.15
S-RA50Vf1E0	730	633.71	655.06	634.00	1.15	1.11	1.15
S-RA100Vf1E0	748	662.35	684.65	641.00	1.13	1.09	1.17
T-RA0Vf1E0	678	627.99	606.25	582.08	1.08	1.12	1.16
T-RA50Vf1E0	700	639.44	617.30	603.00	1.09	1.13	1.16
T-RA100Vf1E0	723	656.88	634.14	633.10	1.10	1.14	1.14
L-RA0Vf1E0	665	622.00	572.04	576.00	1.07	1.16	1.15
L-RA50Vf1E0	692	599.49	551.33	603.30	1.15	1.26	1.15
L-RA100Vf1E0	701	641.26	589.75	596.40	1.09	1.19	1.18
S-RA100Vf0E0.5	190	178.00	200.13	175.90	1.07	0.95	1.08
S-RA0Vf0E0.5	210	187.00	213.38	181.50	1.12	0.98	1.16
T-RA100Vf0E0.5	176	155.50	182.02	171.80	1.13	0.97	1.02
T-RA0Vf0E0.5	172	152.15	191.50	169.20	1.13	0.90	1.02
L-RA100Vf0E0.5	161	140.00	176.81	159.60	1.15	0.91	1.01
L-RA0Vf0E0.5	158	139.00	175.48	157.40	1.14	0.90	1.00
S-RA100Vf1E0.5	223	184.43	206.79	179.63	1.20	1.08	1.24
S-RA0-Vf1E0.5	218	182.00	202.97	177.34	1.19	1.07	1.23
T-RA100Vf1E0.5	186	146.00	192.06	171.50	1.27	0.97	1.08
T-RA0Vf1E0.5	177	145.33	187.54	170.13	1.21	0.94	1.04
L-RA100Vf1E0.5	163	135.10	178.66	161.81	1.20	0.91	1.01
L-RA0Vf1E0.5	168	136.55	181.87	163.87	1.23	0.92	1.02
S-RA100Vf0E1.0	100	84.00	65.68	81.14	1.19	1.52	1.23
S-RA0Vf0E1.0	105	83.00	63.81	80.37	1.27	1.65	1.31
T-RA100Vf0E1.0	76.5	75.50	57.95	76.80	1.01	1.32	1.00
T-RA0Vf0E1.0	80	76.70	60.63	77.84	1.04	1.32	1.03
L-RA100Vf0E1.0	74.5	72.00	56.85	73.68	1.03	1.31	1.01
L-RA0Vf0E1.0	73	71.00	54.44	72.73	1.03	1.34	1.00
S-RA100Vf1E1.0	107	92.00	66.37	85.24	1.16	1.61	1.25
S-RA0Vf1E1.0	112	91.00	64.00	83.60	1.23	1.71	1.33
T-RA100Vf1E1.0	86.5	82.00	58.13	80.60	1.05	1.49	1.07
T-RA0Vf1E1.0	87	83.90	58.99	81.22	1.04	1.47	1.07
L-RA100Vf1E1.0	80.5	77.00	55.37	76.84	1.05	1.45	1.04
L-RA0Vf1E1.0	76.5	76.00	54.28	76.46	1.01	1.41	1.00

5.5 LATERAL DISPLACEMENT

The experimental lateral displacement results at the mid-height of the columns, as presented in Chapter 4, are verified in this section. Equation 5.22, derived earlier, is adopted to calculate the lateral displacement:

$$\Delta_{lat} = \psi_c . \frac{l_u^2}{\pi^2}$$ ---------- 5.23 (repeated)

A concrete strain in compression of 0.003, based on ACI-318, is used. The compression block depth (c) is taken from the PM-interaction diagram analysis for each column. The linear distribution of the strain compatibility is explained in Section 5.2, and a sample spreadsheet calculation is provided in Appendix A, equations 5.26 to 5.28 are used to calculate the value of the strains. The curvatures ψc are calculated based on the specific strain and compressive depth values.

The second method used for verification is called theoretical displacement. This method uses the same equation mentioned above; however, the experimental concrete strain and experimental steel strain are used to determine the compression block depth, which is then used to calculate the curvature and subsequently the displacement.

In both methods, knowing the strain values and the effective depth values in tension and compression, the compression block depth c can be calculated:

$$\varepsilon_s^{;} = \frac{c-d'}{c} \varepsilon_{cu}$$ ----------5.26

$$\varepsilon_s = \frac{d-c}{c} \varepsilon_{cu}$$ ----------5.27

$$\varepsilon_t = \frac{h-c}{c} \varepsilon_{cu}$$ ----------5.28

Table 5.3 compares the lateral displacement values obtained experimentally with those derived from the theoretical methods. Additionally, it displays the ratio of experimental displacement to the ACI displacement and the ratio of experimental displacement to theoretical displacement.

5.6 CONCRETE AND REINFORCEMENT STRAINS.

The calculated strain values displayed in Chapter 4 have been processed as follows. The analysis of the PM interaction diagram is used to determine the depth of the compression block, as well as to calculate the reinforcement and concrete strains. The simple rules of similar triangles are utilized to calculate the strains in equations 5.26 and 5.27. Here, (d) represents the effective depth from the top fiber in compression to centroid of the tension steel, (c) is the distance from the extreme compression fiber to the neutral axis, (d') is the distance from the compression fiber to the centroid of the steel in compression, and (h) is the depth of the section. According to ACI-318-19, the concrete strain in the extreme compression fiber is 0.003. The concrete strain in the tension face is calculated using Equation 5.28.

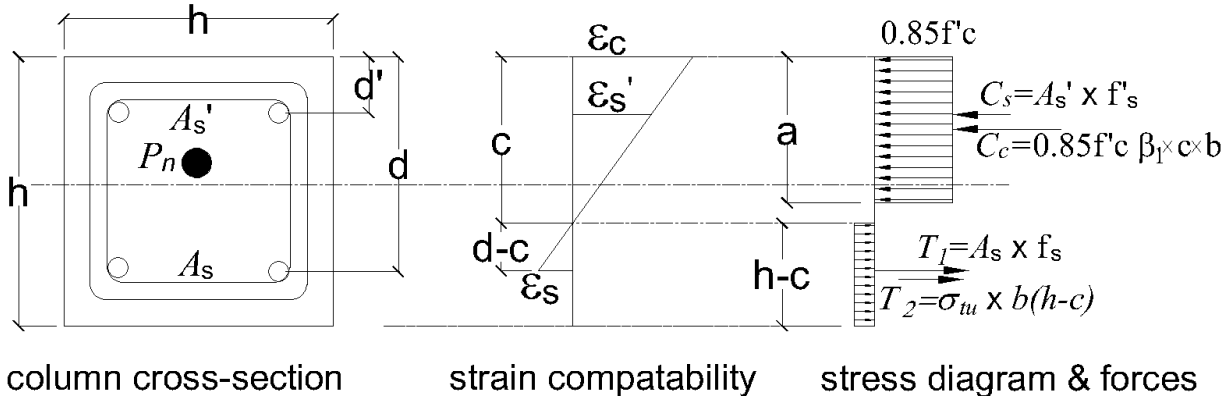

Figure 5.1: Column section analysis (Repeated)

Table 5.3: Comparison of experimental, ACI, and theoretical lateral displacements.

Specimen ID	$\Delta_{Exp.}$(mm)	Δ_{ACI} (mm)	C_{ACI}	$\Delta_{theo.}$ (mm)	$C_{Exp.}$	$\Delta_{Exp/}$ Δ_{ACI}	$\Delta_{Exp.}$/ $\Delta_{Theo.}$
S-RA0Vf0E0	1.03	0.95	125.00	1.01	125.00	1.08	1.02
S-RA50Vf0E0	1.10	0.95	125.00	1.05	125.00	1.16	1.05
S-RA100Vf0E0	0.93	0.95	125.00	1.05	125.00	0.98	0.88
T-RA0Vf0E0	2.55	2.14	125.00	2.35	125.00	1.19	1.09
T-RA50Vf0E0	2.62	2.14	125.00	2.42	125.00	1.23	1.08
T-RA100Vf0E0	2.40	2.14	125.00	2.29	125.00	1.12	1.05
L-RA0Vf0E0	3.50	3.80	125.00	4.16	125.00	0.92	0.84
L-RA50Vf1E0	4.50	3.80	125.00	4.32	125.00	1.18	1.04
L-RA100Vf0E0	4.20	3.80	125.00	4.47	125.00	1.10	0.94
S-RA0Vf1E0	1.11	0.95	125.00	1.08	125.00	1.17	1.02
S-RA50Vf1E0	1.25	0.95	125.00	1.14	125.00	1.31	1.10
S-RA100Vf1E0	1.08	0.95	125.00	1.17	125.00	1.14	0.92
T-RA0Vf1E0	2.65	2.14	125.00	2.54	125.00	1.24	1.04
T-RA50Vf1E0	2.80	2.14	125.00	2.61	125.00	1.31	1.07
T-RA100Vf1E0	2.50	2.14	125.00	2.39	125.00	1.17	1.05
L-RA0Vf1E0	3.73	3.80	125.00	4.88	125.00	0.98	0.77
L-RA50Vf1E0	5.40	3.80	125.00	5.25	125.00	1.42	1.03
L-RA100Vf1E0	4.39	3.80	125.00	5.86	125.00	1.15	0.75
S-RA100Vf0E0.5	2.79	1.93	61.60	2.20	59.12	1.45	1.27
S-RA0Vf0E0.5	3.03	1.94	61.25	2.19	57.53	1.56	1.39
T-RA100Vf0E0.5	6.00	4.68	57.02	5.49	54.76	1.28	1.09
T-RA0Vf0E0.5	5.80	4.67	57.16	5.18	52.48	1.24	1.12
L-RA100Vf0E0.5	10.34	8.52	55.78	9.75	54.07	1.21	1.06
L-RA0Vf0E0.5	10.32	8.51	55.84	9.73	52.35	1.21	1.06
S-RA100Vf1E0.5	3.59	1.88	63.20	2.63	63.09	1.91	1.37
S-RA0-Vf1E0.5	3.45	1.88	63.30	2.45	61.25	1.84	1.41
T-RA100Vf1E0.5	6.65	4.65	57.44	5.94	57.71	1.43	1.12
T-RA0Vf1E0.5	6.70	4.64	57.55	5.74	57.86	1.44	1.17
L-RA100Vf1E0.5	11.06	8.48	56.07	10.46	56.97	1.30	1.06
L-RA0Vf1E0.5	11.58	8.51	55.88	10.92	55.47	1.36	1.06
S-RA100Vf0E1.0	3.87	2.82	42.19	3.28	44.73	1.37	1.18
S-RA0Vf0E1.0	3.52	2.78	42.78	3.35	44.42	1.27	1.05
T-RA100Vf0E1.0	7.70	6.38	41.86	6.79	38.44	1.21	1.13
T-RA0Vf0E1.0	7.90	6.53	40.93	6.86	38.79	1.21	1.15
L-RA100Vf0E1.0	13.13	11.81	40.27	12.38	37.38	1.11	1.06
L-RA0Vf0E1.0	13.03	11.55	41.15	12.29	38.10	1.13	1.06
S-RA100Vf1E1.0	4.79	2.62	45.37	3.36	45.37	1.83	1.43
S-RA0Vf1E1.0	4.13	2.59	45.89	3.44	44.82	1.59	1.20
T-RA100Vf1E1.0	8.25	5.95	44.91	7.36	42.61	1.39	1.12
T-RA0Vf1E1.0	8.50	6.11	43.69	7.41	41.72	1.39	1.15
L-RA100Vf1E1.0	14.10	10.87	43.75	13.30	40.26	1.30	1.06
L-RA0Vf1E1.0	13.49	10.77	44.16	12.72	39.06	1.25	1.06

CHAPTER SIX

CONCLUSIONS AND RECOMMENDATIONS

CHAPTER SIX
CONCLUSIONS AND RECOMMENDATIONS

6.1 CONCLUSIONS

In this study, 42 short and slender columns were cast and tested to examine the effects of recycled aggregate, steel fiber, loading eccentricity, and slenderness. The experimental results and theoretical analysis led to the following conclusions:

1. In concentrically loaded columns, those made with recycled aggregate showed better strength than those with natural aggregate. Columns without steel fiber had a 50% replacement resulting in an average strength increase of 5.4%, while 100% replacement led to an 8% increase. In columns with steel fiber, 50% replacement yielded a 3.2% increase and 100% a 5.6% increase, indicating a greater effect without steel fiber.
2. In concentrically loaded columns, strength loss was attributed to an increased slenderness ratio. For natural aggregate without steel fiber, the loss was 5.4%; with steel fiber, it was 5.9%. Columns with 50% recycled aggregate lost 4.0% without steel fiber and 4.7% with it, while 100% recycled aggregate columns lost 5.5% without and 4.8% with steel fiber. This shows strength loss due to slenderness, regardless of aggregate type.
3. A 1% steel fiber content increased column strength, more so in slender columns ($kl/r = 26$) compared to short ones ($kl/r = 17.24$) or those with $kl/r = 34.5$. This effect intensified with increased eccentricity, peaking at a 10.9% increase in columns with $kl/r = 26$ at $e/h = 1.0$.

4. In concentrically loaded columns, displacement increased with 50% recycled aggregate replacement but decreased with 100% in short, moderately slender, and highly slender columns. In eccentrically loaded columns, displacement was higher with recycled aggregate, regardless of proximity.
5. Mid-height displacement was greater in columns without steel fiber. In concentrically loaded columns, the increase for those with kl/r = 26 was larger than for kl/r values of 17.24 and 34.5. In eccentrically loaded columns, the increase in displacement from steel fiber was more pronounced in short columns than slender ones.
6. In concentrically loaded columns, both natural and recycled aggregates exhibited similar responses, with greater effects in columns without steel fiber, a trend that also applied to eccentrically loaded columns.
7. Vertical displacement in concentrically loaded columns increased with recycled aggregate, peaking at 100% replacement compared to 50%. In eccentrically loaded columns at e/h = 0.5, similar increases were observed, but not for e/h = 1.0.
8. Vertical displacement increased by about 50% in concentrically loaded columns with a slenderness ratio (kl/r) of 26 compared to short columns (kl/r = 17.24), and by about 100% in columns with kl/r = 34.5. In eccentrically loaded columns, the effect on vertical displacement was much lower, with increases of less than 20% for both e/h = 0.5 and e/h = 1.0.
9. In concentrically loaded columns, vertical displacement increased due to steel fiber, with few exceptions where it decreased or remained unchanged. In eccentrically loaded columns, vertical displacement consistently

increased, particularly in columns with kl/r = 34.5, where the increase was about 15-20% for both e/h = 0.5 and e/h = 1.0.

10. The cracking depth in eccentrically loaded columns without steel fiber was greater than in those with steel fiber, with higher slenderness ratios corresponding to deeper cracks. Cracking loads were higher in short columns than slender ones, and were also greater in columns with steel fiber.
11. Concentrically loaded columns failed suddenly and explosively, whereas eccentrically loaded columns exhibited more ductility, allowing for crack observation before failure.
12. Eccentricity significantly affected the failure mode compared to recycled aggregate, steel fiber, and slenderness. Load-carrying capacity decreased markedly with increased eccentricity, causing behavior to shift from compression control to flexural control.
13. Crack patterns in eccentrically loaded columns were comparable for those made with recycled aggregate, regardless of steel fiber presence, and matched those of columns made with natural aggregate.
14. The proposed analytical model predicts the load-carrying capacity of both short and slender columns, accounting for eccentricity, slenderness ratio, recycled aggregate, and steel fiber.
15. Recycling waste concrete reduces landfill waste, which is environmentally beneficial.

6.2 RECOMMENDATIONS:

- Further researches are needed, specifically for the slender columns, high level of eccentricity, and high-strength concrete.
- Construction waste demolition to be used for recycled aggregate.
- Recycled steel fiber to be utilized
- Recycled fine aggregate to be utilized
- 19 mm maximum aggregate size for the larger recycled coarse aggregate to be utilized.
- Different sizes of columns to study size effect
- High-strength concrete is to be used and compared with normal-strength concrete with recycled aggregate.
- Rectangular and circular columns are to be tested using recycled aggregates.
- Different ratios of steel reinforcement to be utilized.
- GFRP and CFRP bars are to be used in normal temperatures and high degrees of temperature.
- Recycled aggregate concrete columns with biaxial loadings to be tested
- Study the performance of recycled concrete aggregate with different ratios of steel fiber.
- More researches in the field of recycled materials is required to assist officials in making decisions on incorporating provisions to the design codes for using recycled materials.

REFERENCES

REFERENCES

ABDELAZIM, W., MOHAMED, H. M. & BENMOKRANE, B. 2020. Inelastic second-order analysis for slender GFRP-reinforced concrete columns: Experimental investigations and theoretical study. *Journal of Composites for Construction,* 24**,** 04020016.

ABDULLA, N. A. 2020. Mechanical behavior of slender composite columns under axial compression load. *KSCE Journal of Civil Engineering,* 24**,** 208-218.

ACI-318-19 ACI 318-19 Building Code Requirements for Structural Concrete (ACI 318-19) and Commentary (ACI 318R-19). ACI Committee 318.

AHMAD, S. H. & BARKER, R. 1991. Flexural behavior of reinforced high-strength lightweight concrete beams. *Structural Journal,* 88**,** 69-77.

AJDUKIEWICZ, A. B. & KLISZCZEWICZ, A. T. 2007. Comparative tests of beams and columns made of recycled aggregate concrete and natural aggregate concrete. *Journal of Advanced Concrete Technology,* 5**,** 259-273.

AL-TAAN, S. A. & ALDOSKI, A. J. S. A. A. 2020. Strength of steel fiber high-strength reinforced concrete columns under concentric and eccentric loads. *Jordan Journal of Civil Engineering,* 14.

ALI, F., HASAN, Q. & MOHAMMED, D. Behavior of Recycled Aggregate Concrete Slender Column under Concentric Axial Loading. E3S Web of Conferences, 2023. EDP Sciences, 02016.

ASAD-UR-REHMAN KHAN, S. F., SYED MUHAMMAD SHAMAIM ALI 2019. Behavior of Recycled Aggregate Reinforced Concrete Columns under Uniaxial Loading.

ASTM-A615/A615M 2022. ASTM A615.

ASTM-A820-01 2001. Standard Specification for Steel Fibers for Fiber-Reinforced Concrete.

ASTM-C33/C33M-18 2018. ASTM C33/C33M-18 Standard Specification for Concrete Aggregates.

ASTM-C39/C39M-21 2021. Standard Test Method for Compressive Strength of Cylindrical Concrete Specimens.

ASTM-C78-09 2009. Standard Test Method for Flexural Strength of Concrete.

ASTM-C127-15 2015. ASTM C127 Standard Test Method for Density, Relative Density (Specific Gravity), and Absorption of Coarse Aggregate.

ASTM-C150/150M 2022. ASTM C150-07 Standard Specification for Portland Cement.

ASTM-C469/C469M-22 2022. Standard Test Method for Static Modulus of Elasticity and Poisson's Ratio of Concrete in Compression.

ASTM-C496-96 1996. Standard Test Method for Splitting Tensile Strength of Cylindrical Concrete Specimens.

AZIZINAMINI, A., PAVEL, R., HATFIELD, E. & GHOSH, S. K. 1999. Behavior of lap-spliced reinforcing bars embedded in high-strength concrete. *Structural Journal,* 96**,** 826-835.

BALANJI, E. K., SHEIKH, M. N. & HADI, M. N. Behaviour of high strength concrete columns reinforced with steel fibres under different eccentric loads. Australasian Structural Engineering Conference: ASEC 2016: ASEC 2016, 2016. Engineers Australia Barton, ACT, 115-121.

BAZANT, Z. 1998. Size effect in tensile and compression fracture of concrete structures: Computational modeling and design. *AEDIFICATIO Publishers, Fracture Mechanics of Concrete Structures,* 3**,** 1905-1922.

BAZANT, Z. P., CEDOLIN, L. & TABBARA, M. R. 1991. New method of analysis for slender columns. *ACI Structural Journal,* 88**,** 391-401.

BAŽANT, Z. P., ZI, G. & MCCLUNG, D. 2003. Size effect law and fracture mechanics of the triggering of dry snow slab avalanches. *Journal of Geophysical Research: Solid Earth,* 108.

BENTUR, A. & MINDESS, S. 2006. *Fibre reinforced cementitious composites*, Crc Press.

CABALLERO-MORRISON, K. E., BONET, J. L., NAVARRO-GREGORI, J. & MARTÍ-VARGAS, J. R. 2012. Behaviour of steel-fibre-reinforced normal-strength concrete slender columns under cyclic loading. *Engineering Structures,* 39**,** 162-175.

CHAN, D. & SUN, P. C. 2006. Effects of fine recycled aggregate as sand replacement in concrete. *HKIE Transactions,* 13**,** 2-7.

CHOI, W.-C. & YUN, H.-D. 2012. Compressive behavior of reinforced concrete columns with recycled aggregate under uniaxial loading. *Engineering structures,* 41**,** 285-293.

CHUNYANG LIU1, *, JIA XU1, YIFAN GU1, RUOFAN SHI1 2021. Experimental Study on the Axial Compression Behavior of Short Columns of Steel-Fiber-Reinforced Recycled Aggregate Concrete. *Fluid Dynamics & Materials Processing 2021*.

CRANSTON, W. 1972. Analysis and design of reinforced concrete columns.

DE BRITO, J. & SAIKIA, N. 2012. *Recycled aggregate in concrete: use of industrial, construction and demolition waste*, Springer Science & Business Media.

DERESA, S. T., XU, J., DEMARTINO, C., HEO, Y., LI, Z. & XIAO, Y. 2020. A review of experimental results on structural performance of reinforced recycled aggregate concrete beams and columns. *Advances in Structural Engineering,* 23**,** 3351-3369.

EL-GOHARY, H. Test on slender concrete columns under eccentric compression. Eleventh International Colloquium on Structural and Geotechnical Engineering, Faculty of Engineering, Ain Shams University, Cairo, Egypt, 2005. 17-19.

GAO, D., LI, W., PANG, Y. & HUANG, Y. 2021. Behavior analysis and strength prediction of steel fiber reinforced recycled aggregate concrete column under axial compression. *Construction and Building Materials,* 290**,** 123278.

HADI, M. N. & ELBASHA, N. 2007. Effects of tensile reinforcement ratio and compressive strength on the behaviour of over-reinforced helically confined HSC beams. *Construction and Building Materials,* 21**,** 269-276.

HAMID, F. L. & YOUSIF, A. R. 2024. Behavior of Short and Slender RC Columns with BFRP Bars under Axial and Flexural Loads: Experimental and Analytical Investigation. *Journal of Composites for Construction,* 28**,** 04023072.

HANNANT, P. 1978. Fibre cements and fibre concretes.

HAO, T., ZHAO, L. T. & DU, Z. H. 2012. Experimental study on compressive performance of RC columns with recycled aggregate. *Key Engineering Materials,* 517**,** 589-594.

HOSINIEH, M. M., AOUDE, H., COOK, W. D. & MITCHELL, D. 2015. Behavior of ultra-high performance fiber reinforced concrete columns under pure axial loading. *Engineering Structures,* 99**,** 388-401.

HUNG, C.-C. & HU, F.-Y. 2018. Behavior of high-strength concrete slender columns strengthened with steel fibers under concentric axial loading. *Construction and Building Materials,* 175**,** 422-433.

JIANG, T., AND J. G. TENG 2013. Behavior and design of slender FRP-confined circular RC columns. *ournal of Composites for Construction 17.4 (2013): 443-453.*

KHAFAGA, M. & SAYED, M. 2011. Behavior of Axially Loaded Reinforced Concrete Short Columns Contain Recycled Coarse Aggregates.

KHALIL, W. I., GORGIS, I. N. & MAHDI, Z. R. 2012. Behavior of high performance fiber reinforced concrete columns. *ARPN Journal of Engineering and Applied Sciences,* 7**,** 1455-1467.

KHELIL, A., BOISSIÈRE, R., AL MAHMOUD, F., WURTZER, F. & BLIN-LACROIX, J. L. 2021. Experimental and numerical investigation on

axial compression of reinforced concrete columns made from recycled coarse and fine aggregates. *Structural Concrete,* 22**,** E193-E206.

KIM, J.-H., SUNG, J.-H., JEON, C.-S., LEE, S.-H. & KIM, H.-S. 2019. A study on the properties of recycled aggregate concrete and its production facilities. *Applied Sciences,* 9**,** 1935.

KNAACK, A. M. & KURAMA, Y. C. 2020. Effect of recycled concrete coarse aggregates on service-load deflections of reinforced concrete columns. *Engineering Structures,* 204**,** 109955.

KOTTB, H. A., EL-SHAFEY, N. F. & TORKEY, A. A. 2015. Behavior of high strength concrete columns under eccentric loads. *HBRC Journal,* 11**,** 22-34.

KOU, S.-C. & POON, C.-S. 2013. Long-term mechanical and durability properties of recycled aggregate concrete prepared with the incorporation of fly ash. *Cement and Concrete Composites,* 37**,** 12-19.

LI, C., GENG, H., DENG, C., LI, B. & ZHAO, S. 2019. Experimental investigation on columns of steel fiber reinforced concrete with recycled aggregates under large eccentric compression load. *Materials,* 12**,** 445.

LI, R., DENG, M. & ZHANG, Y. Behavior of highly ductile fiber–reinforced concrete columns under eccentric loading. Structures, 2021. Elsevier, 3357-3370.

LIMA, L., TRINDADE, E., ALENCAR, L., ALENCAR, M. & SILVA, L. 2021. Sustainability in the construction industry: A systematic review of the literature. *Journal of Cleaner Production,* 289**,** 125730.

LIU, S., WANG, X., ALI, Y. M., HUANG, H., ZHOU, J. & WU, Z. 2023. Experimental study on eccentric compression behavior of slender rectangular concrete columns reinforced with steel and BFRP bars. *Engineering Structures,* 293**,** 116626.

LYSE, I. & KREIDLER, C. Fourth progress report on the column tests at Lehigh University. Journal Proceedings, 1932. 317-346.

MACGREGOR, J. G. 1993. Design of slender columns revisited. *Structural Journal,* 90**,** 302-309.

MACGREGOR, J. G. & BREEN, J. E. Design of slender concrete columns. Journal Proceedings, 1970. 6-28.

MALEŠEV, M., RADONJANIN, V. & MARINKOVIĆ, S. 2010. Recycled concrete as aggregate for structural concrete production. *Sustainability,* 2**,** 1204-1225.

MAMLOUK, M. S. & ZANIEWSKI, J. P. 2014. *Materials for civil and construction engineers*, Pearson London, UK:.

MARTI, P., PFYL, T., SIGRIST, V. & ULAGA, T. 1999. Harmonized test procedures for steel fiber-reinforced concrete. *Materials Journal,* 96**,** 676-685.

MAZHOUD, B., SEDRAN, T., CAZACLIU, B., COTHENET, A. & TORRENTI, J.-M. 2022. Influence of residual mortar volume on the properties of recycled concrete aggregates. *Journal of Building Engineering,* 57**,** 104945.

MCNEIL, K. & KANG, T. H.-K. 2013. Recycled concrete aggregates: A review. *International journal of concrete structures and materials,* 7**,** 61-69.

MIRZA, S. 1990. Flexural stiffness of rectangular reinforced concrete columns. *ACI Structural Journal,* 87**,** 425-435.

MOCKRY, E. F. & DARWIN, D. 1982. Slender Columns Interaction Diagrams. *Concrete International,* 4**,** 44-50.

NEMATZADEH, M., MOUSAVIMEHR, M., SHAYANFAR, J. & OMIDALIZADEH, M. 2021. Eccentric compressive behavior of steel fiber-reinforced RC columns strengthened with CFRP wraps: Experimental investigation and analytical modeling. *Engineering Structures,* 226**,** 111389.

NEWMARK, N. M. 1943. Numerical procedure for computing deflections, moments, and buckling loads. *Transactions of the American Society of Civil Engineers,* 108**,** 1161-1188.

NG, T., HTUT, T. & FOSTER, S. 2012. Fracture of steel fibre reinforced concrete–The unified variable engagement model. *UNICIV Rep. No. R-460, May 2012*.

OTHMAN, Z. S. & MOHAMMAD, A. H. 2019. Behaviour of eccentric concrete columns reinforced with carbon fibre-reinforced polymer bars. *Advances in civil engineering,* 2019.

OZBAKKALOGLU, T., GHOLAMPOUR, A. & XIE, T. 2018. Mechanical and durability properties of recycled aggregate concrete: effect of recycled aggregate properties and content. *Journal of Materials in Civil Engineering,* 30**,** 04017275.

PACHECO TORGAL, F., JALALI, S., TORGAL, F. P. & JALALI, S. 2011. Construction and demolition (C&D) wastes. *Eco-efficient construction and building materials***,** 51-73.

PAULTRE, P., EID, R., LANGLOIS, Y. & LÉVESQUE, Y. 2010. Behavior of steel fiber-reinforced high-strength concrete columns under uniaxial compression. *Journal of Structural Engineering,* 136**,** 1225-1235.

PFRANG, E. & SIESS, C. 1961. Analytical Study of the Behavior of Long Restrained Concrete Columns Subjected to Eccentric Loads. *Civil Engineering Studies, Structural Research Series*.

PRADHAN, S., NAYAK, T. K., KUMAR, S. & BARAI, S. V. 2023. Experimental and numerical study of recycled aggregate concrete column. *Structural Concrete,* 24**,** 3498-3519.

QUANG, N. T., CUONG, T. V., TAN, N. N., TAN, N. H., KAWAMOTO, K. & GIANG, N. H. 2022. Experimental studies on behaviors of reinforced concrete column structures made of recycled aggregates under concentric loads. *Journal of Science and Technology in Civil Engineering (JSTCE)-HUCE,* 16**,** 1-11.

RAGAB, K. S. & EISA, A. S. 2015. Effect of Steel Fibers Reinforced High Strength Self-Consolidating Concrete (SFRHSCC) on axially loaded columns reinforced longitudinally and transversely by GFRP bars. *International Journal of Civil & Structural Engineering,* 5**,** 227-242.

RAMESH, R. B., MIRZA, O. & KANG, W. H. 2019. Mechanical properties of steel fiber reinforced recycled aggregate concrete. *Structural Concrete,* 20**,** 745-755.

RAMPIT, R., SMITH, J. & RAY, I. 2020. A review of recycled concrete aggregates as a sustainable construction material.

REN, F., WU, D., CHEN, G., XIE, P., XIONG, M.-X. & LIANG, Y. 2021. Slender FRP-confined steel-reinforced RAC columns under eccentric compression: Buckling behavior and design calculation models. *Engineering Structures,* 246**,** 113059.

REYNOLDS, C. E. & STEEDMAN, J. C. 2017. *Examples of the design of reinforced concrete buildings to BS8110*, CRC Press.

RIDZUAN, A., IBRAHIM, A., ISMAIL, A. & DIAH, A. Durablity performance of recycled aggregate concrete. Achieving Sustainability in Construction: Proceedings of the International Conference held at the University of Dundee, Scotland, UK on 5–6 July 2005, 2005. Thomas Telford Publishing, 193-202.

SAMANI, A. K., ATTARD, M. M. & FOSTER, S. J. 2015. Ductility in concentrically loaded reinforced concrete columns. *Australian Journal of Structural Engineering,* 16**,** 237-250.

ŞENER, S., BARR, B. I. & ABUSIAF, H. F. 2004. Size effect in axially loaded reinforced concrete columns. *Journal of Structural Engineering,* 130**,** 662-670.

SEZEN, H. & MOEHLE, J. P. Strength and deformation capacity of reinforced concrete columns with limited ductility. Proceedings of the

13th World Conference on Earthquake Engineering, 2004. Vancouver, Canada, 1-15.

SHATARAT, N., ALHAQ, A. A. & KATKHUDA, H. 2019. Investigation of axial compressive behavior of reinforced concrete columns using Recycled Coarse Aggregate and Recycled Asphalt Pavement aggregate. *Construction and Building Materials,* 217**,** 384-393.

SHI, C., LI, Y., ZHANG, J., LI, W., CHONG, L. & XIE, Z. 2016. Performance enhancement of recycled concrete aggregate–a review. *Journal of cleaner production,* 112**,** 466-472.

SHIN, S.-W., GHOSH, S. K. & MORENO, J. 1989. Flexural ductility of ultra-high-strength concrete members. *Structural Journal,* 86**,** 394-400.

SURYA, M., VVL, K. R. & LAKSHMY, P. 2013. Recycled aggregate concrete for transportation infrastructure. *Procedia-Social and Behavioral Sciences,* 104**,** 1158-1167.

TABSH, S. W. & ABDELFATAH, A. S. 2009. Influence of recycled concrete aggregates on strength properties of concrete. *Construction and building materials,* 23**,** 1163-1167.

TOKGOZ, S., DUNDAR, C. & TANRIKULU, A. K. 2012. Experimental behaviour of steel fiber high strength reinforced concrete and composite columns. *Journal of constructional steel research,* 74**,** 98-107.

VERIAN, K. P., ASHRAF, W. & CAO, Y. 2018. Properties of recycled concrete aggregate and their influence in new concrete production. *Resources, Conservation and Recycling,* 133**,** 30-49.

WANG, Q., ZHAO, D. & GUAN, P. 2004. Experimental study on the strength and ductility of steel tubular columns filled with steel-reinforced concrete. *Engineering Structures,* 26**,** 907-915.

XU, C., LIU JIN, ZIXING DING, DONG LI, AND XIULI DU 2016. Size effect tests of high-strength RC columns under eccentric loading. *Engineering Structures 126 (2016): 78-91.*

YANG, I. H., JOH, C. & KIM, B.-S. 2010. Structural behavior of ultra high performance concrete beams subjected to bending. *Engineering structures,* 32**,** 3478-3487.

ZHANG, F., LIU, X., GE, F.-W. & CUI, C. 2023. Investigation on the Ductility Capacity of Concrete Columns with High Strength Steel Reinforcement under Eccentric Loading. *Materials,* 16**,** 4389.

ZHOU, J., HE, H., MENG, X. & HUAN, S. 2010. Experimental study of recycled concrete columns under large eccentric compression. *Earth and Space 2010: Engineering, Science, Construction, and Operations in Challenging Environments.*